



University of Évora

ARCHMAT

(ERASMUS MUNDUS MASTER IN ARCHaeological MATerials Science)

Mestrado em Arqueologia e Ambiente (Erasmus Mundus–ARCHMAT)

**Phoenician-Punic amphorae from Castro Marim, Portugal:  
provenance and contents of Pellicer amphora types B/C and D**

**Adam Gašpar, m40770**

Prof. José Antonio Paulo Mirão  
(Supervisor - University of Évora)

Prof. Cristina Maria Barrocas Dias  
(Supervisor - University of Évora)

Prof. Ana Margarida Arruda  
(Supervisor – University of Lisbon)

Évora, October 2019





University of Évora

ARCHMAT

(ERASMUS MUNDUS MASTER IN ARCHaeological MATerials Science)

Mestrado em Arqueologia e Ambiente (Erasmus Mundus–ARCHMAT)

**Phoenician-Punic amphorae from Castro Marim, Portugal:  
provenance and contents of Pellicer amphora types B/C and D**

**Adam Gašpar, m40770**

Prof. José Antonio Paulo Mirão  
(Supervisor - University of Évora)

Prof. Cristina Maria Barrocas Dias  
(Supervisor - University of Évora)

Prof. Ana Margarida Arruda  
(Supervisor – University of Lisbon)

Évora, October 2019



## Panel of Jury

President: Prof. Nicola Schiavon, University of Évora;

Examiner: Dr. Elisa de Sousa, Uniarq – University of Lisbon;

Supervisor: Prof. José Antonio Paulo Mirão, University of Évora;

Partner member: Prof. Donatella Magri, Sapienza University of Rome.

## Resumo

Ânforas fenício-púnicas de Castro Marim, Portugal: origem e conteúdos dos tipos B/C e D de Pellicer

O sítio arqueológico de Castelo de Castro Marim fica na parte mais elevada da Vila com o mesmo nome na costa sul de Portugal, perto da fronteira com Espanha. O local está situado no topo de uma colina 30 metros acima do nível do mar erguido numa área pantanosa entre a costa sudeste do Algarve e a foz do rio Guadiana. Várias campanhas de escavações arqueológicas revelaram ocupação durante a Idade do Ferro, período romano e Idade Média. O objetivo do estudo é avaliar a presença de dois tipos específicos de ânforas pré-romanas no sítio de Castro Marim em termos de proveniência e conteúdo. A produção e distribuição de ânforas Pellicer tipo B/C e D podem ser datadas do 5<sup>o</sup> ao 1<sup>o</sup> séculos a.C e estão relacionadas com a ocupação fenício-púnica da baía de Cadis e do vale do Baixo Guadalquivir. A análise petrográfica do material cerâmico com base na abordagem multi-analítica (principalmente XRD, XRF, petrografia e SEM-EDS) será focada em identificar as diferentes proveniências de amostras selecionadas de ânforas. Em casos relevantes, os resíduos extraídos dos materiais cerâmicos são estudados recorrendo a GC-MS para identificar o bem armazenado nas ânforas. Este trabalho discute a origem das ânforas analisadas e contextualiza-as no meio de produção e comércio de alimentos.

Palavras-chave: Ânforas Pellicer B/C; Ânforas Pellicer D; proveniência das ânforas; ânforas conteúdo; comércio

## Abstract

Phoenician-Punic amphorae from Castro Marim, Portugal: provenance and contents of Pellicer amphora types B/C and D

The castle of Castro Marim archaeological site is located at the highest point of the town with the same name on the southern margin of Portugal close to the border with Spain. The site is placed in the hilltop 30 meters above sea level, elevated along a swampy area between the south eastern coast of the Algarve and the mouth of the Guadiana river. Several archaeological campaigns revealed occupation during the Iron Age, Roman period and the Middle Ages. The objective of this research is to evaluate the presence of two specific types of Pre-Roman amphorae in Castro Marim site in terms of provenance and content. Production and distribution of Pellicer type B/C and D can be dated from the 5<sup>th</sup> to the 1<sup>st</sup> centuries B.C and are related with Phoenician-Punic occupation of the Cadiz bay area and the Lower Guadalquivir valley. The Petrographic analyses of the ceramic material, based on a multianalytical approach (mainly XRD, XRF, petrography and SEM-EDS) is focused on identifying the different provenance of selected amphorae. In relevant cases, the residues extracted from the ceramic materials are studied by GS-MS, in order to identify possible past content of the amphorae. This thesis discusses the origin of the analysed amphorae, contextualizing them in their production, commerce and content.

Key words: Pellicer B/C amphorae; Pellicer D amphorae; amphorae provenance; amphorae contents; commerce

## Acknowledgements

Firstly, I would like to express great gratitude to my supervisors, namely prof. Ana Margarida Arruda from The Uniarq – Centre for Archaeology at the University of Lisbon, who provided archaeological material (post-shards) and valuable information. She led several seasons of field works at the Castelo de Castro Marim, and has been systematically working on evaluating and publishing the results. Great appreciation to my supervisors from the Hercules laboratory – University of Évora, namely prof. Cristina Dias and prof. José Mirão. They were close to me during the entirety of the process, from laboratory work, analysis and thesis writing, to having always been ready to provide me with support, advice and further knowledge. Without my supervisors the master thesis could have come to fruition.

I would like also to thank the whole of Hercules laboratory, to each and every one of my colleagues. The working atmosphere in the laboratory was at all times propitious and fruitful. Especial thanks to my colleagues and friends Massimo Beltrame, Anna Tsoupra and Ana Manhita, who gave me greatly needed information and showed me skills associated with sample preparations, their analysis and interpretation. Here I would like to thank Jan Petřík, from the Department of Geological Sciences of Masaryk University in Brno. For his endless friend support and for providing information crucial in the making of this thesis. I would also like to devote my thanks to Elisa de Sousa from The Uniarq for her help, and drawings documentation of shards. I am again very thanks full to Anna Tsoupra for advices and corrections during the text writing. Great appreciation to Tiago Alexandre Carpelho Martins da Silva, he is from a good family.

I would like to thank the ARCHMAT EMMC International Selection Committee for the amazing opportunity to study this master in archaeometry. This adventure and cultural nourishment forever changed my perspective and archaeological thinking. It did not come without grand support. Here, I would like to thank also our coordinator prof. Nick Schiavon, and all professionals and persons related with the program. Thank you, my dear classmates around world, for everything that I had the pleasure of learning with you.

Finally, I must thank my family, especially to my brother, father, grandfather, and closer friends for their constant moral support. The biggest, and final thanks I send to my mother

At the end I thank to everyone and everything, what is not referenced here.

## Outline

Scope	10
1. Introduction	11
1.1. Phoenician colonisation of the Western Mediterranean	11
1.2. The “Castelo de Castro Marim” – typical hilltop site in the delta	13
1.3. The Lower Guadalquivir valley, Pellicer B/C and D amphorae commerce	15
1.4. The geology of Castro Marim	19
1.5. The geology of Lower Guadalquivir valley	20
1.6. Archaeometry of ceramic materials – raw material, modelling and firing	21
1.7. Workshops of amphorae, amphorae distribution, use and discard	24
2. Analytical techniques	27
2.1. Petrography of thin sections	27
2.2. X-ray fluorescence (XRF)	28
2.3. X-ray diffraction (XRD)	29
2.4. Electron microscopy (SEM-EDS)	30
2.5. Organic content analysis (GC-MS)	32
3. Materials and methods	35
3.1. Petrography	37
3.2. ED-XRF	38
3.3. Powder XRD	39
3.4. SEM-EDS	39
3.5. GC-MS	40
4. Results	42
4.1. Petrography	42
4.2. XRD	47
4.3. ED-XRF	49
4.4. SEM-EDS	54
4.5. GC-MS	61
5. Discussion	63
5.1. Ceramic materials study	63
5.2. Content of vessels	70
Conclusion	74
Literature	77
Annex	

## List of figures

**Fig. 1.1** – **A:** Phoenician merchant ship with various traded goods; **B:** The Phoenician-Punic sphere of influence and main sites in the 6<sup>th</sup> century BC.

**Fig. 1.2** – **A:** The Castro Marim in the Iberian Peninsula (after Arruda et al. 2014, Fig. 1); **B:** The Guadiana river, the area of salt production and the archaeological site with the Medieval castle.

**Fig. 1.3** – The topographic plan of the castle and excavated areas (after Arruda et al. 2006, Fig. 2).

**Fig. 1.4** – Lower Guadalquivir and surroundings of the ancient Lacus Ligustinus – the marshy area of the Guadalquivir delta with main surrounding Iron Age settlements (after Garcia-Fernandez 2015, Fig. 1).

**Fig. 1.5** – **A:** Amphorae Pellicer B, C and D (after Pellicer Catalán 1978, Fig. 13); **B:** The selected bottoms of Turdetani amphorae founded in Cerro Macareno, Sevilla (after Pellicer Catalán 1978, Fig. 12).

**Fig. 1.6** – **A:** Amphorae Pellicer D and example the variability of rims (after Vargas 2016); **B:** Local amphorae of the Turdetani region: I - Pellicer C (Cerro Macareno), II - Pellicer B (Cerro Macareno), III - Pellicer D (Las Cumbres); Amphorae with Punic-Gadiz origins: IV - T-12.1.1.1 and T-12.1.1.1/2 (Cádiz), V - T-8.2.1.1 (Sevilla), VI - T-9.1.1.1 (prototype from Cádiz), VII- T-8.1.1.2 (Cerro Naranja; after Garcia-Fernandez 2015, Fig. 2).

**Fig. 1.7** – Cross sections of Pelicer B/C and D amphorae sorted to the material groups (after Megías 2017).

**Fig. 1.8** – Geological map of the lower Guadalquivir basin (map adapted from IGME's 1:50.000 geological maps, after Salvany et al. 2011).

**Fig. 1.9** – Sediment grain size and sorting; **A:** The grain size dimensions in millimetres (mm) from pebbles to silt and clay; **B:** the degree of uniformity of grain size: sorting (Moura et al. 2017, Annex III - credits: S. Oliveira).

**Fig. 1.10** – Support of the grate: **A:** Central pillar; **B:** Radial support; **C:** Axial support (after Cuomo di Caprio 2007).

**Fig. 1.11** – Technological choices, material properties and schema of ceramic life cycle (after Sillar, Tite 2000).

**Fig. 2.1** – Petrographic (polarized light) microscope configuration.

**Fig. 2.2** – Principle of X ray fluorescence spectroscopy.

**Fig. 2.3** – Reflection of an X-ray beam by the planes of a crystal with interplanar spacing (after Bannert 2017).

**Fig. 2.4** – Scanning electron microscope.

**Fig. 2.5** – Schematic plot of the main components of standard GC–MS instruments (Emwas et al. 2015, Fig. 1).

**Fig. 3.1** – **A:** Pellicer B/C amphora with the smaller, pointed protrusion and concave wall (sample 4, 12356); **B:** Pellicer B/C amphora with the smaller oval protrusion (sample 10, 12655), **C:** Pellicer B/C amphorae with the bigger and oval protrusion (sample 12, 3698), **D:** The bottom similar to Pellicer B/C amphora without significant protrusion (sample 15, 12658), **E:** The bottom similar to MPA4 amphora with probable Cadiz origin (sample 16, 11078), **F:** The concave bottom of local common ware (sample 19, 12047).

**Fig. 4.1** – Stereo-images of cross sections: number of sample and petrographic group represented by letter; more images and details about petrography is possible to see in the catalogue of samples (**Annex I**).

**Fig. 4.2** – Thin section image with significant intrusion in selected sample. 10 – A: amphibole, 16 – A: fossil, 9 – A3: slate, 6 – A4: limestone, 22 – A5: shell, 30 – C2: gabbro.

**Fig. 4.3** – Selected diffractograms and main mineral phases (x -  $2\theta$ , y - Intensity (a.u.)) with the numbers of samples and the letter of fabric group. Q – quartz, F – feldspar, Dio – diopside/pyroxene, Geh – gehlenite, M – mica/illite, A – amphibole, Hor – hornblende, Ca – calcite.

**Fig. 4.4.** – Box plots of main oxides and LOI with marked outliers as circles.

**Fig. 4.5** – The ED-XRF data in the bi-axial graphs. **A:** CaO-Fe<sub>2</sub>O<sub>3</sub>, **B:** Na<sub>2</sub>O- CaO, **C:** Na<sub>2</sub>O-K<sub>2</sub>O (dot – Pellicer B/C, cross – amphorae without protrusion, square – local common wares, X – Pellicer D).

**Fig. 4.6** – The ED-XRF data in the bi-axial graphs. **A:** Al<sub>2</sub>O<sub>3</sub>-Zr, **B:** Rb-Sr, **C:** Rb-Zr (dot – Pellicer B/C, cross – amphorae without protrusion, square – local common wares, X – Pellicer D).

**Fig. 4.7** – Selected surface electron images (SE) with the numbers of samples and the letter of fabric group.

**Fig. 4.8** – SEM EDS: sample 1 – A; **A:** Backscattering image, **B:** elemental mapping, **C:** spectra of the mapping, **D:** table with point EDS analysis in the atomic % (the number of points correspond with the numbers in mapping).

**Fig. 4.9** – SEM EDS: sample 10 – A; **A:** Backscattering image, **B:** elemental mapping, **C:** spectra of the mapping, **D:** table with point EDS analysis in the atomic % (the number of points correspond with the numbers in mapping).

**Fig. 4.10** – SEM EDS: sample 6 – A4; **A:** Backscattering image, **B:** elemental mapping, **C:** spectra of the mapping, **D:** table with point EDS analysis in the atomic % (the number of points correspond with the numbers in mapping).

**Fig. 4.11** – SEM EDS: sample 16 – A2; **A:** Backscattering image, **B:** elemental mapping, **C:** spectra of the mapping, **D:** table with point EDS analysis in the atomic % (the number of points correspond with the numbers in mapping).

**Fig. 4.12** – SEM EDS: sample 24 – B; **A:** Backscattering image, **B:** elemental mapping, **C:** spectra of the mapping, **D:** table with point EDS analysis in the atomic % (the number of points correspond with the numbers in mapping).

**Fig. 4.13** – SEM EDS: sample 30 – C2; **A:** Backscattering image, **B:** elemental mapping, **C:** spectra of the mapping, **D:** table with point EDS analysis in the atomic % (the number of points correspond with the numbers in mapping).

**Fig. 4.14** – Detail of glassy vitrification; sample 21 – B. **A:** Backscattering image, **B:** Al mapping, **C:** Ca mapping, **D:** Si mapping, **E:** Mg mapping, **F:** Fe mapping.

**Fig. 4.15** – SEM-EDS data. Ternary diagram illustrating the composition of feldspars in selected samples (dots – Pellicer B/C, triangles – amphorae without protrusion, squares – local common ware, diamonds – Pellicer D).

**Fig. 5.1** - Bi-axial graph: MgO and CaO obtained by ED-XRF.

**Fig. 5.2.** – Calcareous rich clays – mineral forming during the firing (after Noll, Heimann 2016).

**Fig. 5.3** – **A:** Simplified ternary phase diagram SiO<sub>2</sub>- Al<sub>2</sub>O<sub>3</sub>-(CaO+MgO) for calcareous-dolomitic clays (after Noll, Heimann 2016), **B:** Top part of the simplified ternary diagram. Symbols reflect the main ceramic typology (dot – Pellicer B/C, cross – amphorae without protrusion, square – concave bottoms, X – Pellicer D).

**Fig. 5.4** – Principal component analysis (PCA) of main oxides. The values of oxides were transformed into the logarithmic scale (loading data: **Annex III**), the group of petrographic fabrics marked in circles (**Table 2-5**).

**Fig. 5.5** – **A:** Chromatogram of GC-MS for sample 6 and **B:** sample 9, with compounds identified (FA- fatty acids; AL- Alcohols; MAG: monoacylglycerols; CXY- Alcanes).

## Scope

The amphorae were broadly used as containers for storage and export of various food product in the ancient time. There are various types of Phoenician-Punic amphorae related with the time scale and production centres ([Garcia-Fernandez 2015, Fig. 2](#); [Ramón Torres 1995](#)). The main objective of this study is to evaluate the overall meaning of the presence of two specific types of pre-Roman amphorae, Pellicier B/C and D, in the archaeological site of the Castro Marim, Portugal. The production and distribution of these “Punic” amphorae are dated from the end of 6<sup>th</sup> to the 1<sup>st</sup> century BC, and it is associated with commercial food supply from the Lower Guadalquivir valley or Cadiz area, in the Southwest Andalusia ([Garcia-Fernandez 2019](#)).

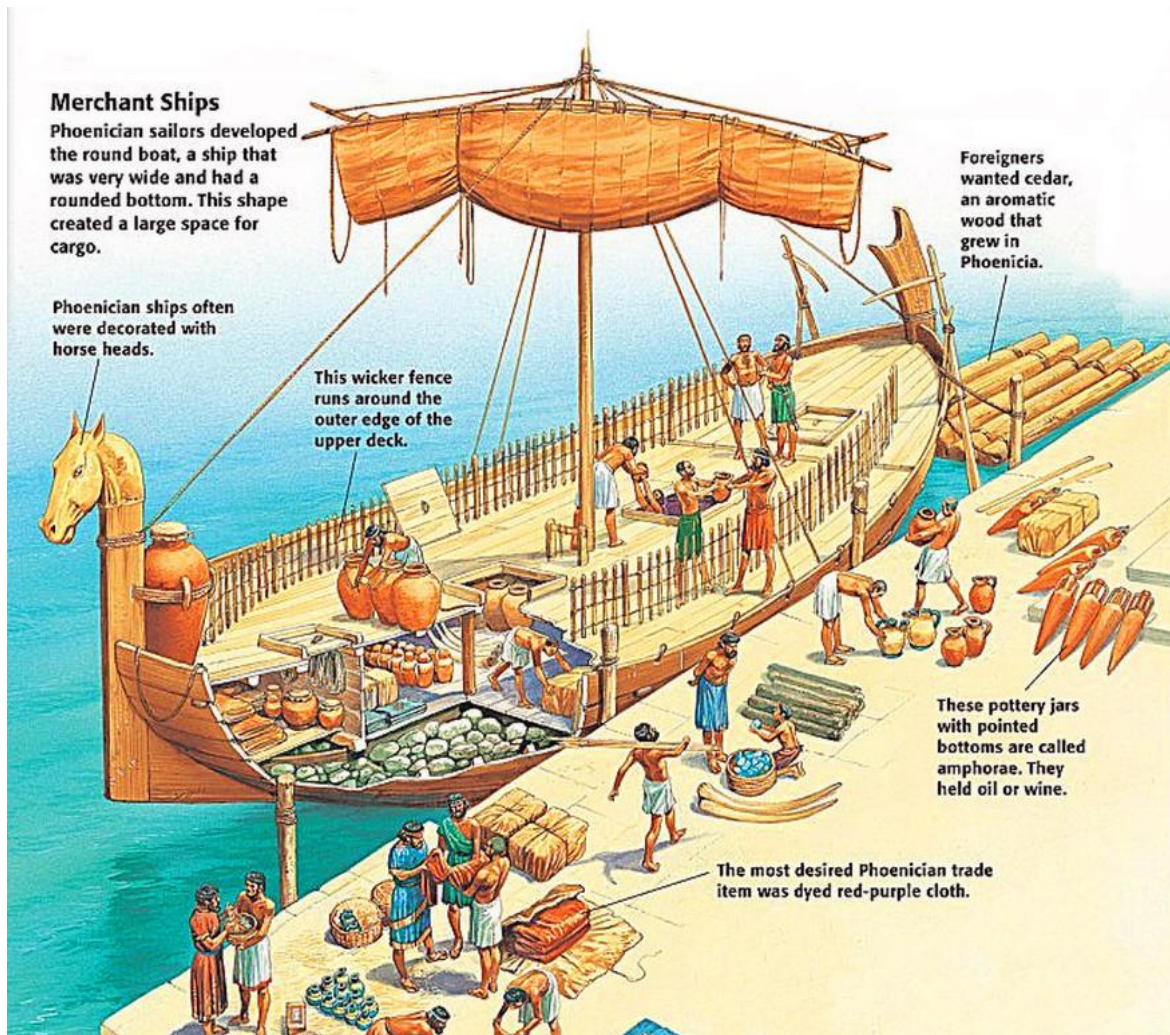
The shards of 14 bottoms of Pellicier B/C amphorae with protrusions (I), 2 bottoms of amphorae without significant protrusion (III), 4 concave bottoms identified as local common wares (III), and 10 rims of Pellicier D amphorae (IV) were selected with the aim to identify the provenance and the content of the vessels. A multianalytical protocol combining petrography of thin sections, chemical analysis of ceramic material in the form of fused beads, and determination of main mineralogical composition of the bulked powder by XRD was implemented. SEM-EDS analysis was applied on selected thin sections to obtain more details about the temper and microstructure. The primary goal of the study is the material characterisation of the composition of vessels, and to identify different fabric groups. The firing temperature and atmosphere, partially manufacturing process and used raw material are discussed. Based on the provenance results, the contents of selected bottoms were investigated by GC-MS. The research objective of content study is to determine the food products residues presented in the bottoms.

## 1. Introduction

### 1.1. Phoenician colonisation of the Western Mediterranean

The term Phoenicians derives from ancient Greek and it is a commonly accepted name for Semitic-speaking populations settled in city-states (e.g. Tyre, Sidon, Byblos) along the Eastern Levantine Mediterranean coast. The culturally developed population excelled at navigating. Phoenician traders and settlers began spreading to the southern coast of the Mediterranean in the early 1<sup>st</sup> millennium BC (**Fig. 1.1: A**). Carthage was established in the 9<sup>th</sup> century, as well as other colonies, where Algeria and Morocco are located nowadays. Based on archaeological data, systematic Phoenician colonisation continued in the Balearic Islands, Iberian Peninsula and Western North Africa during the 9<sup>th</sup> and 8<sup>th</sup> century BC. The Phoenician settlers established a network of trading posts aiming at commerce with indigenous populations and direct exploitation of local resources. The centres of trade attracted more and more natives, and soon grew into cities of their own. During the Orientalising period (9<sup>th</sup>/8<sup>th</sup> – 6<sup>th</sup> century BC), in the Atlantic shoreline of Iberia, the most prominent centres of exchange were Cadiz and Huelva, due to metal trading ([Dietler 2009](#)).

Taking the 6<sup>th</sup> century as a starting point, the Carthage had been rising to the power and began to incorporate former Phoenician cities in Sicily, Sardinia and Iberia. After the city of Tyro and the Levantine coast was conquered by the Babylonian empire in 573 BC, Carthage established itself as the dominant maritime power in the Mediterranean and created an autonomous “Punic” commercial sphere. Punic is the Latin equivalent for Phoenician, but the term Punic is more relevant for Carthaginians and Carthage’s sphere of influence in the Central and Western Mediterranean (**Fig. 1.1: B**; [Dietler 2009](#)). These circumstances in the 6<sup>th</sup> century, but also environmental and societal factors led to the economic destabilization and changing of settlement patterns in mostly of the regions. In the Cadiz bay, the centres based on the mining and trading metals were affected, and the subsistence strategy had been changed to the local oriented economic based on agriculture. In the area of the Lower Guadalquivir valley, the long-distance trade related with the Tartessos ecumene collapsed ([Aubet 1995](#)). After a few decades of revitalisation and consolidation, commerce of different goods and food products started to flourish from the fertile region such as the Lower Guadalquivir valley again ([Garcia-Fernandez 2015](#); [Megías 2017](#)).



A



B

Fig. 1.1 – A: Phoenician merchant ship with various traded goods<sup>1</sup>; B: The Phoenician-Punic sphere of influence and main sites in the 6<sup>th</sup> century BC<sup>2</sup>.

<sup>1</sup> <https://phoenicianresearch.weebly.com/uploads/1/7/3/5/17357749/8122590.jpg?875> (10.7.2019)

<sup>2</sup> <https://phoenicia.org/imgs/phoeniciancolontradedposts.jpg> (10.7.2019)

## 1.2. The “Castelo de Castro Marim” – typical hilltop site in the delta

The archaeological site is situated in the upper part of the small town, Castro Marim, in the south-east coast of the Algarve in Portugal. The town is placed in the delta of the Guadiana river which nowadays forms parts of the border with Spain (**Fig. 1.2: A**). The site with the medieval castle is situated at a hilltop (30-40 m a. s. l.) rising from a swampy area between the coast and the Guadiana river (**Arruda 1996; 2000; Bargão, Arruda 2014**). Nowadays the marshy area is modified artificially due to the industrial salt production. In the 16<sup>th</sup> century the river was closer to the hilltop and the area was well protected (**Arruda 1996**). Hypothetically during the Iron Age, the hilltop might have been an island in the delta, and such might have been possible reaching the hilltop by ships either from the river or from the sea (**Fig. 1.2: B; Arruda et al. 2006**).



**Fig. 1.2 – A:** The Castro Marim in the Iberian Peninsula (after **Arruda et al. 2014, Fig. 1**); **B:** The Guadiana river, the area of salt production and the archaeological site with the Medieval castle<sup>3</sup>.

The castle was occupied mainly during the Iron Age, Roman Age and Modern time, as the archaeological campaigns in the eighties and at the beginning of new millennium proved (**Fig. 1.3**). However, the evidence of first human activity at the site date to the Late Bronze Age (**Arruda 1996**). The privileged location of the Castro Marim, crucial for the controlling of the

<sup>3</sup> [https://www.visitalgarve.pt/pt/menu/39/castro-marim.aspx#prettyPhoto\[1\]/1/](https://www.visitalgarve.pt/pt/menu/39/castro-marim.aspx#prettyPhoto[1]/1/) (10.7.2019)

delta area, attracted the Phoenician colonists. Such, during the Orientalizing period (7th – 6<sup>th</sup> century BC), the indigenous settlers of Castro Marim came to interact with Phoenicians, which were already installed in Southern Andalusia (Arruda et al. 2006). The Phoenicians made use of big rivers as trade routes with inland indigenous populations (Arruda 2009).

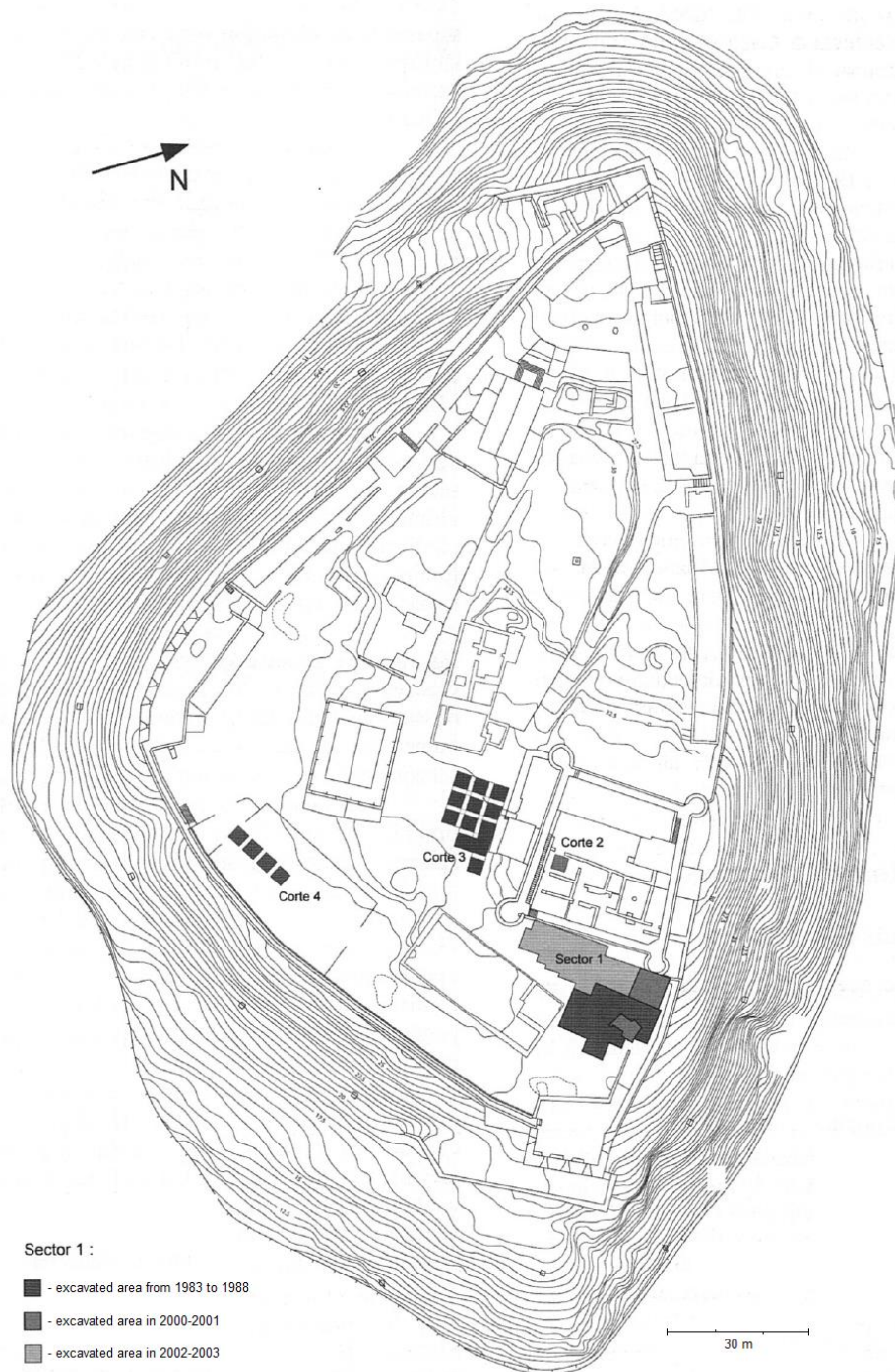


**Fig. 1.3** – The topographic plan of the castle and excavated areas (after Arruda et al. 2006, Fig. 2).

A lack of imports and a decrease in human activity on the hilltop is recorded at the end of the 6<sup>th</sup> and at the beginning of the 5<sup>th</sup> century as proved the radiocarbon dating. This phase did not go beyond the second half of the 5<sup>th</sup> century BC, when the settlement at the hilltop restructured (Arruda, Freitas 2008; Arruda et al. 2014). From the second half of 5<sup>th</sup> century BC, Castro Marim started again to be fully integrated into trade network, including several distant settlements and sites associated with Phoenician-Punic tradition. In the Pre-Roman time, the Castro Marim population was exchanging various goods and especially food products with the Western Andalusian region (mainly the Lower Guadalquivir valley and Cadiz bay). In the same time the Castro Marim site was the centre of exchange in the Guadiana river region. After the Carthaginians were defeated by the Romans, the socio-economic sphere had been transforming, and the significant period of the hilltop occupancy is the second half of 1<sup>st</sup> century BC, when the Roman trade based at the Italian production culminated (Arruda et al. 2006; Arruda, Freitas 2008; Arruda et al. 2014).

### 1.3. The Lower Guadalquivir valley, Pellicer B/C and D amphorae commerce

The presence of Pellicer B/C and Pellicer D amphora types in the Castro Marim site is related with their export from the Lower Guadalquivir river valley and the area of Cadiz in the second half of the first millennium BC (Fig. 1.4; Arruda et al. 2006; Vargas 2016). The boundaries of the Turdetani region were formed by The Guadalquivir river to the west, the Sierra Morena to the North, the foothills of the Baetic Cordillera to the East (Bastetania) and according to Strabo, it also comprised the coast from the Strait of Gibraltar to the mouth of the Guadiana river. The crisis of the Orientalising period during the 6<sup>th</sup> century BC causes the emergence of the Turdetani culture (from 5<sup>th</sup> to 2<sup>nd</sup> century BC) in the region. This culture was not a homogenous ethnic group, but a melting pot containing mainly indigenous population affected by Phoenician-Punic influence. The production in this fertile region formed by the delta was supported by the distinctive eating habits. Due to the interaction of various communities in central sites, and vigorous trade, food consumption habits and cuisine were exchanged as well. On the list of favourite commodities was fish sauce, but a broad scale of other goods related with rural production were also traded (Garcia-Fernandez 2015).

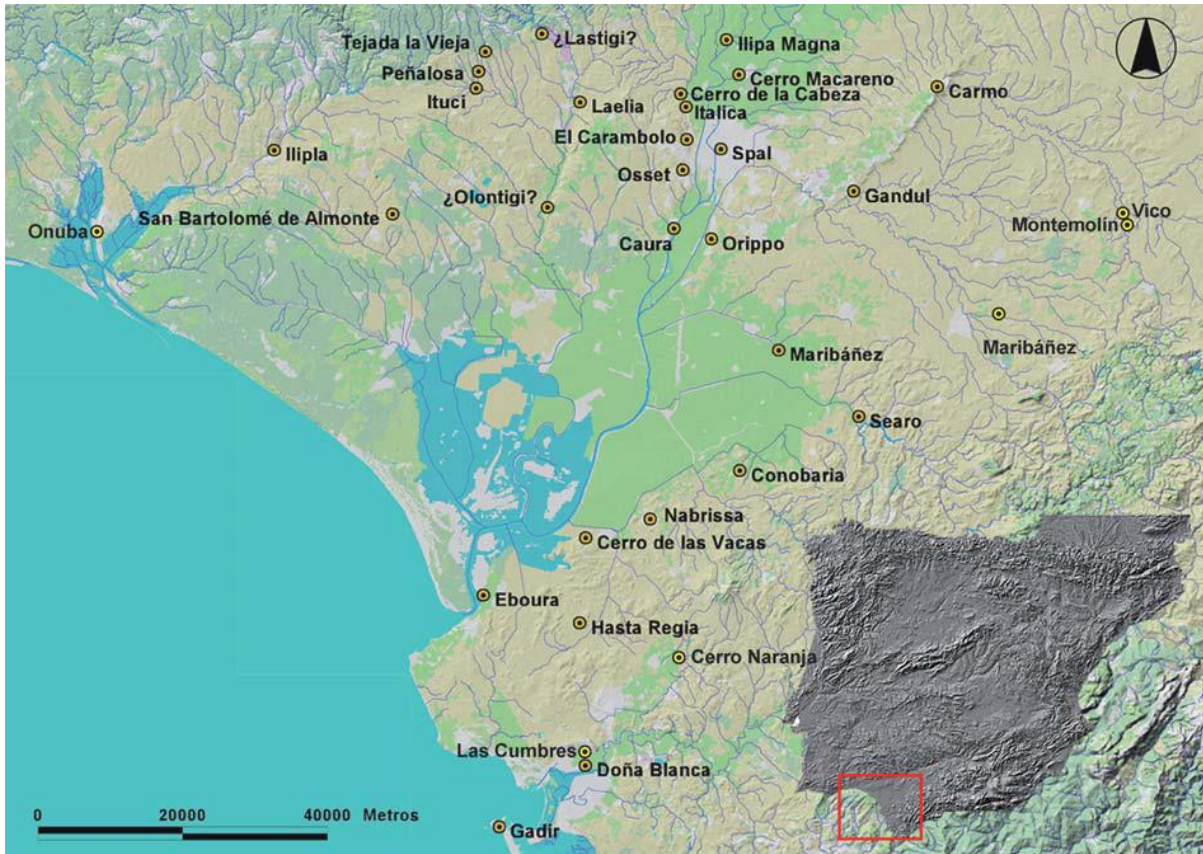


Fig. 1.4 – Lower Guadalquivir and surroundings of the ancient Lacus Ligustinus – the marshy area of the Guadalquivir delta with main surrounding Iron Age settlements (after Garcia-Fernandez 2015, Fig. 1).

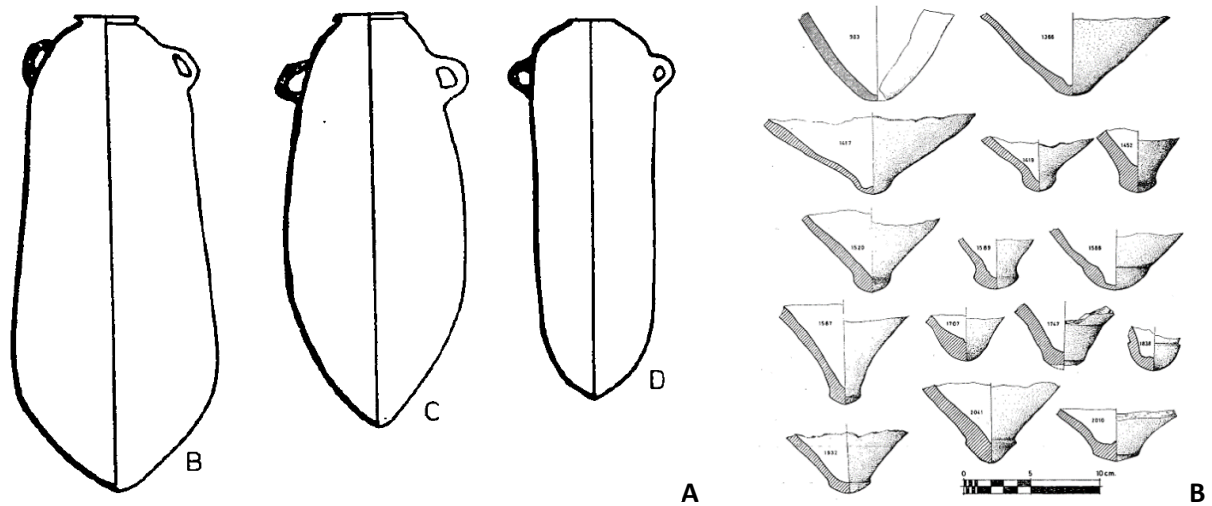
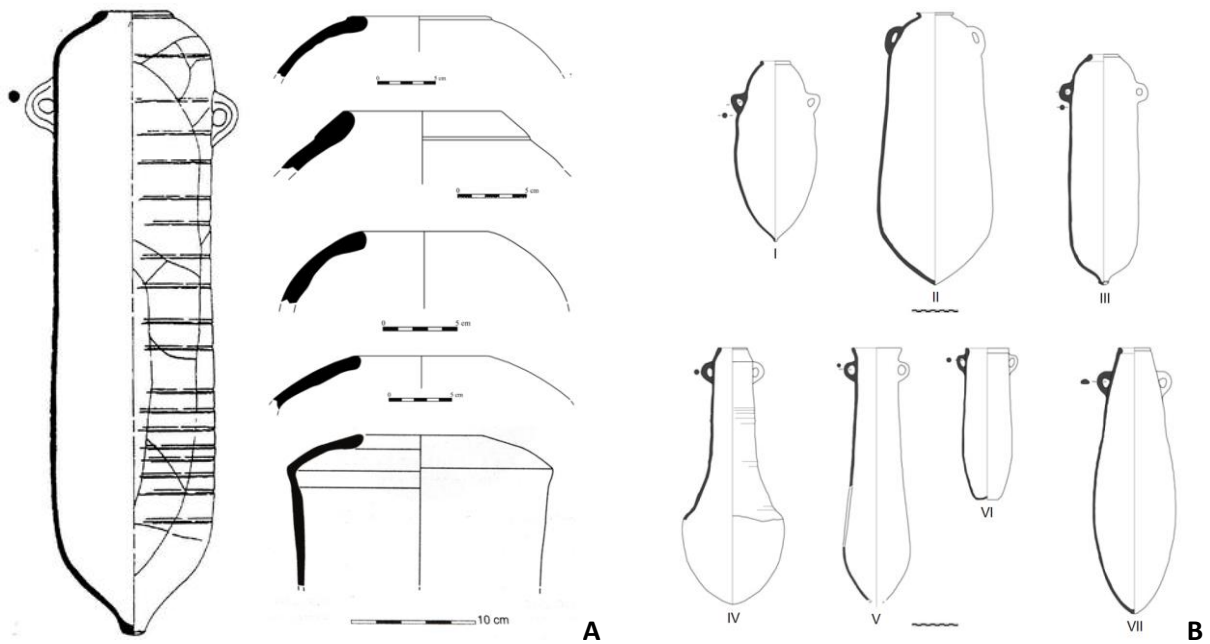


Fig. 1.5 – A: Amphorae Pellicer B, C and D (after Pellicer Catalán 1978, Fig. 13); B: The selected bottoms of Turdetani amphorae founded in Cerro Macareno, Sevilla (after Pellicer Catalán 1978, Fig. 12).



**Fig. 1.6 – A:** Amphorae Pellicer D and example the variability of rims (after Vargas 2016); **B:** Local amphorae of the Turdetani region: I - Pellicer C (Cerro Macareno), II - Pellicer B (Cerro Macareno), III - Pellicer D (Las Cumbres); Amphorae with Punic-Gadiz origins: IV - T-12.1.1.1 and T-12.1.1.1/2 (Cádiz), V - T-8.2.1.1 (Sevilla), VI - T-9.1.1.1 (prototype from Cádiz), VII- T-8.1.1.2 (Cerro Naranja; after Garcia-Fernandez 2015, Fig. 2).

The amphorae of Phoenician-Punic tradition Pellicer B/C and D were used for the transport of various food products (Fernandes et al. 2017). The Pellicer B/C type is dated from the 6/5<sup>th</sup> to 3<sup>rd</sup> century BC. The younger variant of similar shape Pellicer D occurred from the 4<sup>th</sup> to the 1<sup>st</sup> century BC. The overall features of these amphorae are the oval protrusion or pointed end at the bottom of elongate body and concave throat with mouth about 10-12 cm wide. After the classification mainly based on sections of rims, various inner sub-types were described. The body shapes of amphorae vary from oval-saccate to cylindrical, especially in the case of Pellicer B/C, while Pellicer D amphorae have predominantly the cylindrical body with maximum weight about 100 cm (Fig. 1.5, 1.6). However, there are other defined types of amphorae with similar morphological features which could pose the problems in typological classification (Fig. 1.6; Arruda et al 2006; Garcia-Fernandez 2009; Megías 2017; Romero Sáez, Niveau de Villedary 2016; Vargas 2016).

Although the origin of Pellicer B/C amphorae has been agreed to be the Lower Guadalquivir valley, their contents are under debate (olives, olive oil, wine, fish sauce, etc.). The

provenance of younger, Pellicer D amphora, so called “Coastal type” is still not certain. The study based solely on the macroscopic observation of the ceramic paste, suggests two distinct geographical regions, the Lower Guadalquivir valley, or the area of Cadiz. The amphorae were being produced concurrently in more places in the Lower Guadalquivir. This demonstrates a different sub-classification based on the composition of ceramic (**Fig. 1.7**), and a few distinct sites with the kilns (Megías 2017). Primary commodities as well as secondary food products like wine, olive oil or fish sauce were transported and traded. The Pellicer amphorae B/C and D were probably used and re-used as common containers in a local scale trade too (Garcia-Fernandez et al. 2017). Various food products and surplus were exported, and in this view, the Pellicer amphorae B/C and D are encountered in many sites of the Iberian Peninsula and North Africa. Punic Cadiz had in that time function as the commercial hub and distribution centre of these amphorae (Garcia-Fernandez 2019; Megías 2017; Sáez Romero, Niveau de Villedary 2016; Sáez Romero 2018; Vargas 2016).

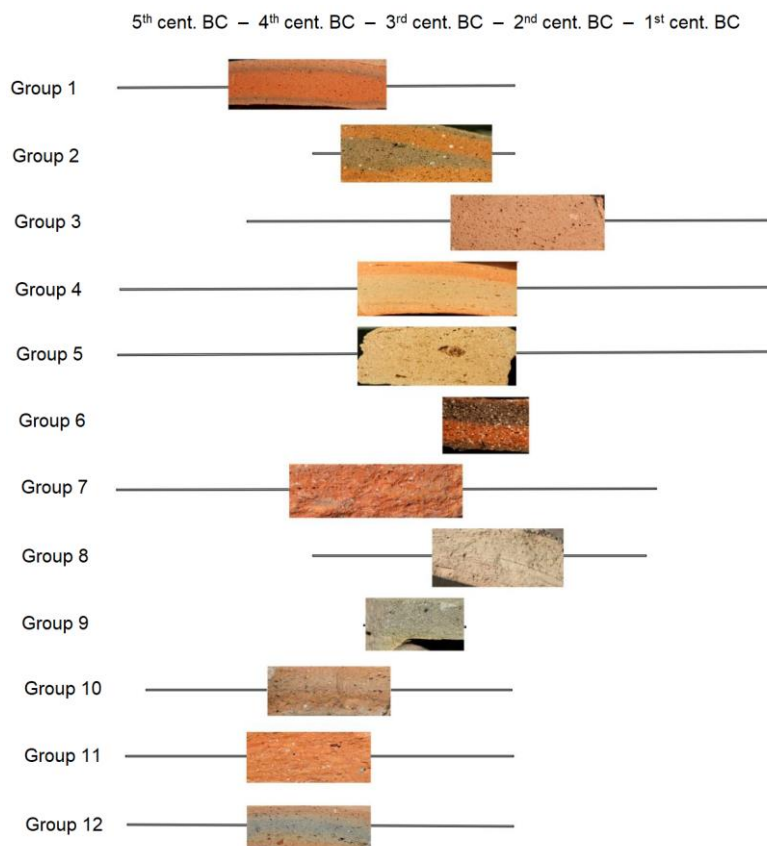


**Fig. 1.7** – Cross sections of Pellicer B/C and D amphorae sorted to the material groups (after Megías 2017).

#### 1.4. The geology of Castro Marim

The Castro Marim site is situated in an area with a geological evolution that involves periods of marine transgression and regression, formation of mountains, erosion, volcanism and seismic activity. The oldest rocks in Castro Marim region are the slate and greywacke from Baixo Alentejo Flysh formation, created at about 320 million years ago, in the Carboniferous Period, due to the deposition at sea floor of terrigenous sediments coming from the erosion of an emerging continent. During Hercynian orogeny (from 290 to 260 million years ago) these strata were intensively folded. The foothill located north of Castro Marim is essentially made up of this geological formation ([Oliveira et al. 1982](#)).

During the Mesozoic period, in the Triassic, the intense erosion of the Hercynian reliefs originated the formation of sandstones, conglomerates and clay stones, of predominant red colour, commonly known as "Grés de Silves". Above this unit, a marl with evaporitic rocks geologic formation is identified.

Intense igneous activity affected the geology of Castro Marim region in the transition between the Triassic and the Jurassic periods. These basic volcanic and doleritic rocks are characterized by the presence of plagioclases and pyroxenes. The overlying dolomitic limestone related with the doleritic rocks is lower Jurassic dated ([Oliveira et al. 1982](#); [Romariz, Almeida, Oliveira 1979](#)).

From the Lower Jurassic to the Miocene there are almost 200 million years, the geological history is unknown, since sediments from this time interval were not found. In the Upper Miocene (from 8 to 5 million years ago), in the deltas, were deposited sandy clays and silts, which form the main cliffs in the East Algarve ([Moura et al. 2017](#)).

Most of the landscape of the Castro Marim has origin in a recent geological period, the Quaternary, which began 2,5 million years ago. The alluvial formations of black clays have been deposited in the final section of the Guadiana for about 8000 years. They progression to the sea is blocked by large masses of sand. The alluvial plain, subject to flooding, was developed and furrowed by sinuous streams originating in the surrounding reliefs. The salty swampy area was developed during the last 5000 year. The sediment in the delta has 2 main sources: fluvial and marine. The top sediment in the riverbed is formed by mud, clay and silt

with sandy layers, while the riverbanks contain mainly substrate of carboniferous shale (Fletcher 2005; Morales 1997; Moura et al. 2017).

### 1.5. The geology of Lower Guadalquivir valley

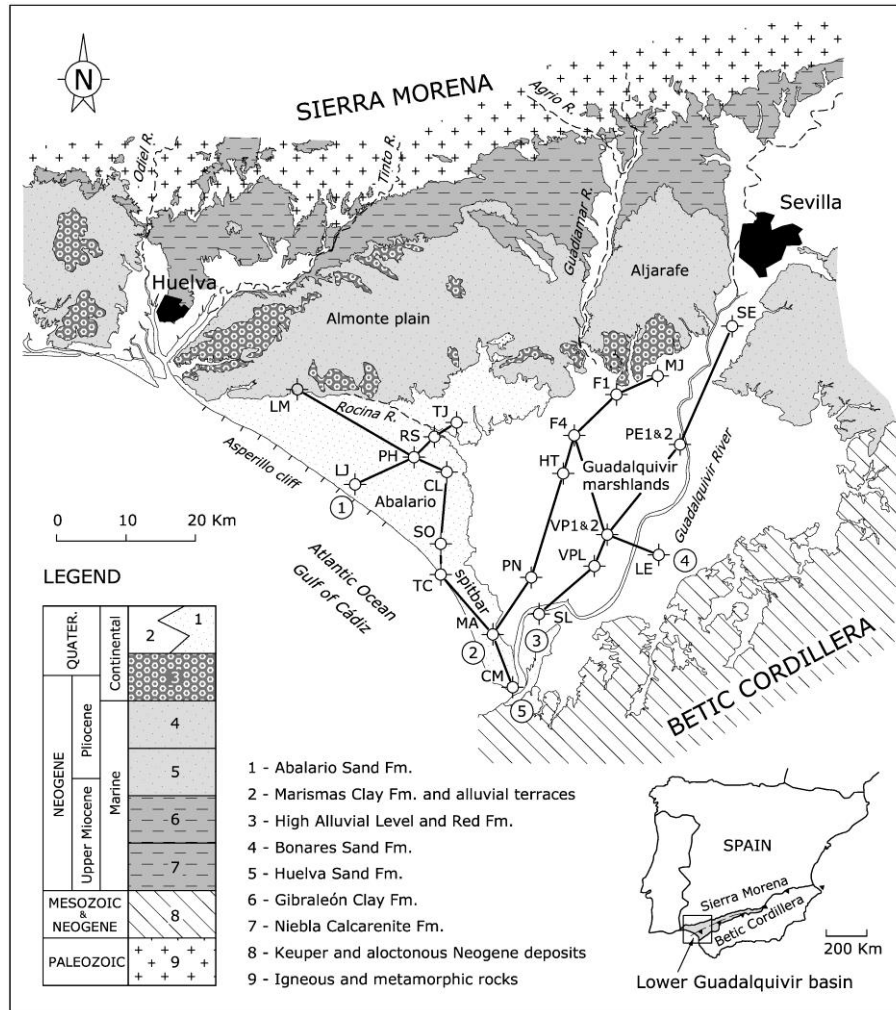


**Fig. 1.8** – Geological map of the lower Guadalquivir basin (map adapted from IGME's 1:50.000 geological maps (after Salvany et al. 2011).

The depression of the Guadalquivir is a broad foreland basin between two orogenic units: the Iberian Massive (i.e. Sierra Morena) with the origin in Hercynian orogeny in the North, and much younger Betica Cordillera formed in Neogene in the South. The continental sedimentary basin was created in the Neogene and Quaternary (Villalobos, Pérez 2006). The southern half is formed by younger mesozoic materials from the Betica Cordillera, while the north-western

edge remained more stable, with compact sediments from the erosion of older Iberian massif. The geology here is more like in the area of Castro Marim site. In the Southeast edge of basin, the Paleogenic and Neogenic sediments are much diverse, because of a constant elevation of the Beatica mountains. In this area, the presence of volcanic and plutonic rocks is clear (**Fig. 1.8**; [Montealegre, Barrios 1996](#); [Fernandez et al. 1998](#)).

From the stratigraphic point of view, the sedimentary fill of the basin can be divided into two large groups. The lower set, dated to the middle Miocene, includes the facies of "moronitas" or "albarizas", and white marls deposited in environments deep marine, rich in microfossils such as foraminifera, coccoliths, diatoms, radiolaries, silicoflagellates, spicules, etc.

The highest levels of the basin stretch were mainly formed during the Quarternary. The marls are the more abundant sediments and can be considered as calcareous clays with impregnations of iron oxides and sporadic more plastic intercalations.

#### 1.6. Archaeometry of ceramic materials – raw material, modelling and firing

The routine archaeometric targets are the identification of ceramic groups and their origin, as well as aspects related to the manufacturing of ceramics. Production centres and workshops offer an ideal framework to recover ceramic manufacturing processes, with the necessary involvement for technical/technological choice, and fabric groups could function as localized references for provenance studies. On the contrary, consumption centres are ideal for discussing the interaction of artefacts with people. Archaeological classification is usually based on the morphological properties of ceramics, together with the compositional and structural properties determined or hypothesized by macroscopic and/or stereoscope observations. Portable analytical facilities and instruments may allow preliminary overview, which would improve the initial sampling frame for the archaeometric study. Archaeometric results allow us to infer the exact composition of post-excavated shards and creating a new classification of ceramics with similar morphological and macroscopic properties ([Buxeda i Garrigós, Madrid Fernández 2017](#)).

The objective of studying ancient ceramic material is to understand the ceramic life cycle in past societies: extracting, procuring, and processing of raw material; shaping and firing of the

vessel; use, exchange, trade; discarding of the ceramic (Heimann, Maggetti 2014; Tite 1999, 2008). To find a proper answer, material nature of ceramics must be also studied and evaluated from an archaeometric point of view, mainly on a chemical, mineralogical and petrographic level. The archaeometry of ceramics is an inverse problem and it must consider the weathering and post-depositional processes in the archaeological record. The archaeometric data can also be influenced by an archaeological post-excavational treatment (e. g. washing of shards, labelling with reference information, storage conditions, etc.). But, research questions are mainly related with states of ceramic in their life cycle – finished pottery, unfired pottery, the manufacture processes (preparation of material, shaping of vessels, etc.), raw ceramic materials and their provenance. To understand the complexity of these problems a multianalytical study is appropriate (Buxeda i Garrigós, Madrid Fernández 2017; Heimann, Maggetti 2014; Tite 1999, 2008).

The final properties of ceramic material are directly linked with the used raw materials and the process of manufacturing and firing (Quinn 2013; Noll, Heimann 2016). Information regarding ancient technology can be derived from the pottery itself, but also from the production places. In this view, it is important for the cryptanalysis of the ceramic elaboration, besides precise material studies, to collect historical, ethnographic or ethnoarchaeological information (Heimann, Maggetti 2014; Noll, Heimann 2016; Roux 2017).

First, the raw material with the required properties for ceramic production was extracted and transported to the site. As accessible fine clay sources are limited, there is a premise, that raw material has been extracted from the distinctive places for longer (Shephard 1985). The material in ceramic production should have had enough plasticity, and at the same time it couldn't shrink too much during the drying and firing. To obtain the efficient properties of the material, the coarse particles were removed, and the clay was grinded. Then usually, some temper was added, either from an organic or inorganic material, such as plant remains, bones, shells or crushed rocks and sand. The identification of the temper is a particularly important factor in provenance studies. Different kind of temper affects differently the final quality of the pottery, thus the selection of the temper added is related to the ceramic tradition. The final step, in clay preparation, after of any kind of manipulation is its stay for few days in order to "mature" (Heimann, Maggetti 2014; Noll, Heimann 2016; Petřík 2017; Quinn 2013).

The sphericity and roundness of the temper grains depends on the distances of transportation in sedimentary environments. The rounder grains, the longer distances were transported. In this respect, the observation of these attributes could provide as information regarding the initial places of the raw materials and thus to associate to potential sources. For example, in a river, round temper grains indicate that their place of exploitation were on the downstream. However, in a case like the roundness of the grains could also be from various other processes, such as wind erosion or tidal regime (**Fig. 1.9**). The size of the temper grains depends on the sorting and/or sieving that underwent and its relative homogeneity (unimodal, bimodal) could be an attribute in ceramic studies ([Grotzinger et al. 2006](#); [Quinn 2013](#)). Another characteristic of the temper is the orientation of the elongated grains, which can be linked to the use of pottery wheel. For instance, if the fast pottery wheel was used, the particles are oriented along the ceramic body ([Quinn 2013](#)).

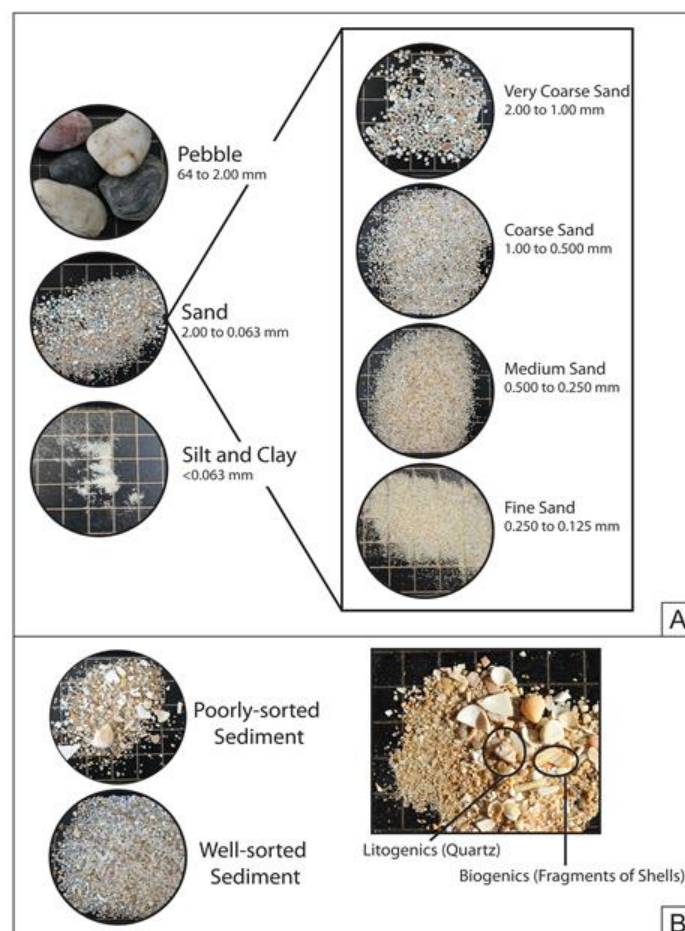


**Fig. 1.9** – Sediment grain size and sorting; **A:** The grain size dimensions in millimetres (mm) from pebbles to silt and clay; **B:** the degree of uniformity of grain size: sorting ([Moura et al. 2017, Annex III - credits: S. Oliveira](#)).

During the firing of ceramic material, the minerals either from the clay and temper interact, transform, decompose or form new mineral-like phases. The final mineralogical composition of the ceramic from certain material depends on the temperature regime and the atmosphere in ceramic kiln (Noll, Heimann 2016; Quinn 2013; Riccardi, Messiga, Duminuco 1999). In the case of calcareous or dolomitic clays, so called marl, specific features appear in the pottery. Calcium and magnesium have function as a flux, and, if the clay contains enough iron or iron oxide, it allows to form hematite in relative low temperature. If the temperature reached 900°C, other minerals *e.g.* gehlenite and diopside could form (Nodari et al. 2007; Noll, Heimann 2016; Trindade et al. 2009). In the case of extremely rich calcite and dolomitic clays from the Algarve, if temperature goes over 900°C, the ceramics shows a vitrified microstructure and potassium–calcium sulphates are created (Trindade et al. 2009).

#### 1.7. Workshops of amphorae, amphorae distribution, use and discard

Many archaeological sites are not yet found or have already been destroyed and will never be documented (Renfrew, Bahn 2012). Beside the lack of archaeological components from the Second Iron Age, in the Lower Guadalquivir region, four archaeological sites with ceramic workshops, as indicate by the kilns and other related structures were excavated. Based on these four sites, we might sum up that ceramic workshops of Turdetani-Punic culture within the region of the Lower Guadalquivir were located at strategic points, close to main distribution routes, urban centres and raw material sources. Three of them are in a district of Seville, here the high concentration of Turdetani-Punic sites does not only reflect the state of research, but also its importance as a settlement area in that time (Chic, García Vargas 2004; Mégias 2017).

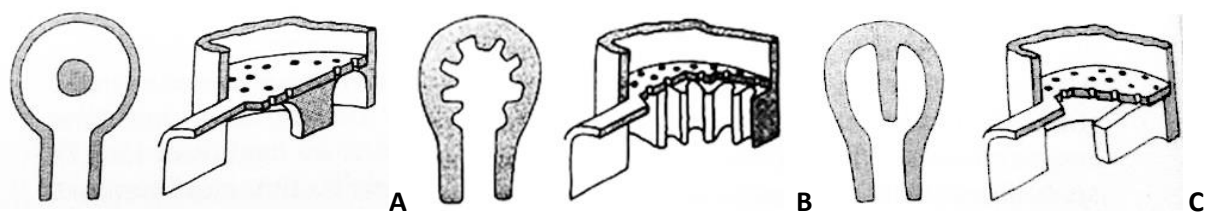


Fig. 1.10 – Support of the grate: A: Central pillar; B: Radial support; C: Axial support (after Cuomo di Caprio 2007).

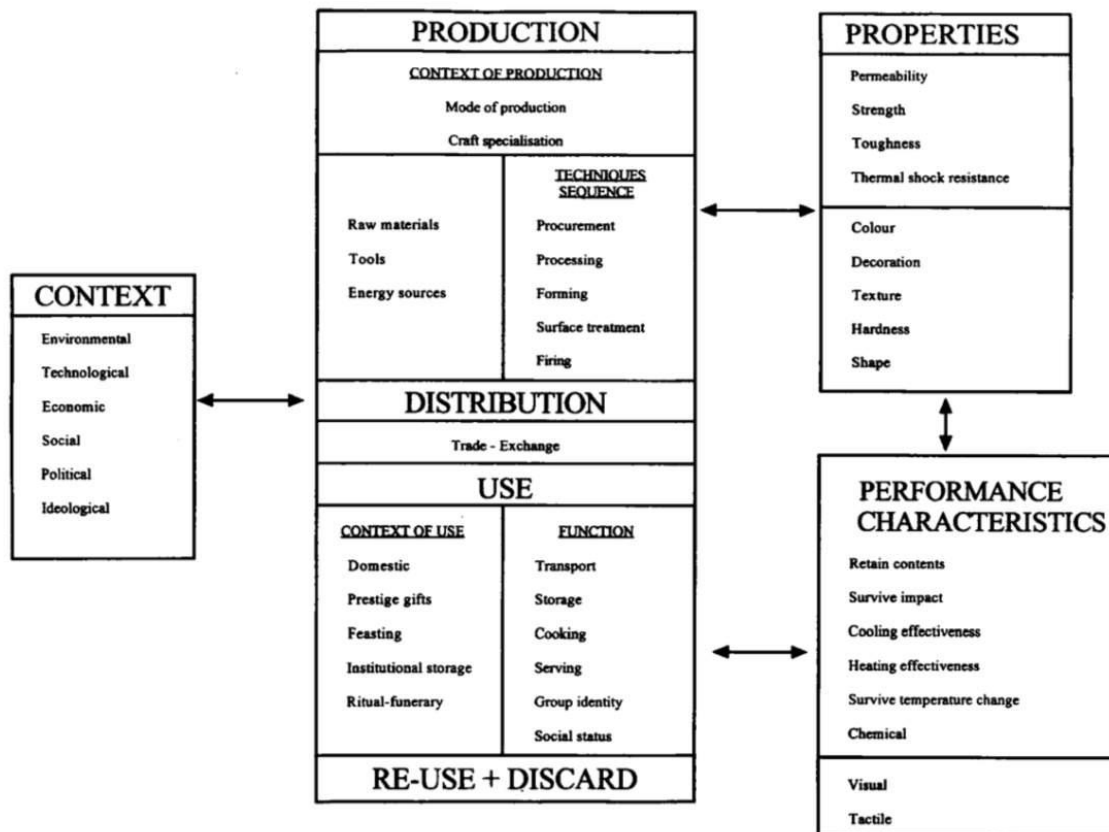


Fig. 1.11 – Technological choices, material properties and schema of ceramic life cycle (after Sillar, Tite 2000).

The potter's wheel and the vertical ceramic kiln are the technological innovations, introduced with the colonialism that took place during the First Iron Age, and spread fully in the Second Iron Age (García Fernández, García Vargas 2012). A feature that differentiates these kilns that were discovered in the southwest of the Iberian Peninsula from the Second Iron Age is the supporting grate (Fig. 1.10; Cuomo di Caprio 2007). In all cases the structure is circular, and the kiln is divided into two compartments by a grate made with clay. The above one is used to firing the ceramic, below it can be found the combustion chamber dug onto the ground below the structure (Chic García, García Vargas 2004). The opening for the combustion chamber is also used to control the temperature and firing atmosphere during the firing process. The heat was transferred to the firing chamber through the holes in the grate, without risking having the vessels exposed directly to fire. The upper chamber, which stood at ground level, was made by mud bricks with openings for the smoke to come out. In these ceramic kilns it was possible to have a stable firing atmosphere and to reach relatively higher temperature (Mégias 2017). The process of pottery making in workshops consist of clay

treatment, fuel collection, modelling and firing of the vessels, construction and repair of the kilns, etc. As the complexity of found sites indicates, the Turdetani pottery was made in crafting centres. According to the parallels that we know about the colonial Punic world, potters were specialists and the production was centralized ([García Fernández, García Vargas 2012](#); [Mégias 2017](#)).

The Pellicer amphorae B/C and D were redistributed from the production centres to rural areas and used for in the transport of primary food products. The food goods were probably shipped from the fields to treatment structures or marketplace as raw materials. Many of the goods were processed as secondary food products (e. g. Garum), however, these treatment or shipping sites in and around the area of Seville had not yet been found. The amphorae could have been reused and were circulating in the trade network of the Lower Guadalquivir as common containers for transport of rural products or even secondary food products ([Garcia-Fernandez et al. 2017](#); [Mégias 2017](#)). However, the Pellicer amphorae B/C and D filled with food products were exported by commercial ships from the Lower Guadalquivir or the commercial hub in Cadiz (where ceramic workshops were also found) to the broader area (e.g. [Garcia-Fernandez 2019](#); [Sáez Romero 2018](#)). When the amphorae reached their destination, their content could have been redistributed, and the amphorae reused in a local scale there or even transported again. Ceramic objects as well as other artefacts after the time of usage in a living culture had been discarded and buried in the ground (**Fig. 1.11**). After the discard of the artefacts, depositional and post-depositional processes took place. These processes vary according to the local environment ([Freestone 2001](#)).

## 2. Analytical techniques

### 2.1. Petrography of thin sections

Petrography of ceramics provides us basic information about the mineralogy and changes occurring in ceramic artefacts during long-term deposition in anthropogenic layers. Ceramic petrography is an analytical method based on optical mineralogy. It uses knowledge of optical properties minerals and rocks which can be identified by a petrographic (polarized light) microscope (Quinn 2013; Barker 2014).

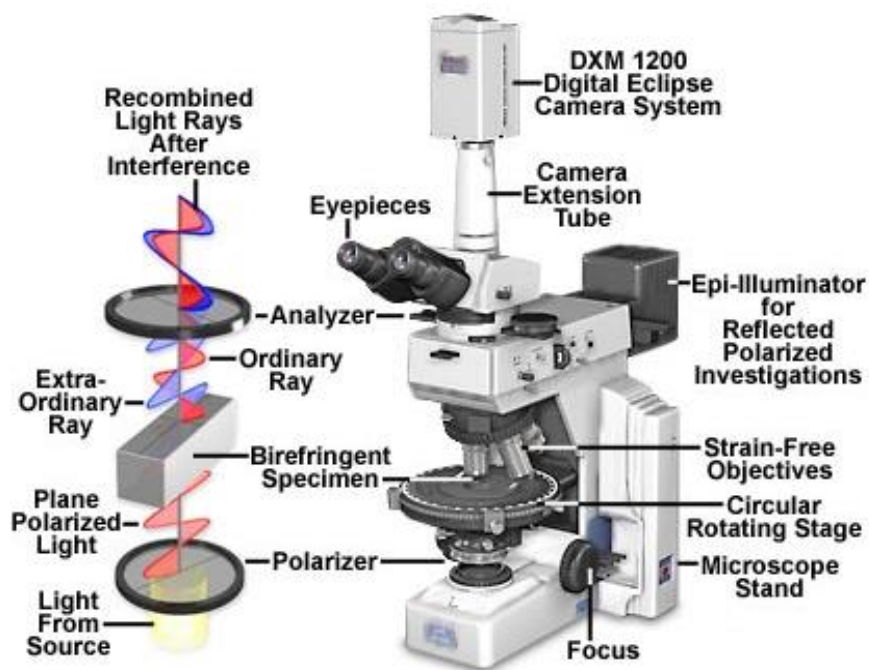


Fig. 2.1 – Petrographic (polarized light) microscope configuration<sup>4</sup>.

The petrographic polarizing microscope allows us to study the sample in transmitted, reflected or combined light. To understand the optical properties of minerals it is necessary to know the basic facts about the symmetry of crystals and the properties of light. In the transmitted light of the microscope, the study is commonly performed on thin sections about 30  $\mu\text{m}$  thick. Cleavage, relief (as a result of refractive index), shape and structure, colour and

<sup>4</sup> <http://soft-matter.seas.harvard.edu/images/9/91/FINALRLK1.jpg> (31.8.2019).

pleochroism are monitored in linear polarized light (PPL). Birefringence and other properties are studied in XPL/CPL – cross polarized light (**Fig. 2.1**; [Barker 2014](#); [Hložek 2012](#)).

In thin sections of ceramic artefacts, fragments of rocks and minerals in the temper can be identified, but also fragments from older ceramics (grog), bones, shells, fossils, etc. The size, shape and spatial orientation of the temper (and pores) are observed as well. From mineral fragments and rocks, we can deduce the degree of thermal transformation, changes in colour and optical properties, enamel formation, etc. Secondary mineralization and changes often reflect the effects of several thousand years in the anthropogenic layers and moving of groundwater. Based on changes of physical and optical properties of selected minerals, firing temperature can be determined as well as it is atmosphere (oxidative, reducing) or multiple lines responsible for an unstable condition. Using the petrographic microscope, we can objectively classify the microstructures of ceramics and characterize the binder. A detailed observation of pottery wares allows us to cluster the samples and recognize fabric and their provenance ([Quinn 2013](#); [Hložek 2012](#)).

## 2.2. X-ray fluorescence (XRF)

X-ray fluorescence (XRF) is the most widely used method of atomic spectroscopy, and it is broadly used for the analysis of solid samples. A great advantage of XRF is the multi-elemental analysis of samples. The XRF technique has been widely used for provenance and technological studies of archaeological ceramics. The analysis can be performed non-destructively, commonly by portable equipment or in the form of powder in pressed-pellets or fused beads by a benchtop instrument ([Artioli 2010](#); [Beckhoff et al. 2006](#)).

The principle of the method is the ionization of the sample atoms by primary X-ray radiation. X-ray spectrometry involves the following processes: generation of primary radiation in the anode of the X-ray tube, transfer of primary radiation to the sample, interaction of the radiation with the sample, secondary X-ray emission from the sample, and its measurement by the detector. In the analysed sample, electrons are ejected from the inner shells of atoms (K, L, M, N) and electrons from higher levels jump to the vacant spots of these released electrons. The energy of the fluorescent X-ray radiation corresponds to the difference of the energies of the two shells (**Fig. 2.2**). Secondary X-ray is emitted and is characteristic of a specific

element. The intensity is proportional to the amount of the element in the sample (Artioli 2010; Beckhoff et al. 2006; Pollard et al. 2007).

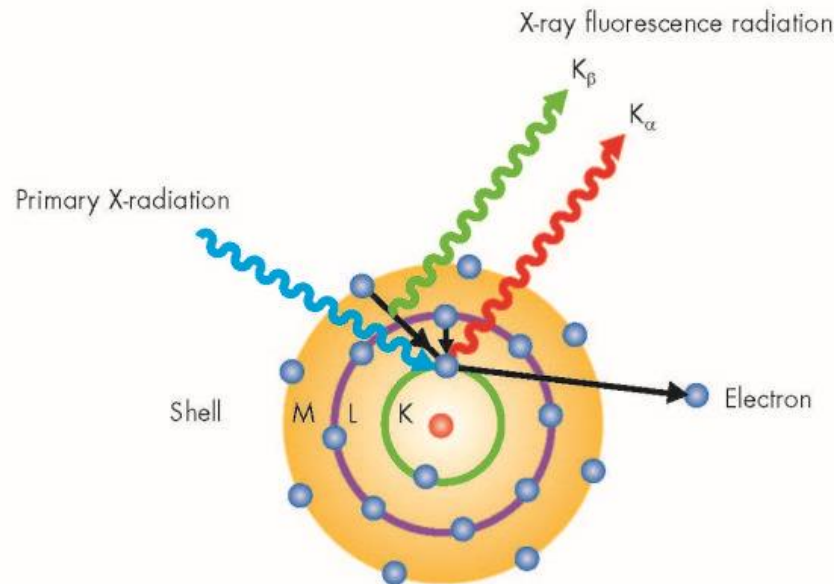
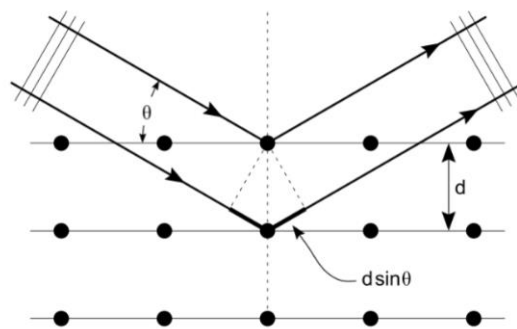


Fig. 2.2 – Principle of X ray fluorescence spectroscopy <sup>5</sup>.

### 2.3. X-ray diffraction (XRD)

X-ray diffraction (XRD) is a very powerful technique for identifying the arrangement of atoms in solid samples. It is a widely applied method for the study of ceramic artefacts. It is possible to work in micro or macro mode, while micro mode allows us to analyse small spots in the samples. For formalized analysis of ceramic body phase composition, samples should be ground into a fine powder (about 1 g of sample is needed). The study of mineral phases by XRD is fundamental for the understanding of thermal transformations occurring during the firing of ceramic. The mineralogical phases also allow identifying the origin of the raw materials used for the manufacture of ceramics. Using this method can be estimated qualitative, and semi-quantitative or quantitative phase composition of the ceramic body commonly after the Rietveld method (Artioli 2010; Stuart 2007).

<sup>5</sup> (<https://xrf-spectroscopy.com/> (25.8.2019)).

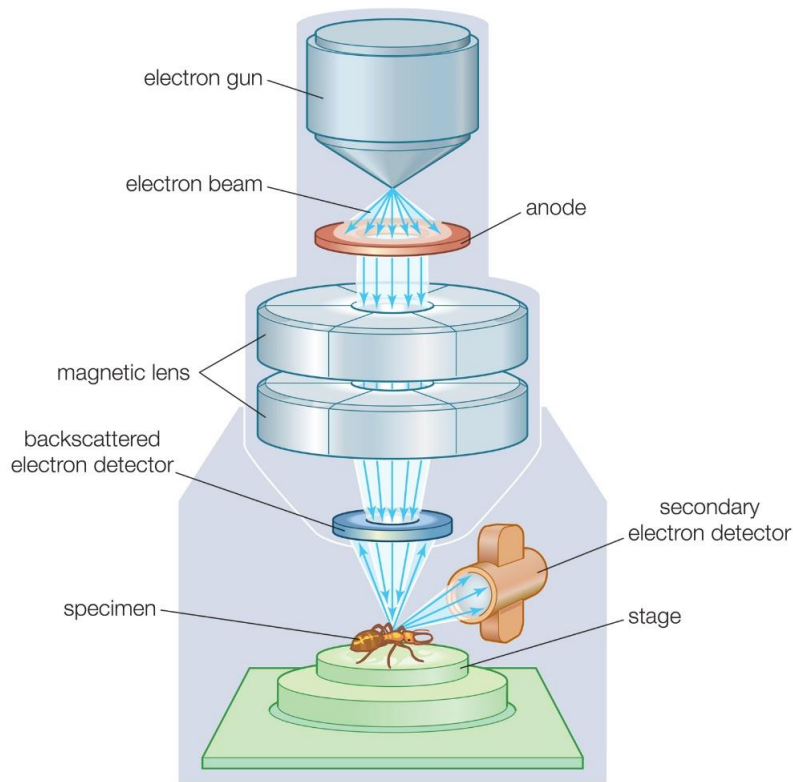


**Fig. 2.3** – Reflection of an X-ray beam by the planes of a crystal with interplanar spacing (after [Bannert 2017](#)).

The geometrical conditions for X-ray diffraction depend on the difference path taken by the monochromatic X-rays in crystal planes with the same orientation. This condition is expressed by Bragg's Law ( $n\lambda = 2d \sin\theta$ ), where  $\lambda$  corresponds to the wavelength of the incident radiation, “n” represents the diffraction order, “d” corresponds to the interplanar distance for the set of planes of the crystal structure and  $\theta$  to the X-ray incidence angle – measured between the incident beam and the crystalline planes (**Fig. 2.3**). ([Bannert 2017](#); [Pollard et al. 2007](#); [Stuart 2007](#)).

#### 2.4. Electron microscopy (SEM-EDS)

The scanning electron microscope (SEM) has been used in a broad scale for analysis of samples related with Cultural Heritage and in plenty of studies about archaeological ceramics. SEM provides detailed images at a magnification range up to 100,000 times, and it is commonly associated with the X-ray Dispersive Spectroscopy (EDS) technique, which allows a quantitative point or area analysis of the chemical elements on the surface of the samples (**Fig. 2.4**). SEM analysis is based on the incidence of an accelerated electron beam on the sample surface and the subsequent collection of the electronic signals emitted by it. The sample's surface is scanned sequentially by the electron beam. A respective image of the scanning is plotted as a raster image. The brightness of each point is determined by the intensity of the surface radiation emitted. Higher atomic number elements (heavy elements) backscatter electrons stronger than lower atomic number elements ([Stuart 2007](#); [Artioli 2010](#)).



© 2012 Encyclopædia Britannica, Inc.

**Fig. 2.4** – Scanning electron microscope<sup>6</sup>.

Samples analysed by electron microscopy must have certain characteristics: surface electrical conductivity; withstand the vacuum; and being physically and chemically stable under the conditions of observation – interaction with the electromagnetic beam. When the samples do not have electrical conductivity, they should either be metallized by applying an ultra-thin gold or carbon coating, or the SEM should be performed on a variable pressure mode. If the sample is small, it can be used non-destructively, however, there can be a problem with a morphology of the sample. To get representative structural information, common is analysis of samples in cross sections or thin sections which are also flat (Pollard et al. 2007).

The interaction of the electron beam with the sample results in the emission of radiation and electrons, including secondary electrons (SE) used in the formulation of the sample image. Secondary electrons are electrons in the sample that excite and “escape” from the surface.

<sup>6</sup> <https://163602-560839-raikfcquaxqncofqfm.stackpathdns.com/wp-content/uploads/2018/10/The-scanning-electron-microscope-SEM.jpg> (25.8.2019).

Observation of images obtained through SE detection has strong topographic contrast. Retrodifused electrons, whose intensity is increasing with the atomic number (chemical composition of the sample), are electrons that hit the surface of the sample with high energy and are dispersed.

The interaction of the electron beam results in the emission of X-rays, which are used to identify the elements present in a “point” or a large “area” of the sample surface by EDS. The elements are identified by database in the computer system associated with the spectrometer. The results are plotted in a spectra, tables or elementary mapping distribution with only qualitative analysis (Pollard et al. 2007).

## 2.5. Organic content analysis (GC-MS)

Chromatography is based on the separation of compounds using two immiscible phases - mobile (eluent) and immobile (stationary). Considering the mobile, chromatography can be divided into a liquid and gas chromatography. The gas chromatography coupled with mass spectrometer (GC-MS) has been widely used for the separation, identification and quantification of organic residues preserved in archaeological ceramics (Fig. 2.5; Dune et al. 2018; Roffer-Salque et al. 2017). The ceramic material is porous and can retain the chemical signature of the organic material stored inside it. Among the classes of organic compounds preserved in archaeological materials, lipids are prominent. The presence of lipids, particularly saturated compounds, is due to their resistance to degradation by chemical and microbial processes. Saturated carbon chains give them a hydrophobic character. According to patterns of saturated molecules or biomarkers, distinct matter can be identified. The study of archaeological organic residues is hampered by the frequent complexity of the recovered extracts (Barnard, Eerkens 2017; Evershed 2008).

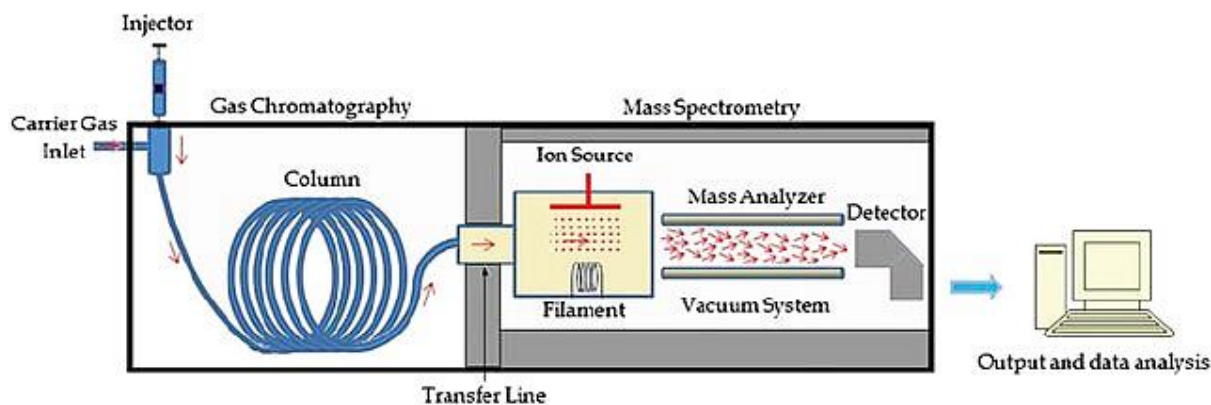


Fig. 2.5 – Schematic plot of the main components of standard GC–MS instruments (Emwas et al. 2015, Fig. 1).

Before a possible organic residue of ceramic is analysed, it must be extracted from the ceramic material. The conventional extraction method uses a mixture of solvents ( $\text{CHCl}_3$  / MeOH, 2:1 v/v) added to a test tube with grounded ceramic powder. The lipid classes that are usually recovered using this method include fatty acids, acyl glycerols, long chain ketones, wax esters, n-alkanols and n-alkanes, which are derived from animal fats and/or oils, vegetables and waxes. For specific questions and samples can be used other organic solvent (Evershed, 2008).

Samples analysed by GC-MS must be also sufficiently volatile and thermally stable. Gas chromatography is applied for the separation and identification of all components which can be converted into the gas phase without decomposition. Thermolabile compounds can only be analysed after their chemical derivatization. In general, derivatization reactions have the advantage of increasing volatility and stability of the compounds. One of the most frequent reaction is silylation. The mechanism involves the replacement of active hydrogen atoms (in -OH, -COOH, -NH, -NH<sub>2</sub>, -SH) by a trimethylsilyl group (TMS). The most versatile and common derivatizing reagent is N,O-Bis- (trimethylsilyl) trifluoroacetamide with 1% trimethylchlorosilane (BSTFA-TMCS), which produces trimethylsilyl ether derivatives, allowing this reagent to derivatize a wide range of polar organic compounds. Reaction products are more volatile and thermally stable than the original compounds (Moldoveanu, David 2018).

After the extraction and derivatization, the sample is injected into the GC equipment. The injection can be in the split (if the sample is very concentrated) or splitless mode. Then the sample is vaporized and dragged onto a chromatographic column with the aid of a gas. The

carrier gas must be inert and pure as it must not react with the sample, stationary phase or instrument. The flow of this gas (mobile phase) passes through the chromatographic column, which separates the substances based on their lower or higher affinity with the stationary phase. The capillary columns are nowadays widely used: they are efficient due to their small diameter, quite large length, and requirement of a small amount of sample. There is wide range of columns with different polarity ([Rahman 2015](#)). Apart from the polarity of the column, a temperature program is an essential factor in the separation of the compounds. Increasing column temperature results in decreased retention times which may lead to the loss of resolution. Therefore, a heating ramp is used to shorten the analysis time of complex samples and improve the chromatographic separation ([Pollard et al. 2007](#)).

As the compounds elute from the column, they are detected on the mass spectrometer (MS), which count them according to the mass/charge ratio ( $m/z$ ). The mass spectrometer consists of an ionization source, analyser and detector in a vacuum system connected to a data processing system. Among the various types of MS, the quadrupole is the most common mass analyser. Regarding ionization sources, the most used is electron ionization (EI). In ionisation source, gas phase with sample is bombarded by high-energy electrons. This leads to the production of a cation molecular ion (represented by mass  $M^+$ ). In a mass spectrum, the resulting signal of each ion is observed. This information is used to identify compounds of interest and to elucidate the structure of components of unknown mixtures. EI is suitable for volatile, low molar mass and thermostable compounds ([Hoffmann, Stroobant 2007](#)).

### 3. Materials and methods

For the purpose of study, 30 ceramic shards were elected (20 bottoms and 10 rims). The shards were previously processed by archaeologists and labelled by a varnish sticker. The samples of bottoms contain: 14 bottoms of Pellicer B/C amphorae – type I, 2 bottoms of amphorae without a distinctive protrusion – type II, and 4 local common wares with probable local provenance – type III. All 10 rims are defined as the Pellicer D amphorae - type IV.<sup>7</sup> The bottoms of amphorae are possible to divide after the oval protrusion (**Fig. 3.1**). The samples of bottoms are mainly dated from the second half of 5<sup>th</sup> century BC to the beginning of 4<sup>th</sup> century. The rims of Pellicer D are mostly associated with the second half of 1<sup>st</sup> century BC (**Table 1**). Commonly, the shards have on the surface, red areas related with the oxidation of iron in the ground. One shard of the bottom of Pellicer B/C amphora (13167) has 3 holes in the sides as probable reminiscence of the vessel repairing ([South 1968](#); **Annex I**).

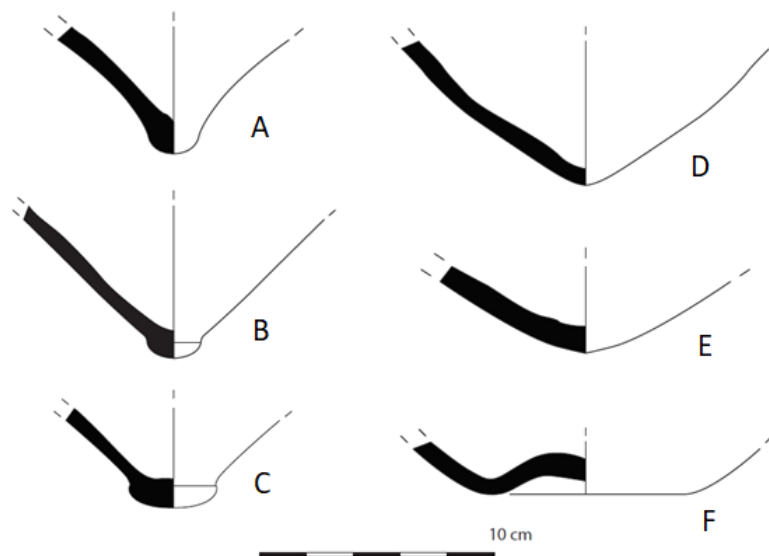


**Fig. 3.1** – **A:** Pellicer B/C amphora with the smaller, pointed protrusion and concave wall (sample 4, 12356); **B:** Pellicer B/C amphora with the smaller oval protrusion (sample 10, 12655), **C:** Pellicer B/C amphorae with the bigger and oval protrusion (sample 12, 3698), **D:**The bottom similar to Pellicer B/C amphora without significant protrusion (sample 15, 12658), **E:** The bottom similar to MPA4 amphora with probable Cadiz origin (sample 16, 11078), **F:** The concave bottom of probable local common ware (sample 19, 12047).

<sup>7</sup> The information about typology and probable provenance provided prof. A. M. Arruda and Dr. E. de Sousa.

**Table 1** – List of samples with primary information about ceramic typology, dating and shard characteristic; additional information is referenced in the **Annex I**.

Sample number	General type of vessel	Type notation	Probable provenance	Contextual dating	Outside colour	Inside colour	Fragment size	Part of the vessel	Shape (Fig. 3.1)
1	Pellicer B/C amphora	I	Guadalquivir	?	beige	red	medium	bottom	A
2	Pellicer B/C amphora	I	Guadalquivir	5 <sup>th</sup> -4 <sup>th</sup> c. BC	beige	orange	big	bottom	A
3	Pellicer B/C amphora	I	Guadalquivir	2 <sup>nd</sup> half of 5 <sup>th</sup> c. BC	pale yellow	orange	small	bottom	A
4	Pellicer B/C amphora	I	Guadalquivir	2 <sup>nd</sup> half of 5 <sup>th</sup> c. BC	pale yellow	pale pink, orange	big	bottom	A
5	Pellicer B/C amphora	I	Guadalquivir	2 <sup>nd</sup> half, 5 <sup>th</sup> c. BC	pinkish beige	orange	small	bottom	A
6	Pellicer B/C amphora	I	Guadalquivir	2 <sup>nd</sup> half, 5 <sup>th</sup> c. BC	greyish beige	greyish beige	small	bottom	B
7	Pellicer B/C amphora	I	Guadalquivir	?	beige	orange	medium	bottom	B
8	Pellicer B/C amphora	I	Guadalquivir	?	pale yellow	pinkish orange	small	bottom	B
9	Pellicer B/C amphora	I	G. - Queimada	2 <sup>nd</sup> half of 5 <sup>th</sup> c. BC	orange, grey	greyish beige	small	bottom	B
10	Pellicer B/C amphora	I	Guadalquivir	2 <sup>nd</sup> half of 5 <sup>th</sup> c. BC	pale yellow	pale pink, orange	medium	bottom	B
11	Pellicer B/C amphora	I	G. - Gatada	1 <sup>st</sup> half of 5 <sup>th</sup> c. BC	pale yellow	pale orange	medium	bottom	B
12	Pellicer B/C amphora	I	Guadalquivir	2 <sup>nd</sup> half, 5 <sup>th</sup> c. BC	beige	pale pink	small	bottom	C
13	Pellicer B/C amphora	I	Guadalquivir	4 <sup>th</sup> c. BC	beige	orange	big	bottom	C
14	Pellicer B/C amphora	I	Guadalquivir	5 <sup>th</sup> -4 <sup>th</sup> c. BC	beige	beige-orange	small	bottom	C
15	Amphora without protrusion	II	Guadalquivir	2 <sup>nd</sup> half of 5 <sup>th</sup> c. BC	brownish beige	pinkish orange	medium	bottom	D
16	Amphora without protrusion	II	Cadiz	5 <sup>th</sup> -4 <sup>th</sup> c. BC	pale orange, olive brown	olive grey	medium	bottom	E
17	local common ware	III	Castro Marim	5 <sup>th</sup> -4 <sup>th</sup> c. BC	pale pink	pale pink	medium	bottom	F
18	local common ware	III	Castro Marim	4 <sup>th</sup> c. BC	orange	brownish red	big	bottom	F
19	local common ware	III	Castro Marim	5 <sup>th</sup> -4 <sup>th</sup> c. BC	reddish orange	reddish orange	big	bottom	F
20	local common ware	III	Castro Marim	5 <sup>th</sup> -4 <sup>th</sup> c. BC	pale pink	pale pink	big	bottom	F
21	Pellicer D amphora	IV	Cadiz area	1 <sup>st</sup> c. BC	pale yellow	pale yellow	big	rim	
22	Pellicer D amphora	IV	Guadalquivir	1 <sup>st</sup> c. BC	orange	orange	medium	rim	
23	Pellicer D amphora	IV	Cadiz area	1 <sup>st</sup> c. BC	pale yellow	pale yellow	medium	rim	
24	Pellicer D amphora	IV	Guadalquivir	1 <sup>st</sup> c. BC	pale yellow	pale yellow	big	rim	
25	Pellicer D amphora	IV	Cadiz area	1 <sup>st</sup> c. BC	pale yellow	pale yellow	medium	rim	
26	Pellicer D amphora	IV	Cadiz area	1 <sup>st</sup> c. BC	pale yellow	pale yellow	medium	rim	
27	Pellicer D amphora	IV	Cadiz area	1 <sup>st</sup> c. BC	pale yellow	pale yellow	medium	rim	
28	Pellicer D amphora	IV	Cadiz area	1 <sup>st</sup> c. BC	pale yellow	pale yellow	medium	rim	
29	Pellicer D amphora	IV	Guadalquivir	?	pale orange	pale yellow	medium	rim	
30	Pellicer D amphora	IV	Cadiz	1 <sup>st</sup> c. BC	red	red	small	rim	

Before any additional work, the samples of shards were documented with a scale by a digital camera (Nikon D3100 equipped with 18-55mm objective) placed at a stand desk. Information from the label at the surface of shards are written in the catalogue of samples (**Annex I**).

The ceramic itself has specific nature according to the used raw material, manufacturing process and firing. For identifying provenance and understanding the ancient technology, the proper description and scientific analysis is necessary. For formalized characterization of ceramic material, multianalytical protocol containing petrography of thin-sections, X-ray fluorescence (ED-XRF), powder X-ray diffraction (powder XRD) and scanning electron microscope coupled with X-ray Dispersive Spectroscopy (SEM-EDS) was implemented.

To discover possible past content of ceramic, gas chromatography coupled with mass spectrometer (GC-MS) was carried out to the selected bottoms after the provenance.

### 3.1. Petrography

To complete each thin section, a piece of shard from the sample was cut along ceramic body to have representative section and fine size for a standard glass slide (7x5 cm) by a saw (Discoplan TS Struers). Then the samples were washed and dried. The cut pieces were embedded in an epoxy resin (Epofix Fix, Struers A/S, Ballerup, Denmark; resin / hardener; 7:1) and kept 24 hours to get hard. The shards in resin were polished by sandpapers from bigger grain size to fine one (Struers, SiC, FEPA P # 320, 500, 800, 1200, 2000 and 4000). Cleaned and dried cross sections were glued on the pre-polished glass slide (standard thickness 1,161 mm) with Araldite (1:1) and hardening few hours pressed at a hot plate. After 24 hours the cross sections were cut from the glass slide by the saw. The glass slides were ground smoothly by the saw until they were approximately 1,3 mm thick. Next, thin sections were polished by a silicon carbide grid powder (< 5 µm) and water until they reached a fine thickness about 30 µm of sample at the glass slide. The fine thickness was checked by the petrographic microscope. Quartz was used as thickness standard, respectively its first-order interference grey-white colour under cross polarized light. The final thin sections were not covered by a permanent glass for a possibility to do SEM-EDS analysis.

The petrographic analysis of thin sections was performed in all 30 samples using a Leica DM2500P polarized microscope. The images were captured with a Leica MC 170HD digital camera attachment to the equipment (Leica microsystems, Wetzlar, Germany). The thin sections and rock minerals or other intrusions were described and identified after the standard keys (Quinn 2013; Barker 2014). The cross sections were documented as well by a stereomicroscope (Leica DFC 295) to have representative images in smaller magnification.

### 3.2. ED-XRF

For purpose of XRD and XRF analysis, the parts of shards were cut and each one was completely cleaned by a Dremel multitool (DREMEL® 3000) with a diamond wheel point 4,4mm (7105) to avoid a contamination. Then, the samples were ground to the fine powder in the agate mortar by pestle. The grinding tools were always carefully washed and dried.

For ED-XRF analysis, beads were made in a Claisse Fluxer® LeNeo™ fusion instrument. A 1,2g of powdered sample was mixed with 12 g of lithium iodide in a crucible and fused in 1065°C. After the fusion, the instrument cast a fluid into a mould for the bead.

Since the calibration of XRF data require the exact value of total loss of ignition (LOI), a slightly modified standard protocol with porcelain crucibles was applied (Heiri, Lotter, Lemcke 2001). The crucibles with scrapped reference were firstly calcinated in a furnace. When the temperature reached 1065 °C, the crucibles were 90 minutes heated. After that, they were directly placed to a desiccator with a silica gel and closed. When the crucibles cooled down in the desiccator, they were weighted and 0,5g of sample powder was placed inside. After, all crucibles with samples were again heated to 1065°C for 90 minutes, placed to the desiccator, cooled and weighted. The loss of weight was calculated after the initial weight of crucible, sample and final weight of the calcinated crucible with the sample.

The chemical compositions of the ceramic materials were determined in a Bruker S2 Puma energy dispersive XRF (ED-XRF). Spectrometer is equipped with a silver anode X-ray tube. All 30 samples were analysed as the glass disks. The quantitative data were obtained after careful calibration using siliceous commercial standard beads. The results were evaluated in bi-axial

and ternary plots and by Principal component analysis (PCA) in software PAST-3.<sup>8</sup> The values of main oxides (except P<sub>2</sub>O<sub>5</sub> and SO<sub>3</sub>) were transformed into logarithmic scale (function – log; **Appendix III**) and multivariate by PCA ([Carlson 2017](#)).

### 3.3. Powder XRD

To get mineral composition of samples powdered bulk samples, approximately 1g of sample was analysed by a Bruker D8 Discover X-Ray Diffractometer with Cu K $\alpha$  source at 40 kV and 40 mA. The analysis was done for all 30 samples. The patterns were collected at a 2 $\theta$  angular range of 3°-75°, with 0,05° step size and 1s measuring time by a point. The LYNXEYE linear detector provides an increased signal. Identification of minerals was performed using the DIFFRAC.SUITE EVA software and the ICDD PDF-2 database. The semi-quantitative determination of the mineral abundance in the bulk samples was obtained by the Reference Intensity Ratio (RIR) method (the reference standard was corundum). The intensities of distinct peaks were compared between the samples as well.

### 3.4. SEM-EDS

SEM-EDS analysis of 12 elected thin sections was performed with a HITACHI S-3700N SEM interfaced with a Quanta EDS microanalysis system to identify chemical composition of specific intrusions. The microanalysis system was equipped with a Bruker XFlash 5010 Silicon Drift Detector (SDD) with a resolution of 129 eV at Mn Ka and the EDS chemical data were acquired in the form of elemental distribution maps processes with Bruker ESPRIT 1.9 software. The EDS quantitative analysis was carried out by point micro-analyses. The EDS analysis were done in BSEM mode by accelerating voltage of 20 kV, 10 mm working distance, 120  $\mu$ A emission current, and chamber pressure of 40 Pa. The detection limits for major elements (N<sub>Na</sub>) were in the order of 0.1 weight % (after [Schiavon et al. 2015](#)). The SEM images were captured in backscattering (BSE) and secondary electron (SE) modes.

---

<sup>8</sup> <https://folk.uio.no/ohammer/past/> (25.8.2019).

### 3.5. GC-MS

The powder for GC-MS analysis was prepared later separately, strictly with cleaned plastic gloves. Eight samples of the ceramic bottoms 3, 6, 8, 9, 10, 15, 17, 20 were selected for analysis after the provenance results. A piece of ceramic was cut from the shard and, after being carefully cleaned by a Dremel multitool (DREMEL® 3000) with a diamond wheel point 4,4mm (7105), it was ground to powder in an agate mortar. The preparation tools used to clean and ground the samples were always carefully washed with a mixture of organic solvents ( $\text{CHCl}_3$  / MeOH, 2:1 v/v) and dried between samples to avoid cross-contamination.

First, the glassware used for the standard sample preparation was brushed and washed with acetone and water. After, the glassware was immersed in a solution of Decon 90 (1:9 v/v) and allowed to stand overnight. Subsequently it was washed with tap water and Milli-Q® water. The material was wrapped into aluminium foil, and with sheets of aluminium foil were placed in the furnace for 12 hours at 600 °C to get completely cleaned from organic matter.

The extraction of organic compounds was performed by following protocol: To a test tube with 2 g of ceramic powder was added 20  $\mu\text{L}$  of n-tetratriacontane (1mg/mL). Then 10 ml of a previously prepared  $\text{CHCl}_3$ /MeOH solution (2:1, v/v) was added to the test tube, and they were capped with the cleaned aluminium foil, and placed in the ultrasonic bath for 15 minutes. After ultrasonification, the test tubes were centrifuged for 15 minutes at 2500 rpm. Subsequently, the supernatant was removed with a Pasteur pipette into a cleaned flask. Except the addition of n-tetratriacontane, the previous procedure was repeated with the remaining solid in the centrifuged tubes. The combined extracts in the flasks were dried under nitrogen ( $\text{N}_2$ ) stream using hot sand (ca 40°C) as a bath. To obtain the total lipid extract, the dried extract was re-dissolved with 250  $\mu\text{L}$   $\text{CHCl}_3$ /MeOH (2:1, v/v). Then 100  $\mu\text{L}$  of this extract were put into a GC vial and dried under  $\text{N}_2$  stream. The sample was re-dissolved with 50  $\mu\text{L}$  of hexane and then derivatized with 50  $\mu\text{L}$  N,O-Bis-(trimethylsilyl)trifluoroacetamide with 1% trimethylchlorosilane (BSTFA-TMCS) in the microwave (700 W) for 30 seconds. In order to evaporate excess of BSTFA-TMCS, the extract was dried under  $\text{N}_2$  stream. For GC-MS analysis is necessary to dissolve the extract with 50  $\mu\text{L}$  hexane and transfer it to a glass insert vial (adapted after [Mukherjee, Gibson, Evershed 2008](#)).

For the analysis by GC/MS, a system consisting of a Shimadzu GC2010 gas chromatographer coupled to a Shimadzu GCMS-QP2010 Ultra mass spectrometer was used. A capillary column Phenomenex Zebron-ZB-5HT (15 m length, 0,25 mm internal diameter, 0,10  $\mu\text{m}$  film thickness) was used for separation, with helium as carrier gas. A column flow of 1,48 mL/min was maintained throughout the analysis. The injector was operated in the splitless mode at a temperature of 250 °C. GC temperature program was as follows: 50 °C during 2 min, ramp until 300 °C at 10 °C/min with a holding time of 5 min., and then another ramp until 400 °C at 10 °C/min, followed by an isothermal period of 5 min. In MS, a source temperature was placed at 240 °C, and the interface temperature was maintained at 280 °C. The mass spectrometer was programmed to acquire data between 40 and 850 m/z.

## 4. Results

### 4.1. Petrography

The petrographic results, based on the observation of the fabric, allowed us to sort out the samples into 3 main fabric groups A, B, C. Some samples (6, 9, 16, 22, 30) are differentiated after distinct features (A2, A3, A4, A5, C2), such as colour and temper specifics (**Fig. 4.1; Table 2, 3**). In general, the temper includes a wide range of rocks and minerals, but the size and the roundness vary. In some samples elongated particles are distinctly oriented after the ceramic body. In the thin sections, a secondary precipitation of calcium carbonates is commonly registered. The petrographic groups in general reflect the ceramic typology<sup>9</sup>.

The group A contain nineteen samples and mainly is related with Pellicer B/C type, however, 3 samples (22, 23 and 29) of Pellicer D present similar characteristics and two sample of amphorae without protrusion (15, 16), especially considering the fabric. The colour in section is commonly bright brown, orange or brown, except 3 samples with dark grey colour (6, 9, 16). Predominantly is isotropic, but anisotropic fabric in 6 samples (1-4, 7, 13) are presented as well. The temper is usually bimodal with the temper size about 0,2 and 0,5 cm and the temper ratio about 10%. Samples 6 (A4), 9 (A3) and 16 (A2) have in the matrix grey colour. The A2 contains fossils and limestone. The A3 has many black slates and fragment of shell. For the A4 is typical with big rounded temper containing quartz and limestone. Sample 22 (A5) has red homogenous colour of matrix and in the temper many shells (**Fig. 4.2**). The temper of fabric group A contains mainly grains of quartz, iron oxide and fragments of low-grade metamorphic rocks (e.g. slate, quartzite), sedimentary rocks, biotite, mica, feldspar and amphibole. The grains are usually subangular or poorly rounded and various voids are commonly presented (**Table 2, 3, Annex I**).

The fabric group B is represented only with the rims of amphorae of Pellicer D and it contains 6 samples (21, 23, 25-28). The colour is, except sample 26, homogenous in beige-green colour and typical is vitrification. The temper is well sorted sand with a size of about 0,2 mm, however, sporadically the iron oxide is presented as bigger intrusions. The temper is in the

---

<sup>9</sup> Sample 1-14: bottoms of Pellicer B/C amphorae (I); sample 15, 16: bottoms of amphorae without significant protrusion (II); sample 17-20: concave bottoms of local common ware (III); sample 21-30: rims of Pellicer D amphorae (IV).

ratio about 15 % and contains primary quartz, but also iron oxides, biotite and feldspar. In the temper of this group sedimentary rocks, slate or amphibole were not identified (**Table 2, 3**).

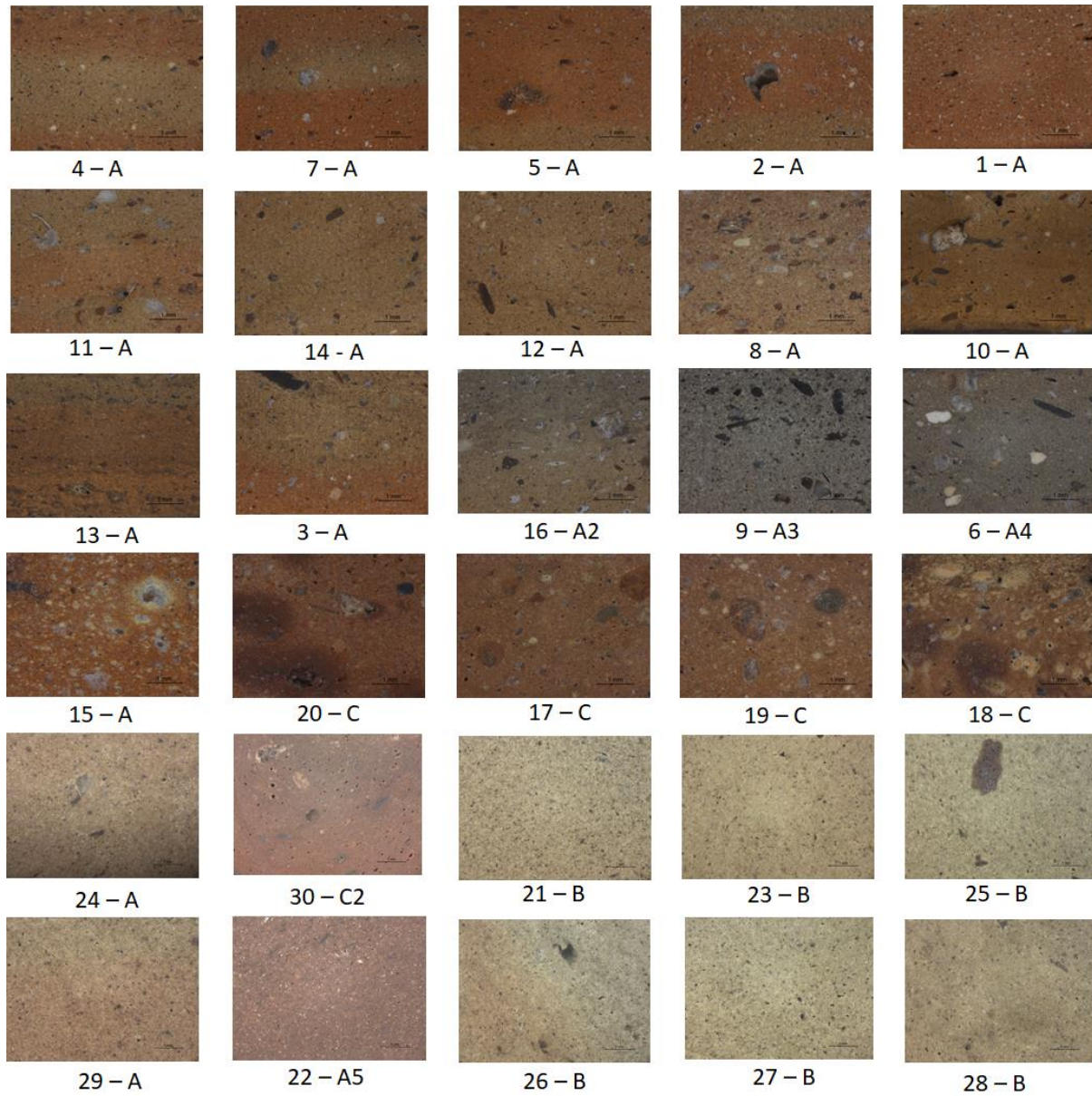


**Fig. 4.1** – Stereo-images of cross sections: number of sample and petrographic group represented by letter; more images and details about petrography is possible to see in the catalogue of samples (**Annex I**).

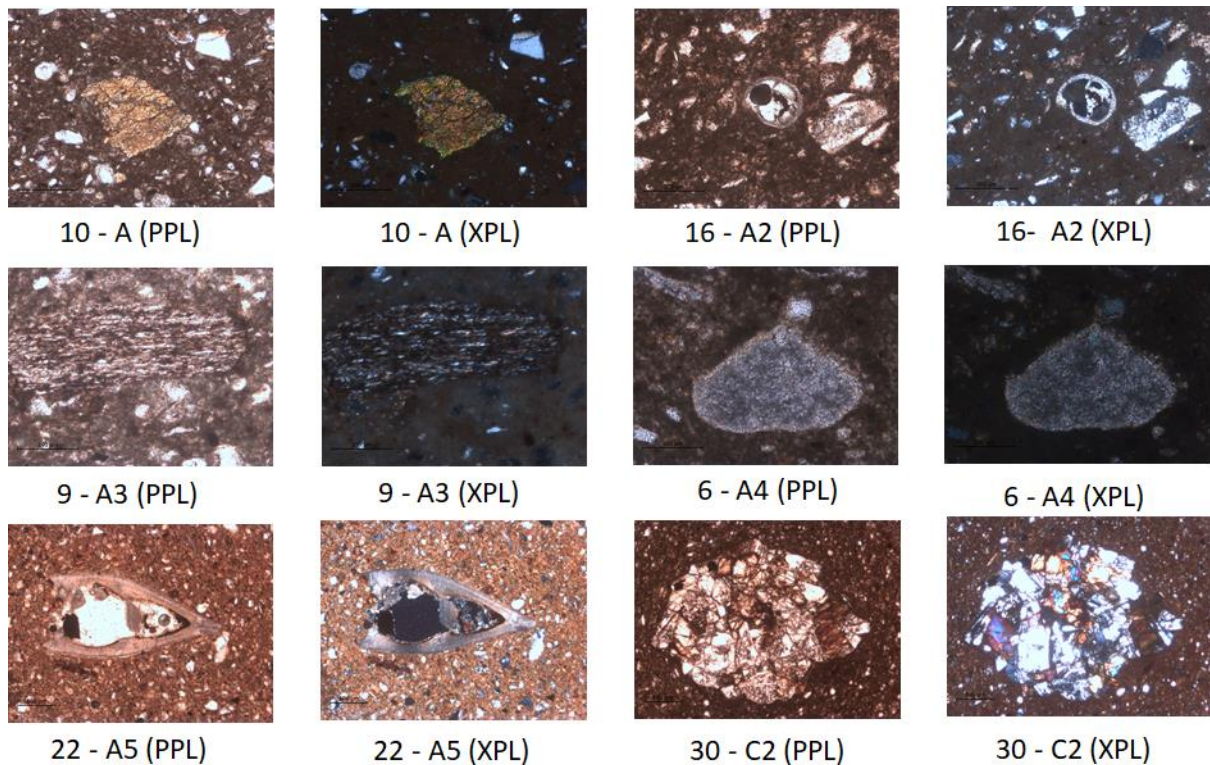


**Fig. 4.2** – Thin section image with significant intrusion in selected sample. 10 – A: amphibole, 16 – A: fossil, 9 – A3: slate, 6 – A4: limestone, 22 – A5: shell, 30 – C2: gabbro.

The group C contains 5 samples, 4 samples of the concave bottoms identified by archaeologists as local common wares (17-20) and one rim of Pellicer D (30 – C2) show similar features. The texture is mainly isotropic, in two cases anisotropic (18, 30). Dominant colour is orange brown but also red brown (15, 30) and red (20). The main feature that characterizes the C group is the bimodal matrix and the highest ratio of the temper (about 20%) and clay. The matrix contains smaller temper (0,2-0,5 mm) and big fractions of rocks inclusions (1-2 mm). The temper includes rounded quartz, iron oxide, and sometimes limestone, greywacke and amphibole. The temper of sub-grouped samples 30 (C2) – has smaller unimodal matrix (0,3-0,5 mm) with biotite and volcanic rocks as gabbro (**Fig. 4.2**) and amphibole.

**Table 2** – Standard description and characteristic of thin sections; Voids semi-quantity: (xxx) – abundant, (xx) – frequent, (x) – sporadic, (-) – no voids.

Sample number	Fabric group	Homogeneity of matrix	Colour of matrix	Temper/ clay %	Temper modality	Temper size mm	Temper sorting	Roundness	Sphericity	Voids (semi-quantity)
1	A	anisotropic	orange, brown	5	unimodal	0,1-0,2	well sorted	subangular	more equant	channels, vugs (xx)
2	A	anisotropic	red, orange, brown	10	bimodal	0,2	well sorted	subangular	half-half	vesicles (x)
3	A	anisotropic	orange, brown	15	bimodal	0,3, 0,5<	poorly sorted	poorly rounded	more equant	channels (xxx)
4	A	anisotropic	orange, brown	10	bimodal	0,2	well sorted	poorly rounded	more equant	channels (xx)
5	A	isotropic	orange	10	unimodal	0,2-0,3	moderately sorted	subangular	more equant	vesicles, vugs (xxx)
7	A	anisotropic	orange, brown	7	bimodal	0,2, 0,5	moderately sorted	subangular	more equant	vesicles (xx)
8	A	isotropic	brown	15	bimodal	0,2, 0,5	moderately sorted	poorly rounded	half-half	vesicles/channels (x)
10	A	isotropic	orange brown	10	bimodal	0,2, 0,5	well sorted	poorly rounded	more equant	channels (xxx)
11	A	isotropic	orange, brown	10	bimodal	0,2, 0,5	moderately sorted	subangular	more equant	channels (xx)
12	A	isotropic	brown	15	bimodal	0,2, 0,5	moderately sorted	poorly rounded	more equant	vesicles (xx)
13	A	anisotropic	orange, brown	7	bimodal	0,2, 0,5	well sorted	poorly rounded	more equant	vesicles (xx)
14	A	isotropic	orange brown	10	bimodal	0,2, 0,5	moderately sorted	poorly rounded	equant	vesicles (xx)
15	A	isotropic	red brown	15	unimodal	0,2-0,5	moderately sorted	poorly rounded	equant	mainly channels (xx)
24	A	anisotropic	orange, brown	10	unimodal	0,1-0,3	well sorted	poorly rounded	more equant	channels (xx)
29	A	anisotropic	orange, brown	10	unimodal	0,1-0,2	well sorted	poorly rounded	more equant	vesicles (xx)
16	A2	anisotropic	grey, brown	20	bimodal	0,2-0,5	moderately sorted	poorly rounded	elongate	channels (xx)
9	A3	isotropic	grey (redox)	15	bimodal	0,2, 0,5	well sorted	poorly rounded	more equant	almost no voids (-)
6	A4	isotropic	grey (redox)	20	bimodal	0,2-0,5, 1<	poorly sorted	rounded	more elongate	vesicles (x)
22	A5	isotropic	red brown	10	unimodal	0,1-0,2	well sorted	subangular	more equant	vesicles (xx)
21	B	isotropic	beige-green	15	unimodal	0,1-0,2	well sorted	subangular	more equant	vesicles (x)
23	B	isotropic	beige	5	unimodal	0,1-0,2	well sorted	poorly rounded	more equant	vesicles/channels (x)
25	B	isotropic	beige-green	15	unimodal	0,1-0,2	well sorted	subangular	more equant	channels (xx)
26	B	anisotropic	beige-green	15	unimodal	0,1-0,2	well sorted	poorly rounded	more equant	vesicles (xx)
27	B	isotropic	beige-green	20	unimodal	0,1-0,2	well sorted	poorly rounded	more equant	vesicles (x)
28	B	isotropic	beige	15	unimodal	0,1-0,2	well sorted	poorly rounded	equant	vesicles (x)
17	C	isotropic	orange brown	20	bimodal	0,2-0,5, 1-2	moderately sorted	poorly rounded	more equant	channels (xx)
18	C	anisotropic	orange brown	20	bimodal	0,2-0,5, 1-2	moderately sorted	poorly rounded	more equant	vesicles (x)
19	C	isotropic	orange brown	20	bimodal	0,2-0,5, 1-2	moderately sorted	poorly rounded	more elongate	vesicles (x)
20	C	isotropic	red	15	bimodal	0,2-0,5, 1-2	moderately sorted	poorly rounded	half-half	channels (x)
30	C2	anisotropic	red, brown	15	bimodal	0,2, 0,5	well sorted	rounded	equant	channels (xx)

**Table 3** – Identified particles of temper and other significant features.

Sample	Fabric	Rocks and minerals	Other features, shells and fossils
1	A	primary quartz, iron oxide, sedimentary rock, limestone micrite carbonate, feldspar	secondary carbonates, strong orientation of grains - fast wheel
2	A	primary quartz, iron oxide (big intrusions), sandstones, ferrous quartz arenite, plagioclase,	secondary carbonate, microfossils
3	A	primary quartz, low grade metamorphic rocks (slate)	secondary carbonates, very porous
4	A	quartz, biotite, metamorphic rocks (slate), feldspar ?	secondary carbonates
5	A	primary quartz, iron oxide, metamorphic rocks, amphibole	very porous, secondary carbonates
7	A	quartz, metamorphic rocks, amphibole, quartzite, feldspar	secondary carbonates precipitation ?
8	A	primary quartz, fragments of metamorphic rocks (slate, quartzite), pyroxene/amphibole, quartzite	secondary carbonates
10	A	primary quartz, slate, iron oxide sandstone, quartzite, amphibole	Bimodal also, schist, very porous, without fossils
11	A	primary quartz, iron oxide, lower metamorphic rocks	elongate particles along body
12	A	quartz, metamorphic rocks (slate, quartzite), lot of slate and schist	secondary carbonates
13	A	primary quartz, small fragments of mica, fragments of lower grade metamorphic rocks (quartzite, slate)	secondary carbonates
14	A	quartz, biotite, metamorphic rocks (slate, quartzite)	fragment big shell
15	A	primary quartz, muscovite, biotite, alkali feldspar	without metamorphic rocks
24	A	primary quartz, iron oxide, big grain of calcite	vitrification, secondary carbonates
29	A	primary quartz, iron oxide, calcite	secondary carbonates
16	A2	quartz, iron oxide, limestone, calcite, lower grade metamorphic rocks (slate, quartzite), chert	secondary carbonates, many various fossils (temperature less than 900°C)
9	A3	quartz, iron oxide, muscovite, quartzite, lot of slate, quartzite, feldspar amphibole	shell
6	A4	primary quartz in smaller fraction; big rounded temper with limestone, metamorphic rocks (slate), feldspar	grains slightly along body, preserved limestone
22	A5	quartz, muscovite, biotite, feldspar	many fragments of shells in the temper
21	B	primary quartz various sizes, iron oxide, sporadically quartzite and chert	vitrification
23	B	primary quartz, iron oxide, mica, feldspar	vitrification, circular fossil ?,
25	B	primary quartz, iron oxide, biotite	vitrification, secondary carbonates
26	B	primary quartz, iron oxide, quartzite, mica feldspar	vitrification, secondary carbonates
27	B	primary quartz, iron oxide, mica, feldspar	very well vitrified parts and less or 2 different clays?
28	B	primary quartz, iron oxide, quartzite, feldspar, mica	secondary carbonates, circular fossil ?, strong orientation of grains
17	C	small subangular (inclusions) and big rounded quartz, iron oxide, sedimentary rocks, volcanic rocks as the temper (dolerite, amphibole)	matrix enrich in iron oxide, secondary carbonates,
18	C	small subangular (inclusions) and big rounded quartz, iron oxide, limestone, volcanic rocks as the temper	matrix enrich in iron oxide, secondary carbonates
19	C	small subangular (inclusions) and big rounded quartz, iron oxide, sedimentary rocks, quartzite, volcanic rocks as the temper	matrix enrich in iron oxide, limestone in the temper fired
20	C	small subangular (inclusions) and big rounded quartz, iron oxide, sedimentary rocks as the temper	more aplastic, dusty clay enrich in iron oxide, shell, quartz quite rounded,
30	C2	quartz (subrounded), biotite, matrix carbonate, volcanic rocks as the temper (amphibole, gabbro), plagioclase	matrix very enrich in iron oxide, strong orientation of grains

## 4.2. XRD

Powder X-Ray Diffraction was performed in order to semi-quantify the bulk mineralogical composition. The mineral phases presented in all samples are quartz, potassium (orthoclase/microcline) and plagioclase (anorthite/albite) feldspar, diopside or/and other pyroxene. Quartz is the most ubiquitous and abundant mineral. Diopside is almost so important, except in the C petrography group. Alkaline and plagioclase feldspars are always present (**Table 4; Fig. 4.3**).

**Table 4** – Semi-quantitative presence of mineral phases in ceramic material: xxxx – predominant, xxx – abundant, xx – frequent, x – sporadic, (tr) – traces, empty cell – not presented.

Sample number	Fabric	Quartz	Diopside/Pyroxene	Gehlenite	Calcite	Hematite	Mica/ Illite	Potassium Feldspar	Plagioclase Feldspar	Other minerals
1	A	xxx	xx	x	x	x	x	x	xx	
2	A	xxx	x	x	x	tr	x	xxx	xx	
3	A	xxxx	xx	tr	x	x	tr	x	x	
4	A	xxxx	xx	x	x		x	x	xx	
5	A	xxxx	xx	x	x	tr	tr	x	xx	
7	A	xxxx	xx	x	x	tr	x	x	xx	
8	A	xxx	xx	tr	tr	tr	x	x	xx	Amphibole
10	A	xxxx	xx	x	tr		x	x	xx	Amphibole
11	A	xxx	xx	tr	x	tr	x	x	xx	
12	A	xxx	xx	x	tr		x	xx	xx	
13	A	xxx	xx	x	xx	tr	x	x	xx	
14	A	xxx	x	x	x	tr	x	x	xx	
15	A	xxxx	xx		tr	x	tr	x	xxx	
24	A	xxx	x	x	x	tr	tr	xx	xxx	
29	A	xxx	x	x	x	x		xx	xx	
16	A2	xxx	x		xx	tr	xx	x	xx	
9	A3	xxx	xx	x	tr			x	xx	Amphibole
6	A4	xxxx	x	tr	x		xx	x	xx	
22	A5	xx	x	tr	xx		xxx	xx	xx	
21	B	xxx	xx	tr		tr		xx	xx	
23	B	xx	xxx	x		tr		xxx	xx	
25	B	xxx	xxx	x	x			x	xx	
26	B	xxx	xx	x	x	tr		xx	xx	
27	B	xxx	xxx	x		tr		xx	xx	
28	B	xxx	xx	x		tr	x	xx	xx	Amphibole
17	C	xx	tr	tr	tr	tr	xxx	x	xx	
18	C	xxx	x	tr	tr	tr	xx	x	xxx	Analcime
19	C	xxx	x	tr	tr	tr	xxx	x	xxx	
20	C	xxxx	x	tr	tr	tr	x	x	xx	
30	C2	xxxx	tr				xx	xx	xx	Amphibole

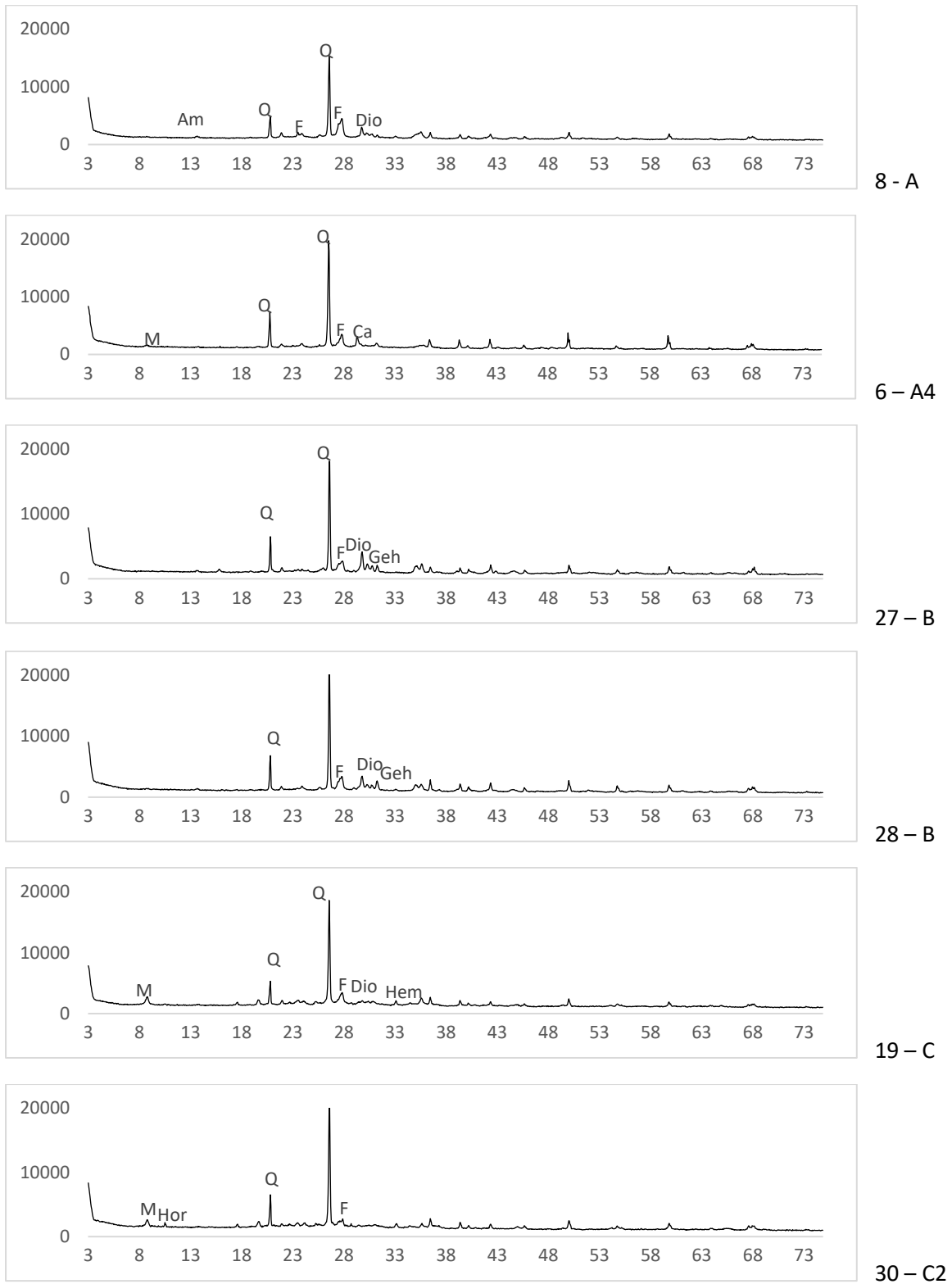


**Fig. 4.3** – Selected diffractograms and main mineral phases (x -  $2\theta$ , y - Intensity (a.u.)) with the numbers of samples and the letter of fabric group. Q – quartz, F – feldspar, Dio – diopside/pyroxene, Geh – gehlenite, M – mica/illite, A – amphibole, Hor – hornblende, Ca – calcite.

Mica/illite, Calcite and gehlenite are frequent. In few samples, amphibole (8-10 – A, 28 – B, 30 – C2) and in one analcime (18 – C) are presented.

The semi-quantitative evaluation of mineralogical phases is in the accordance with the petrographic groups, following the ceramic typology. The XRD data of the petrographic group A show high amount of quartz, a frequent presence of diopside and less of gehlenite. The plagioclase is more abundant than potassium feldspar. Samples 6 (A4), 9 (A3) and 16 (A2) are enriched in quartz and depleted in gehlenite.

The group B demonstrates also abundance in quartz, a higher ratio of diopside than group A, a constant presence of gehlenite and mica is almost lacking. The potassium feldspar is more abundant. The group C is enriched in quartz, plagioclase and sometimes in mica/illite. Diopside and gehlenite are almost absent.

The sample 22 (A5) has a lower amount of quartz, abundant mica/illite and common calcite. In the samples 15 (A), 16 (A2) and 30 (C2), gehlenite was not identified (**Fig. 4.3; Table 4**).

#### 4.3. ED- XRF

ED-XRF was performed to get a general chemical composition of the samples. The chemical results for the major elemental compositions are presented in concentrations of oxides and counted in columns by bars (**Fig. 4.4, Table 5**). The values for other elements are in a supplementary table in ppm (**Appendix II**). Selected elements are presented in bi-axial graphs (**Fig. 4.5, 4.6**) and cross checked after the archaeological groups. Other evaluations and cross check between the ceramic typology and the fabric groups are presented in the discussion. The main oxides obtained by ED-XRF analysis are  $\text{SiO}_2$ ,  $\text{Al}_2\text{O}_3$ ,  $\text{CaO}$  and  $\text{Fe}_2\text{O}_3$ . The silicon oxide is always predominant with a presence ranging from 51,2% to 63,4% without any significant deviation. The aluminium oxide is related with the aluminium-silicate fraction of clay material. The samples contain from 10,5% to 19,5%  $\text{Al}_2\text{O}_3$ . The sample 30 (C2) has the highest amount of  $\text{Al}_2\text{O}_3$  and the lowest percentage of  $\text{CaO}$ .

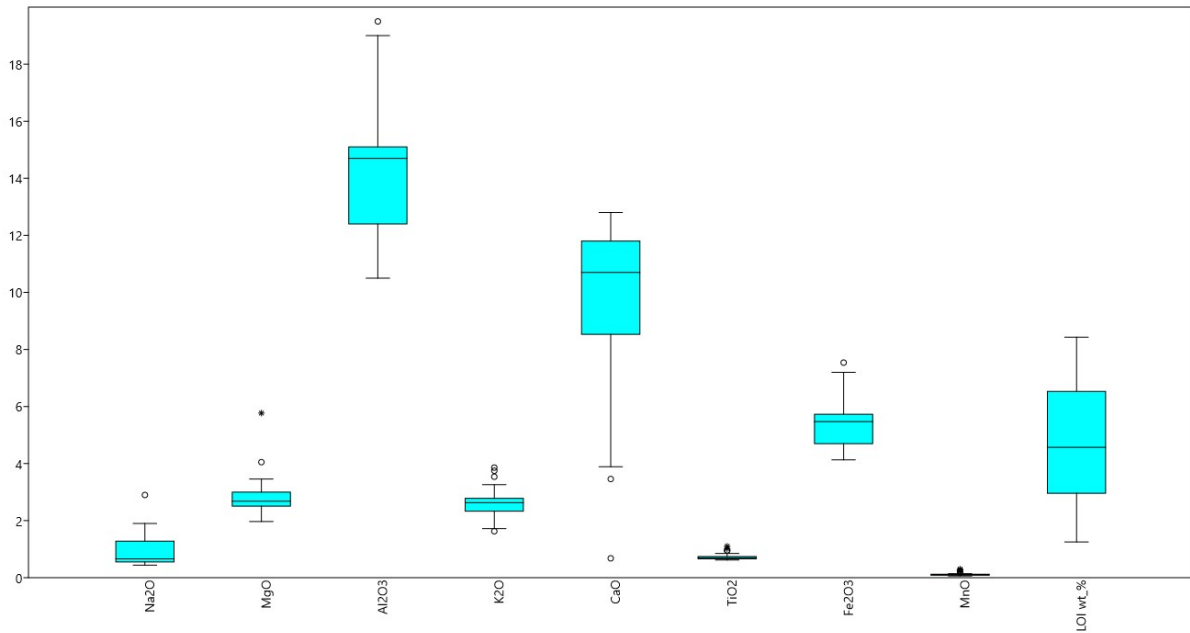


**Fig. 4.4.** – Box plots of main oxides and LOI with marked outliers as circles.

The amount of CaO is similar in the A and B groups (around 10%) and lower in the C group, corroborating the low abundance of diopside and gehlenite reported by the XRD data. The iron oxide is present, from 4,13% to 7,54%. In general, it is more abundant in the C group and less abundant in B group. Other oxides, in general present in lower amounts, are Na<sub>2</sub>O, K<sub>2</sub>O, MgO, TiO<sub>2</sub> and MnO. Sodium, magnesium and manganese oxides are more abundant in the petrographic group C.

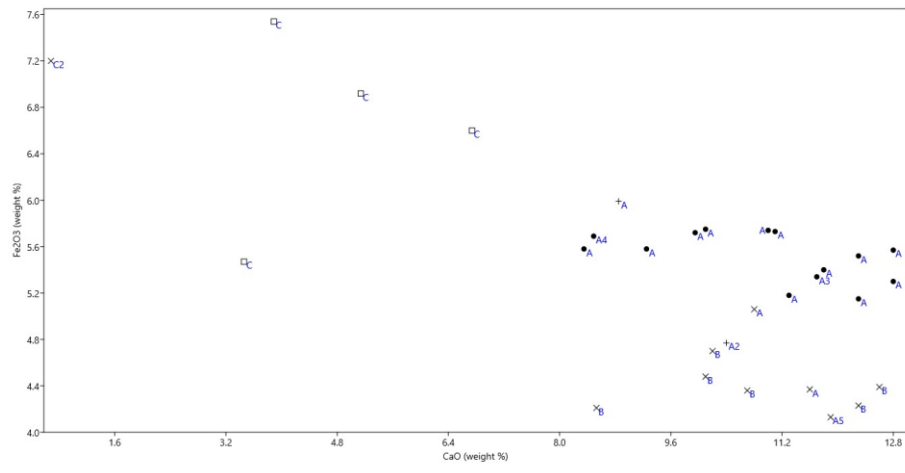
The Linear correlation shows a common positive correlation of the K, Fe, Ti, Al and likely Na oxides; probably due to the clay signature. The negative correlations with SiO<sub>2</sub> and CaO points to the importance of the temper and a limestone contribution, respectively (**Table 6**). The elemental bi-plot graphs (**Fig. 4.5, 4.6**) allow to distinguish between the different typological groups. The petrographic group C is enriched in elements like Fe, Na, Al and Rb and depleted in Ca and Zr. The amount of calcium is similar to Pellicer B/C and Pellicer D, but the amount of iron and rubidium is higher while the amount of sodium, zirconium is lower (**Table 5**).

**Table 5** – ED-XRF table with main oxides in % and loss of ignition (other elements are presented in **Appendix II**).

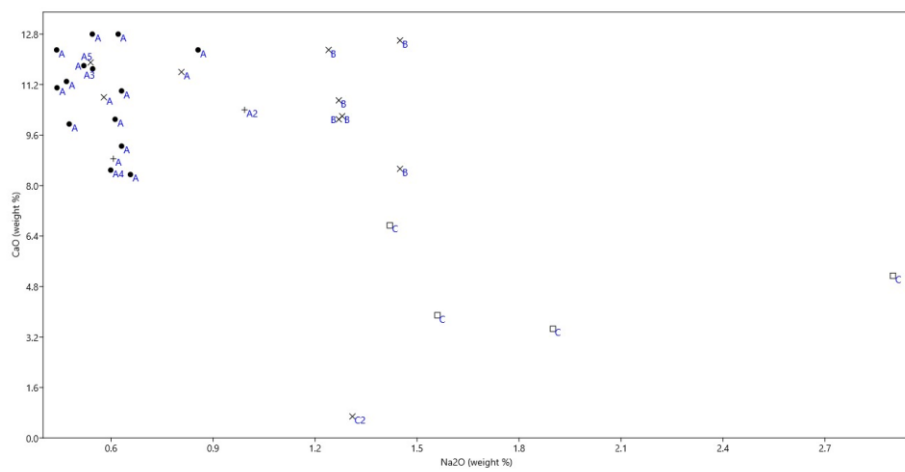
Sample	Fabric	Na2O	MgO	Al2O3	SiO2	K2O	CaO	TiO2	Fe2O3	MnO	P2O5	SO3	LOI
1	A	0.63	3.01	14.9	55.6	2.6	11	0.72	5.74	0.11	0.39	0.13	6.27
2	A	0.47	2.85	14.2	53	2.61	11.3	0.63	5.18	0.09	0.49	0.18	7.74
3	A	0.61	2.79	15.1	54.5	2.72	10.1	0.70	5.75	0.09	0.40	0.14	5.18
4	A	0.86	2.96	14.8	51.5	2.7	12.3	0.66	5.52	0.10	0.35	0.16	6.79
5	A	0.55	2.68	15.1	51.2	2.6	12.8	0.67	5.57	0.10	0.33	0.15	6.84
7	A	0.52	2.75	14.9	52.6	2.64	11.8	0.66	5.40	0.08	0.45	0.13	6.53
8	A	0.66	2.57	15	57.5	3.26	8.35	0.73	5.58	0.09	0.43	0.16	3.52
10	A	0.63	2.51	14.9	56	2.78	9.25	0.74	5.58	0.11	0.44	0.19	4.57
11	A	0.44	2.46	14.5	53.3	2.81	11.1	0.72	5.73	0.12	0.70	0.23	5.64
12	A	0.48	2.61	14.9	54.8	2.97	9.95	0.77	5.72	0.10	0.51	0.13	2.96
13	A	0.62	3.1	14	51.2	2.52	12.8	0.69	5.30	0.10	0.30	0.21	7.65
14	A	0.44	3.09	13.9	50.8	2.63	12.3	0.64	5.15	0.11	0.53	0.21	8.43
15	A	0.61	2.34	15.1	60.1	2.03	8.85	0.72	5.99	0.06	0.30	0.13	1.28
24	A	0.81	2.42	11.8	57	2.32	11.6	0.66	4.37	0.11	0.33	0.21	6.50
29	A	0.58	2.67	11.7	56.5	2.63	10.8	0.72	5.06	0.08	0.37	0.15	6.90
16	A2	0.99	2.58	13.2	55.3	2.9	10.4	0.64	4.77	0.10	0.30	0.14	7.60
9	A3	0.55	2.59	14.7	53.9	2.75	11.7	0.68	5.34	0.09	1.43	0.18	2.40
6	A4	0.60	3.1	13.2	60.5	2.09	8.49	0.72	5.69	0.30	0.33	0.15	5.93
22	A5	0.54	2.03	10.5	54.2	2.33	11.9	0.62	4.13	0.12	0.27	0.17	3.04
21	B	1.45	2.23	11.8	63.1	2.62	8.53	0.70	4.21	0.08	0.24	0.13	4.30
23	B	1.24	3	11.8	57.2	1.98	12.3	0.65	4.23	0.09	0.30	0.13	2.52
25	B	1.27	2.75	12.4	62.5	2.05	10.1	0.69	4.48	0.08	0.31	0.17	4.02
26	B	1.45	2.94	12.1	56.8	1.72	12.6	0.69	4.39	0.12	0.31	0.17	4.64
27	B	1.27	2.66	11.7	61.2	1.63	10.7	0.69	4.36	0.08	0.33	0.15	3.64
28	B	1.28	2.67	12.7	59.1	2.56	10.2	0.74	4.70	0.11	0.32	0.12	3.68
17	C	2.90	3.46	17.7	53.1	3.86	5.14	0.95	6.92	0.23	0.21	0.13	4.33
18	C	1.42	5.77	16.7	53.3	2.65	6.74	0.85	6.60	0.23	0.36	0.16	2.75
19	C	1.56	4.05	19	54.7	3.75	3.89	1.02	7.54	0.27	0.16	0.10	2.90
20	C	1.90	2.46	16.1	63.4	2.7	3.46	0.96	5.47	0.18	0.28	0.16	1.25
30	C2	1.31	1.97	19.5	61.6	3.54	0.68	1.10	7.20	0.14	0.14	0.12	1.44

**Table 6** – Linear correlation matrix of the main oxides and LOI from ED-XRF.

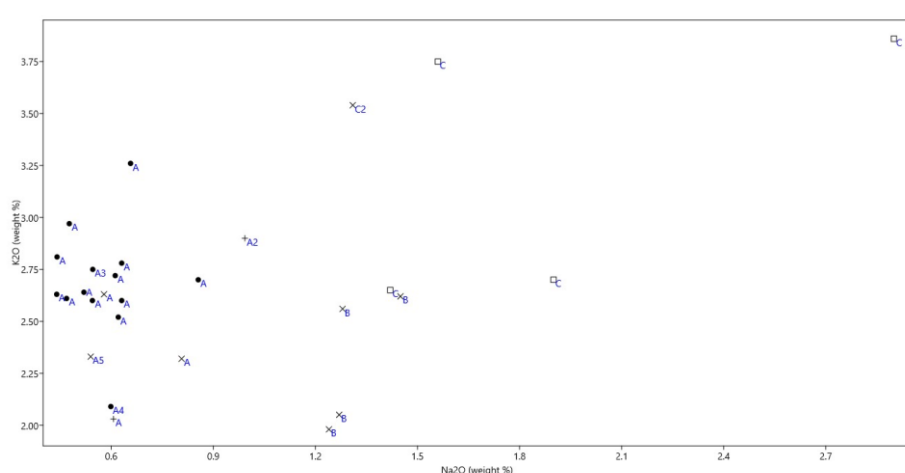
	Na2O	MgO	Al2O3	SiO2	K2O	CaO	TiO2	Fe2O3	MnO	P2O5	SO3	LOI wt. %
Na2O		0.29	0.30	0.34	0.29	-0.59	0.62	0.23	0.46	-0.42	-0.09	-0.34
MgO	0.29		0.34	-0.34	0.14	-0.15	0.24	0.42	0.57	-0.08	0.00	0.13
Al2O3	0.30	0.34		-0.16	0.76	-0.71	0.79	0.95	0.46	-0.05	-0.18	-0.01
SiO2	0.34	-0.34	-0.16		-0.27	-0.46	0.28	-0.20	0.02	-0.30	-0.54	-0.19
K2O	0.29	0.14	0.76	-0.27		-0.60	0.65	0.74	0.36	-0.03	-0.04	-0.19
CaO	-0.59	-0.15	-0.71	-0.46	-0.60		-0.94	-0.68	-0.57	0.35	0.44	0.24
TiO2	0.62	0.24	0.79	0.28	0.65	-0.94		0.77	0.60	-0.32	-0.31	-0.22
Fe2O3	0.23	0.42	0.95	-0.20	0.74	-0.68	0.77		0.58	-0.08	-0.20	0.08
MnO	0.46	0.57	0.46	0.02	0.36	-0.57	0.60	0.58		-0.24	-0.07	0.15
P2O5	-0.42	-0.08	-0.05	-0.30	-0.03	0.35	-0.32	-0.08	-0.24		-0.06	0.28
SO3	-0.09	0.00	-0.18	-0.54	-0.04	0.44	-0.31	-0.20	-0.07	-0.06		0.12
LOI wt. %	-0.34	0.13	-0.01	-0.19	-0.19	0.24	-0.22	0.08	0.15	0.28	0.12	



A

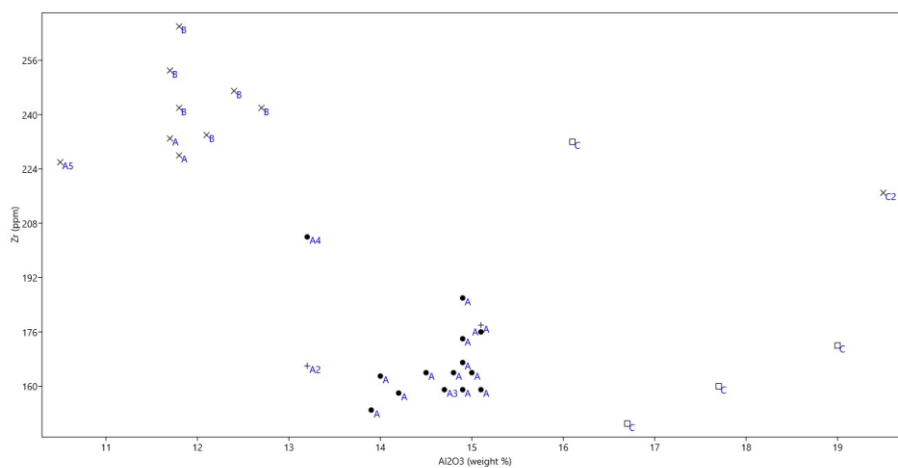


B

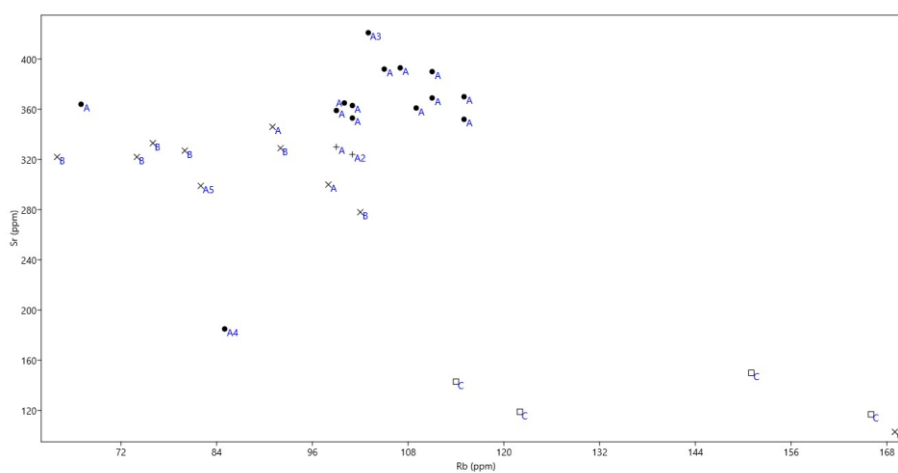


C

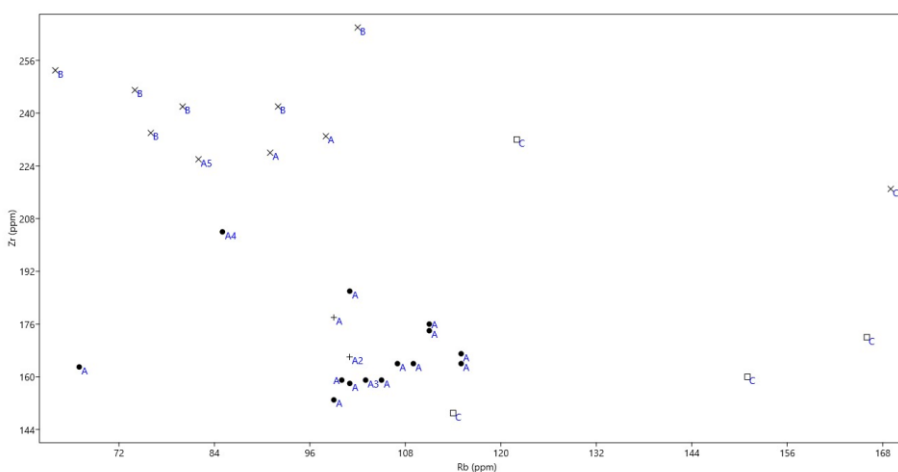
**Fig. 4.5** – The ED-XRF data in the bi-axial graphs. **A:** CaO-Fe<sub>2</sub>O<sub>3</sub>, **B:** Na<sub>2</sub>O- CaO, **C:** Na<sub>2</sub>O-K<sub>2</sub>O (dot – Pellicer B/C, cross – amphorae without protrusion, square – local containers, X – Pellicer D).



**A**



**B**



**C**

**Fig. 4.6** – The ED-XRF data in the bi-axial graphs. **A:** Al<sub>2</sub>O<sub>3</sub>-Zr, **B:** Rb-Sr, **C:** Rb-Zr (dot – Pellicer B/C, cross – amphorae without protrusion, square – local containers, X – Pellicer D).

#### 4.4. SEM-EDS

The SEM-EDS analysis was performed on 12 representative samples (1, 2, 6, 10, 14-16, 18, 20, 21, 24, 30) to complement petrography, XRD and ED-XRF results (**Table 7**).

**Table 7** – List of samples analysed by SEM-EDS.

Sample number	General type of vessel	Type notation	Fabric	Part of the vessel	Shape ( <b>Fig. 3.1</b> )
1	Pellicer B/C amphora	I	A	bottom	A
2	Pellicer B/C amphora	I	A	bottom	A
6	Pellicer B/C amphora	I	A4	bottom	A
10	Pellicer B/C amphora	I	A	bottom	B
14	Pellicer B/C amphora	I	A	bottom	C
15	Amphora without protrusion	II	A	bottom	D
16	Amphora without protrusion	II	A2	bottom	E
18	Local common container	III	C	bottom	F
20	Local common container	III	C	bottom	F
21	Pellicer D amphora	IV	B	rim	
24	Pellicer D amphora	IV	A	rim	
30	Pellicer D amphora	IV	C2	rim	

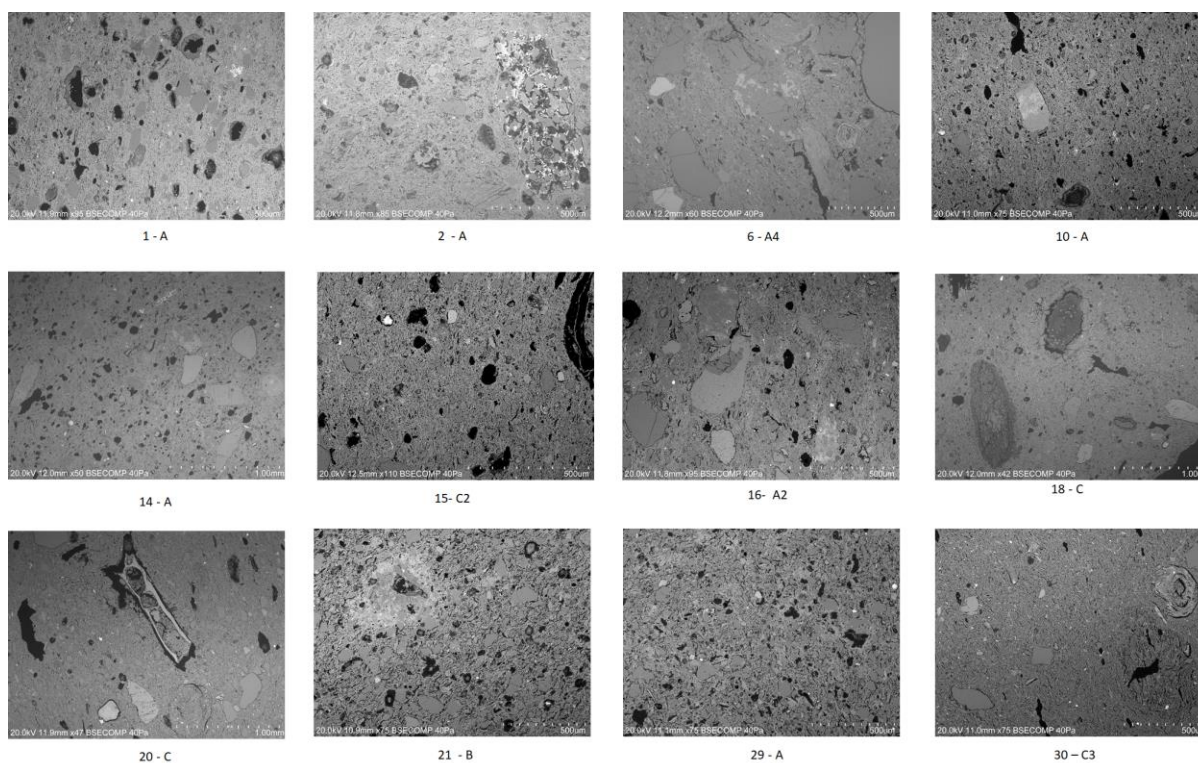


**Fig. 4.7** – Selected surface electron images (SE) with the numbers of samples and the letter of fabric group.

SEM-EDS was used for elemental mapping and point analysis of the ceramic matrix and temper grains in the thin sections. The backscattering imaging provides detailed information about the character of matrix, such as shape and size of the temper grains and voids, and point out chemical differences (**Fig. 4.7**). The general elemental distribution and the major elemental compositions of temper particles, minerals and rock inclusions were examined by EDS analysis. The samples are described after the backscattering images, elemental mapping and chemical composition of distinctive intrusions in atomic % are presented (**Fig. 4.8-29**). The detail of sample 21 (B) with vitrification is illustrated (**Fig. 30**). The EDS analysis of feldspar intrusions is evaluated in the ternary diagram  $\text{CaAl}_2\text{Si}_2\text{O}_8$ ,  $\text{NaAlSi}_3\text{O}_8$ ,  $\text{KAlSi}_3\text{O}_8$  (**Fig. 31**).

The secondary precipitation in the voids is well visible in the backscattering image of samples 1 (A), 10 (A), 18 (C) and 20 (C). The vitrified texture is characteristic for the samples 21 (B), but notable was also in the sample 24 (A). In the sample 18 (C) is presented secondary precipitation of carbonates in the void. The sample 2 (A) presents a sandstone. In the right top part of the backscattering image of sample 15 (A) is an empty space probably after some organic material. In the backscattering image of sample 20 (C) is a fragment of shell. In the sample 30 is a metamorphic rock (**Fig. 4.7**).

The general chemical composition of the matrix of sample 1 presents Si, Al and Ca, then Na, Mg, Cl, K and Fe. P, S and Ti are presented as minor elements. The secondary chemical precipitation in the voids is documented by backscattering. The temper in this sample is mainly quartz and plagioclase feldspars. Other inclusions are sodium-silicate with calcite and magnesium, aluminosilicates, and small grains presenting high amount of titanium (**Fig. 4.8**).

The general chemical composition of the sample 10 (A), based on the mapping, presents Si, Al and Ca; then K, Mg, Na; and Fe. P, S, Cl and Ti are as minor elements. The secondary chemical precipitation around the voids is visible as well as in this sample. The temper grains correspond to feldspar rocks and quartz. The feldspars were analysed by EDS and are close to the orthoclase or microcline and to the albite with variation in Ca and K (**Fig. 4.9**).

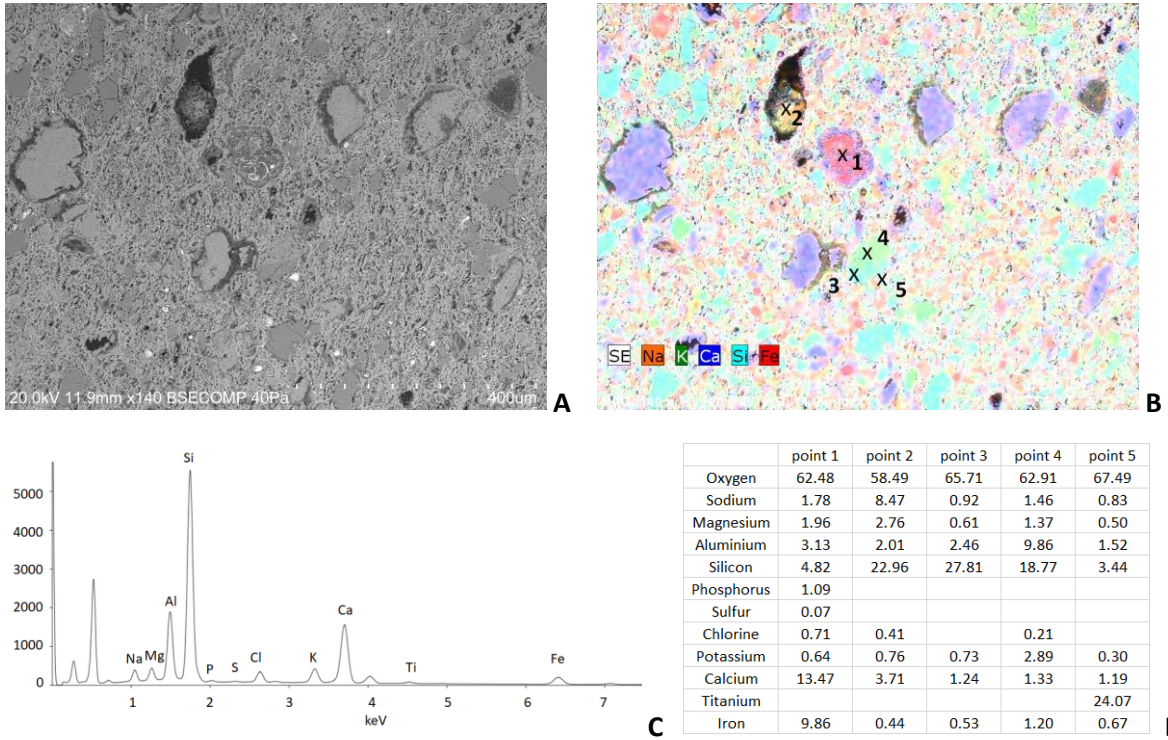


**Fig. 4.8** – SEM EDS: sample 1 – A; A: Backscattering image, B: elemental mapping, C: spectra of the mapping, D: table with point EDS analysis in the atomic % (the number of points correspond with the numbers in mapping).

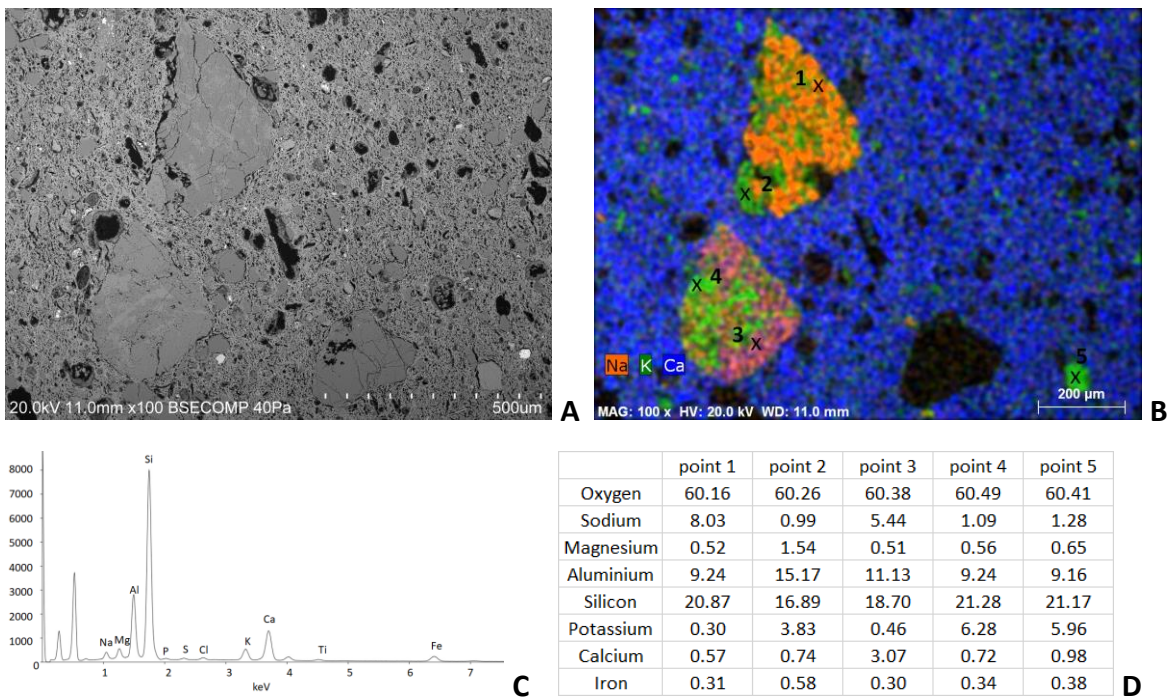


**Fig. 4.9** – SEM EDS: sample 10 – A; A: Backscattering image, B: elemental mapping, C: spectra of the mapping, D: table with point EDS analysis in the atomic % (the number of points correspond with the numbers in mapping).

The representative matrix of sample 6 contains a big fragment of rounded rock with mainly silicon and aluminium silicon parts. Other smaller grains of the temper are limestone and feldspars. The particles of feldspar correspond to albite and andesine in plagioclase series. A particle rich in titanium is documented. The secondary precipitation of calcium is presented. The spectra of mapping, influenced by the big temper particle, point out high amount of Si and Al. Ca is presented in less amount than in the samples 1, 10 and 16. Mg and K are presented as well. Other elements are detected only in traces (**Fig. 4.10**).

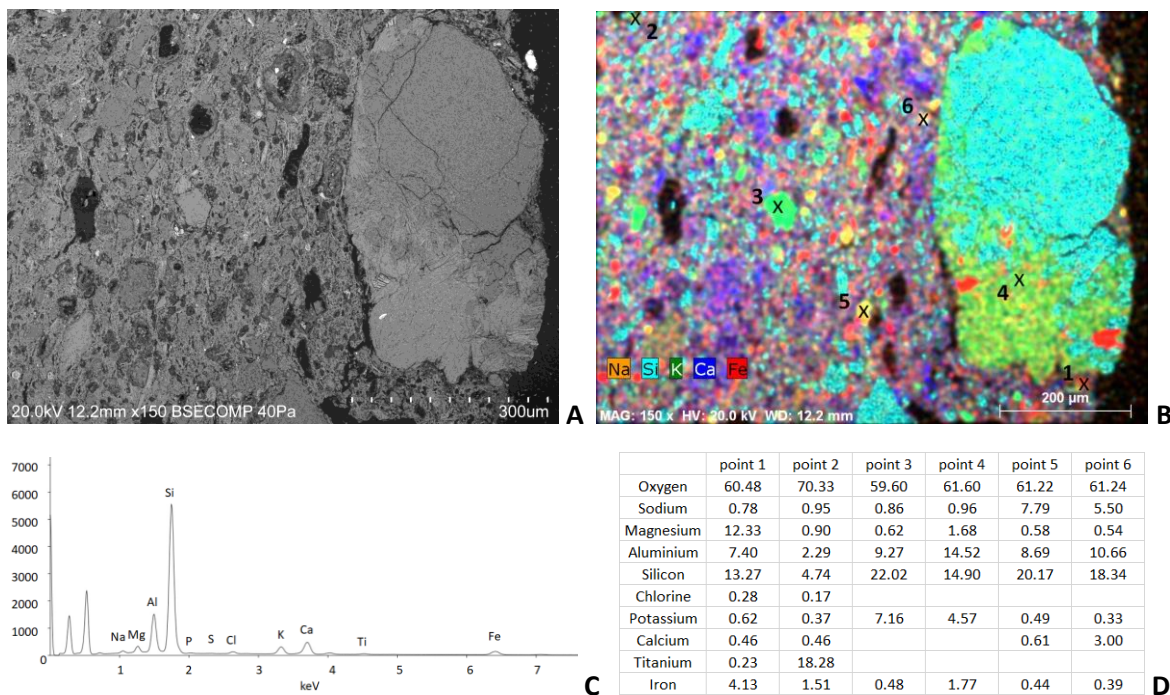


**Fig. 4.10** – SEM EDS: sample 6 – A4; **A**: Backscattering image, **B**: elemental mapping, **C**: spectra of the mapping, **D**: table with point EDS analysis in the atomic % (the number of points correspond with the numbers in mapping).

Representative area of sample 16 contains Si, Al and Ca, then, K, Mg, Na and Fe. P, S, Cl and Ti are presented in traces. The secondary chemical precipitation is presented around some voids. The temper grains are quartz, feldspars and rocks inclusions of limestone. The analysed feldspars are enriched in K (**Fig. 4.11**).

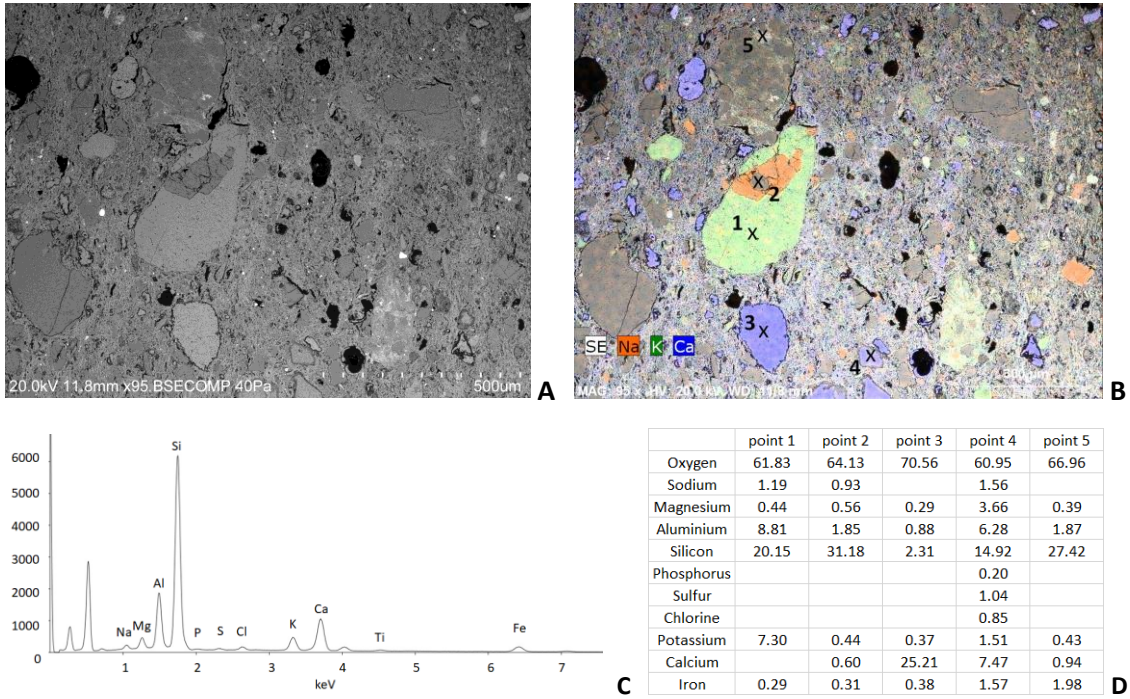


**Fig. 4.11** – SEM EDS: sample 16 – A2; **A**: Backscattering image, **B**: elemental mapping, **C**: spectra of the mapping, **D**: table with point EDS analysis in the atomic % (the number of points correspond with the numbers in mapping).

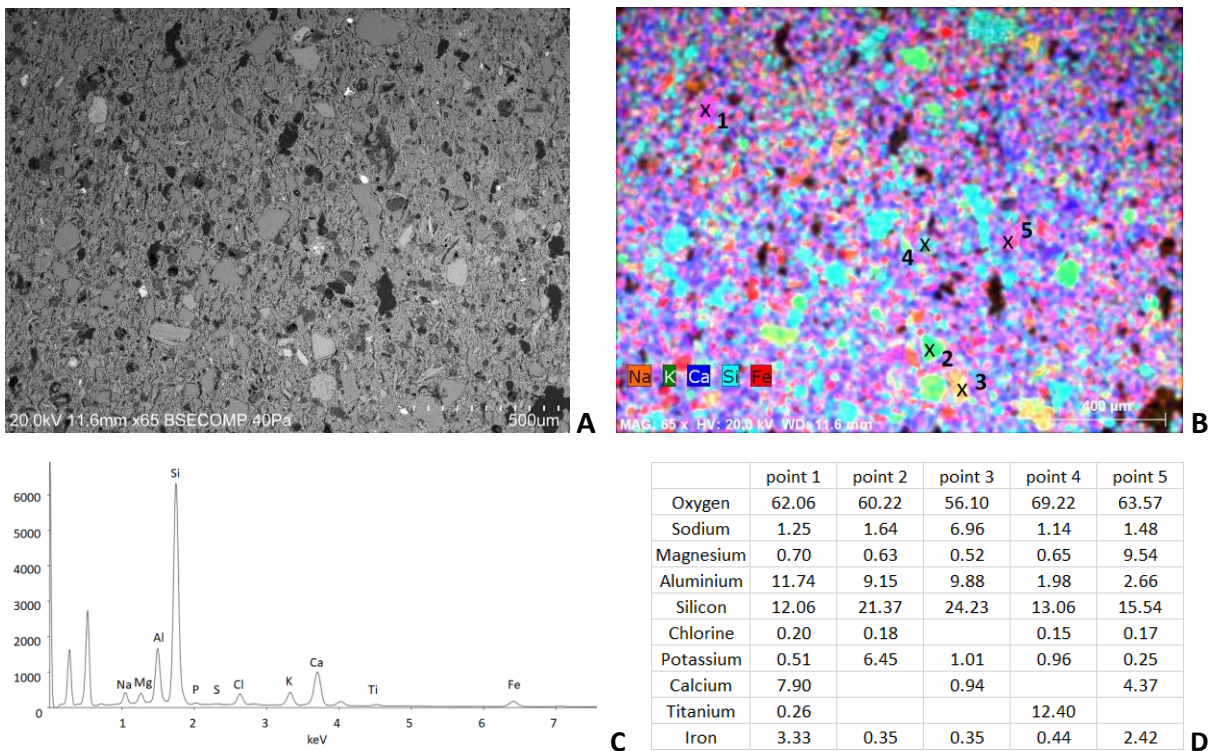


**Fig. 4.12** – SEM EDS: sample 24 – A; **A**: Backscattering image, **B**: elemental mapping, **C**: spectra of the mapping, **D**: table with point EDS analysis in the atomic % (the number of points correspond with the numbers in mapping).

The general chemical composition of the matrix of sample 24 presents Si, Al and Ca, then Na, Mg, Cl, K, where Fe, P, S and Ti are presented in traces. The temper is mainly quartz, but also feldspars. The analysed feldspars are close to the orthoclase or microcline and to the albite. A grain of silica-titanium is documented. The particle with mainly magnesium silicate composition is an amphibole, after the atomic % close to tremolite (**Fig. 4.12**).

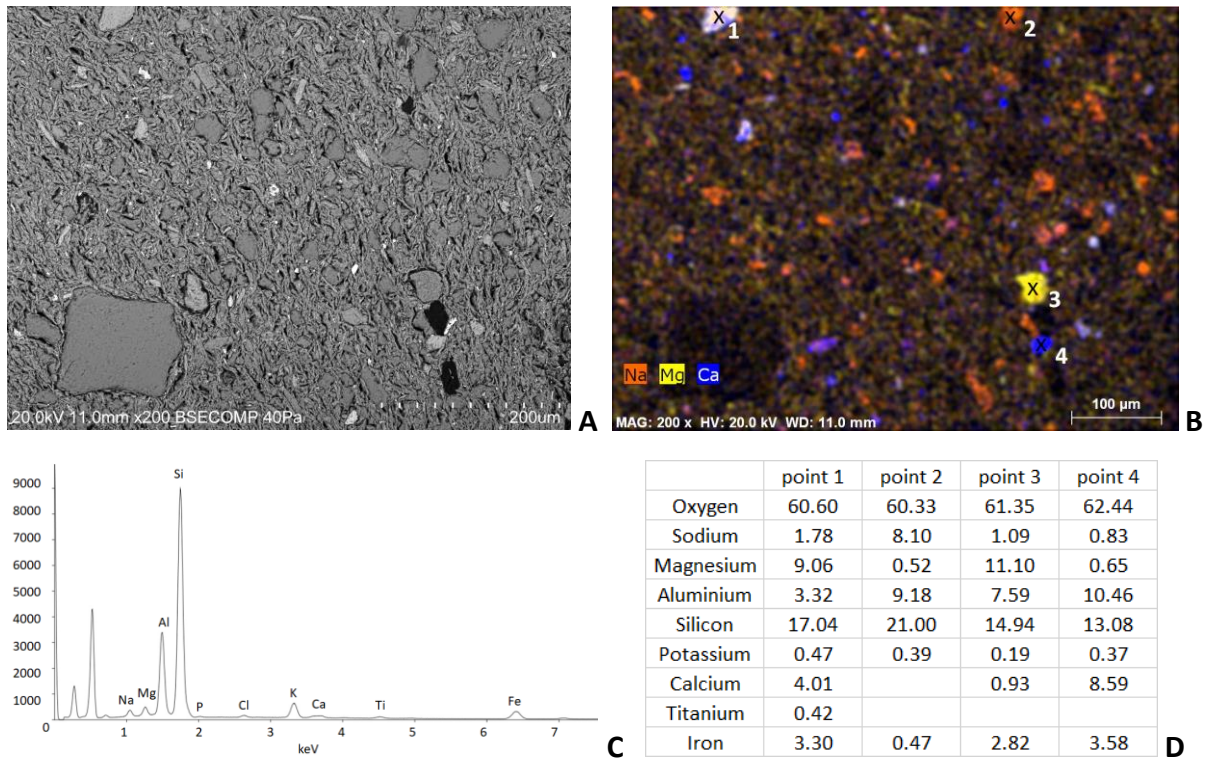


**Fig. 4.13** – SEM EDS: sample 30 – C2; **A**: Backscattering image, **B**: elemental mapping, **C**: spectra of the mapping, **D**: table with point EDS analysis in the atomic % (the number of points correspond with the numbers in mapping).

The presented part of the matrix of sample 30 contains mainly Si and Al. Then, the spectra show peaks of K, Mg, Fe and Na. P, Cl and Ti are presented in minor. Characteristic is the vitrified texture. The temper grains are mainly quartz and feldspars (**Fig. 4.13**).

The calcium-magnesium-iron precipitation in the voids of ceramic is frequent and almost always presented. The vitrified texture (**Fig. 4.14**) was well documented mainly in the samples of Pellicer D but presented is also in some samples of Pellicer B/C.

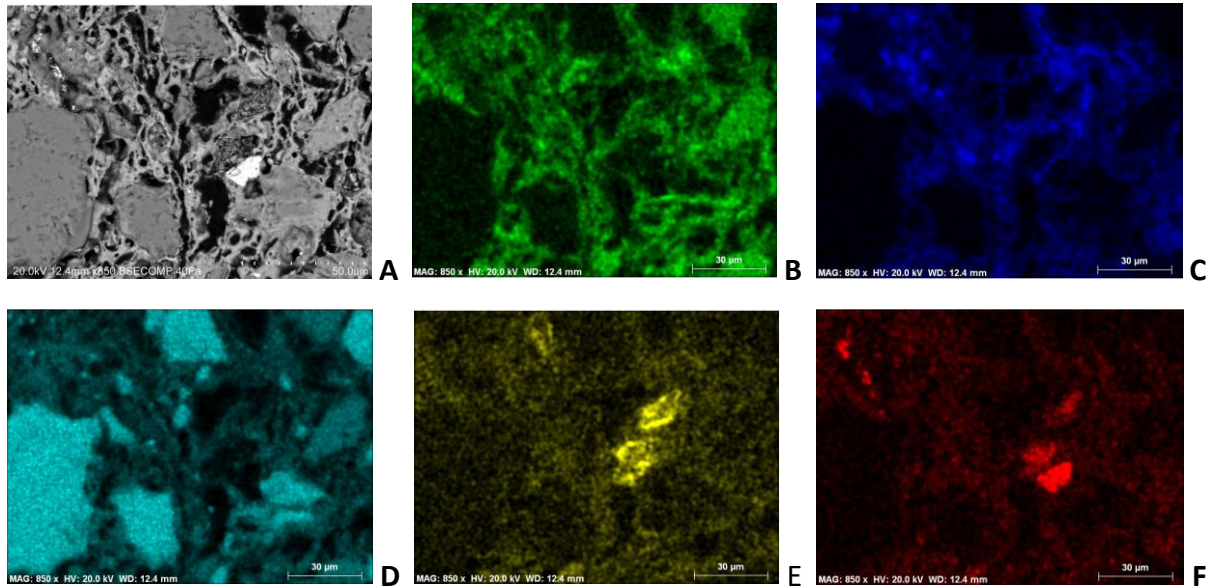


**Fig. 4.14** – Detail of glassy vitrification; sample 21 – B. **A:** Backscattering image, **B:** Al mapping, **C:** Ca mapping, **D:** Si mapping, **E:** Mg mapping, **F:** Fe mapping.

The SEM-EDS data, based on the elemental analyses, show a mineralogical composition mainly with quartz and feldspars, but presented are also iron oxides, low metamorphic rocks, sedimentary rocks, titanium oxides, amphibole etc. Fragments of bones and shells are common as well. Rock inclusions provide similar compositions. The elemental compositions obtained by the EDS analyses of the feldspar grains correspond mainly to sodium and potassium feldspars – albite with tendency to anorthoclase or oligoclase (samples: 1, 2, 6, 10, 16, 21 and 24) and sanidine close to orthoclase or microcline (2, 6, 10, 14, 16, 18, 20, 21). Then sanidine enriched in Na is presented in sample 14 (A). The temper of samples 6 (A4), 10 (A) and 30 (C2) contain andesine and labradorite (**Fig. 4.15**).

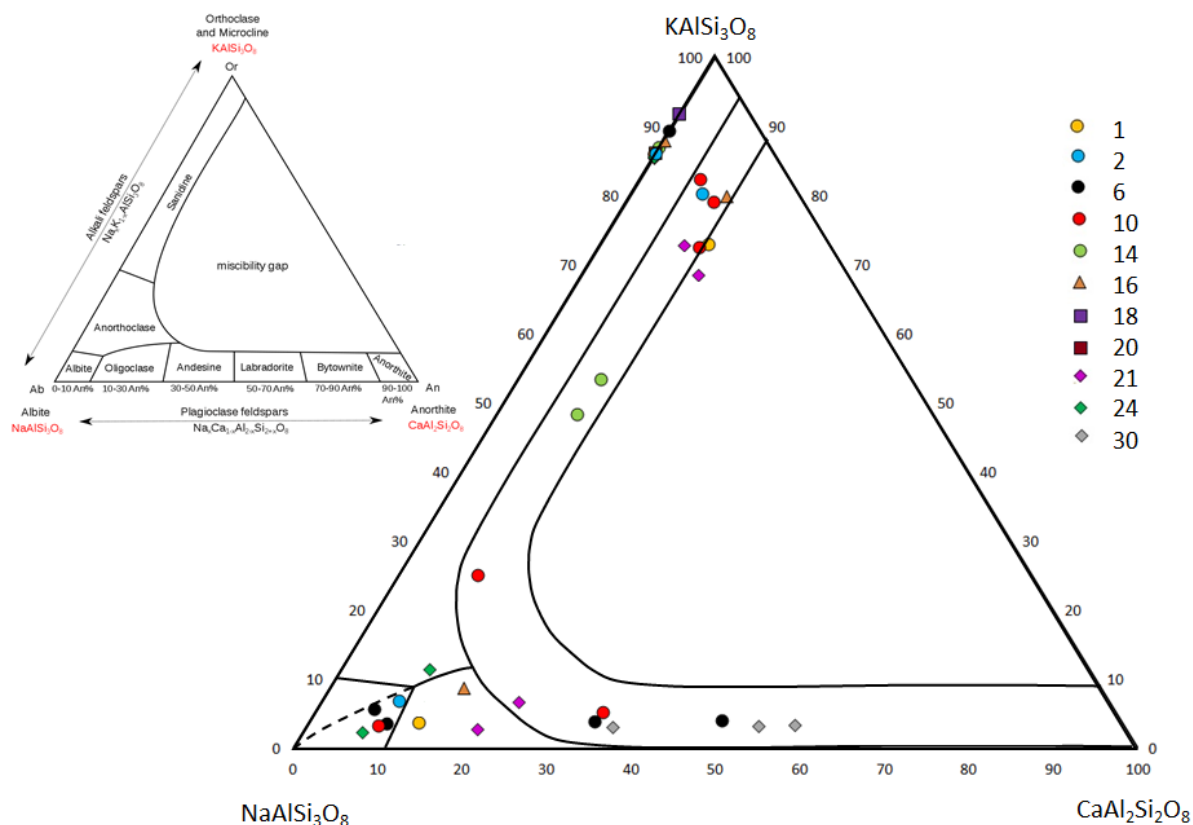


**Fig. 4.15** – SEM-EDS data. Ternary diagram illustrating the composition of feldspars in selected samples (dots – Pellicer B/C, triangles – amphorae without protrusion, squares – local container, diamonds – Pellicer D).

#### 4.5. GC-MS

To investigate organic residues and identify past content 8 samples of bottoms selected after the provenance results (3, 6, 8-10, 15, 17, 20) were analysed by GC-MS (**Table 8**).

**Table 9** – List of samples analysed by GC-MS.

Sample number	General type of vessel	Type notation	Fabric
3	Pellicer B/C amphora	I	A
6	Pellicer B/C amphora	I	A4
8	Pellicer B/C amphora	I	A
9	Pellicer B/C amphora	I	A3
10	Pellicer B/C amphora	I	A
15	Amphora without protrusion	II	A
18	Local common container	III	C
20	Local common container	III	C

**Table 10** – GC-MS: the presence of compounds related with a past content of vessels.

Compound family	Retention time (min)	Compound common name	Abbreviation	Sample				
				6	20	9	10	3
Fatty acids	3,98	Hexanoic acid	C6:0 FA	x				
	6,73	Octanoic acid	C8:0 FA	x				
	8,00	Nonanoic acid	C9:0 FA	x				
	9,21	Decanoic acid	C10:0 FA	x				
	11,43	Dodecanoic acid	C12:0 FA	x				
	13,45	Tetradecanoic acid	C14:0 FA	x				
	15,33	Hexadecanoic acid	C16:0 FA	x				
	17,04	Octadecanoic acid	C18:0 FA	x				
MAG's	18,39	1-Tetradecanoyl-sn-glycerol	C14:0 MAG			x		
	19,62	2-Hexadecanoyl-sn-glycerol	C16:0 MAG	x	x	x		
	19,86	1-Hexadecanoyl-sn-glycerol	C16:0 MAG	x	x	x	x	x
	20,98	2-Stearoyl-sn-glycerol	C18:0 MAG		x	x		
	21,22	1-Stearoyl-sn-glycerol	C18:0 MAG	x	x	x	x	x
Alcohols	10,51	1-Dodecanol	C12:OH AL		x			
	12,61	1-Tetradecanol	C14:OH AL	x	x	x		
	13,59	1-Pentadecanol	C15:OH AL		x			
	14,53	1-Hexadecanol	C16:OH AL	x	x	x	x	
	16,30	1-Octadecanol	C18:OH AL	x	x	x		
	17,93	1-Eicosanol	C20:OH AL		x			
	19,43	1-Docosanol	C22:OH AL		x			
	20,86	1-Tetracosanol	C24:OH AL		x			
	22,19	1-Hexacosanol	C26:OH AL	x	x			
	23,43	1-Octacosanol	C28:OH AL	x	x			
	24,61	1-Triacontanol	C30:OH AL	x				
	25,71	1-Cotriacontanol	C32:OH AL	x	x			x
	26,74	1-Tetratriacontanol	C34:OH AL	x	x			
Alkanes	11,96	n- Heptadecane	C17			x		
	12,9	n- Octadecane	C18	x	x	x		
	13,89	n- Nonadecane	C19	x	x	x		
	14,8	n- Icosane	C20		x	x	x	
	15,73	n- Henicosane	C21	x	x	x	x	
	16,61	n- Docosane	C22		x	x	x	
	17,43	n- Tricosane	C23	x	x	x	x	
	18,23	n- Tetracosane	C24		x	x	x	
	19,02	n- Pentacosane	C25	x	x	x	x	
	19,74	n- Hexacosane	C26	x	x	x	x	
	20,52	n- Heptacosane	C27	x	x			
	21,16	n- Octosane	C28		x			
	21,87	n- Nonacosane	C29	x				
	22,48	n- Triacontane	C30	x				
	23,13	n- Hentriacontane	C31	x	x			
	23,72	n- dotriacontane	C32	x	x			
	24,31	n- Tritriacontane	C33	x	x			
Internal standard	24,91	n- Tertratriacontane	C34 IS	x	x	x	x	x

## 5. Discussion

### 5.1. Ceramic materials study

The expected places of Pellicer B/C (Sevilla district) and D amphorae (Sevilla district and Cadiz) production are approximately 130 km away from the Castro Marim site, however, the geological settings are not so different. The evolution of the Iberian massif, sedimentary basin of both rivers and coastline close to the deltas have comparable patterns. In term of ceramic production and accessibility of raw materials the most prominent clay is calcareous (the Lower Guadalquivir region) or calcareous-dolomitic clay (the Castro Marim region), both called marl. Temper could easily be obtained from river or sea sediments (i.e. gravel, sand, shells; [Megías 2017](#); [Moura et al. 2017](#)).

The ceramic production in the Turdetanii culture was highly manufactured. The workshops had double chamber ceramic kilns and other structures related with raw material manipulation, manufacturing of the vessels and firing. The supply of raw materials is one of the aspects in which the longest lasting tradition seems to exist, since the same macroscopic and petrographic types are preserved during the centuries. Only a few new sources of raw material are detected at the end of the 3<sup>rd</sup> century B.C. in all areas of pottery production in the Lower Guadalquivir. The ceramic recipes were standardized as well as the firing conditions and the morphology of containers ([Megías 2017](#)).

The analysed samples represent four typological groups: Pellicer B/C amphorae (sample 1-14), amphorae without protrusion (15 and 16), local common wares (17-20) and Pellicer D amphorae (21-30). After the petrography study based on analysis of thin sections, the samples were sorted to 3 main fabric groups (A, B, C). Some samples are differentiated after distinct features (A2, A3, A4, A5, C2), such as colour and temper specifics.

The fabric group A is associated with Pellicer B/C, however similar character fabric was found in two amphorae without protrusion (15, 16 – A2) and 3 samples of Pellicer D (22 – A5, 24, 29). The colour in cross sections is commonly bright brown, orange or brown. In case of three samples (6 – A4, 9 – A3, 16 – A2), the grey colour reports a redox firing atmosphere. The temper is usually bimodal with the modes at 0,2 and about 0,5 mm. The temper/clay ratio is about 10%. Some samples show some different details as presenting fossils and limestone (16

– A2), numerous black slates (9 – A3), big rounded quartz and limestone tempers (6-A4) or homogenous colour of matrix and many shells in the temper (22 – A5; **Fig. 19**). Typically, the temper of fabric group A contains mainly grains of quartz, iron oxide and fragments of low-grade metamorphic rocks (e.g. slate, quartzite), sedimentary rocks, biotite, mica, feldspar and amphibole (**Table 2**).

The fabric group B contains 6 samples of Pellicer D amphorae (21, 23, 25-28). The colour is homogenous in beige-green colour and glassy vitrification is typical. The matrix is enriched in calcium and with comparison of other fabric groups in sodium (**Fig. 4.8-14**). The temper is well sorted sand with a size of about 0,2 mm, however, sporadically the iron oxide is presented as bigger intrusions. The temper/clay ratio was estimated about 15 %, but there is difficult to say what is temper and what are natural intrusions. The grains of temper contain primary quartz, but noticed are also iron oxides, biotite and feldspars.

The fabric group C represent 4 local containers and one Pellicer D amphora (30 – C2). The matrix is rich in iron oxide with a typically reddish colour. The temper is bimodal. While a smaller fraction (primary sub-angular quartz) could be a part of clay, the bigger grains (from 1 to 2 mm) had to be intentionally added. The bigger temper represents commonly rounded grains of quartz, iron oxide, sedimentary rocks, quartzite and amphibole.

The semi-quantitative evaluation of mineralogical phases by XRD is in accordance with the fabric groups, following the archaeological typology. The XRD data from fabric group A show a high amount of quartz, a recurrent presence of diopside but less of gehlenite. The plagioclase is more abundant than potassium feldspar. Mineralogical composition corresponds to clay rich in calcite or dolomite. The amount of calcite can be related with secondary precipitation in the ground, but in this case, mainly the samples fired in a redox atmosphere (6 – 4A, 9 – A3, 16 – A2) points out to a presence of shells, limestone or dolomite in the temper. If the firing amphorae were oxidized, the temperature would have been high enough to decarbonize all rocks. The temperature can be estimated to have been less than 900°C as gehlenite started to form and mica/illite is still relatively present ([Vieira Ferreira et al. 2018](#); [Noll, Heimann 2016](#); [Trindade et al. 2009](#)).

Group B also demonstrates an abundance in quartz, a higher amount of diopside than group A, a constant presence of gehlenite and mica/illite is almost lacking. The potassium feldspar is frequent. The mineralogical composition reflects clay rich in calcite or dolomite and firing temperature higher than 900°C as reported diopside, gehlenite, glassy vitrification and the lack in calcite and mica/illite (Noll, Heimann 2016; Trindade et al. 2009; Vieira Ferreira et al. 2018). The vitrification texture clearly shows, that used raw clay was calcite or dolomite marl enriched also in iron oxide. During the firing, calcium works as a flux and allows to new mineralogical phases to form (e.g. diopside or gehlenite; Noll, Heimann 2016; Trindade et al. 2009).

Group C is enriched in quartz, plagioclase and sometimes in mica/illite. Diopside and gehlenite are almost absent. This fabric was made out from less calcareous clay. The higher presence of mica/illite can be related with the clay fraction with lower amount of calcium than the fabric groups A and B (**Fig. 5.1**). The relative high presence of mica/illite can also reflect a lower firing temperature (Vieira Ferreira et al. 2018; Noll, Heimann 2016). The higher amount of magnesium suggests a dolomitic marl or Mg-clay minerals was used as the raw material, however in this group, the chemical pattern is more variable because of the bigger size of temper (**Table 5**). The variance is noticeable in an amount of quartz obtained by XRD, from predominant to frequent (**Table 4**).

While in some vessels of fabric C a Mg-enriched raw clay was used (**Table 5**) in fabric groups A and B, the higher amount of calcium is evident. The linear correlation between the samples of fabric group A and B readable from the bi-plot graph reveals that clay calcareous-dolomitic marl with similar enrichment in the calcite was used. The fabric C has much lower amount of calcium (**Fig. 5.1**). The material of the temper was very likely already sorted material from the river or sea. In the group A is common intentional bimodality of the temper reached by adding of two different fractions. Whereas fabric C has also bimodal temper, the smaller subangular fragments, containing mainly quartz, were probably present in the used clay as inclusions and only the bigger rounded fraction was added intentionally as the temper. The group B has mainly quartz temper with smaller granulometry than other fabrics and there is not easy to distinguish between clay intrusions and added temper. In the terms of modelling of vessels,

the data commonly report the fast-rotating wheel as the orientation of elongated particles of the temper indicates.

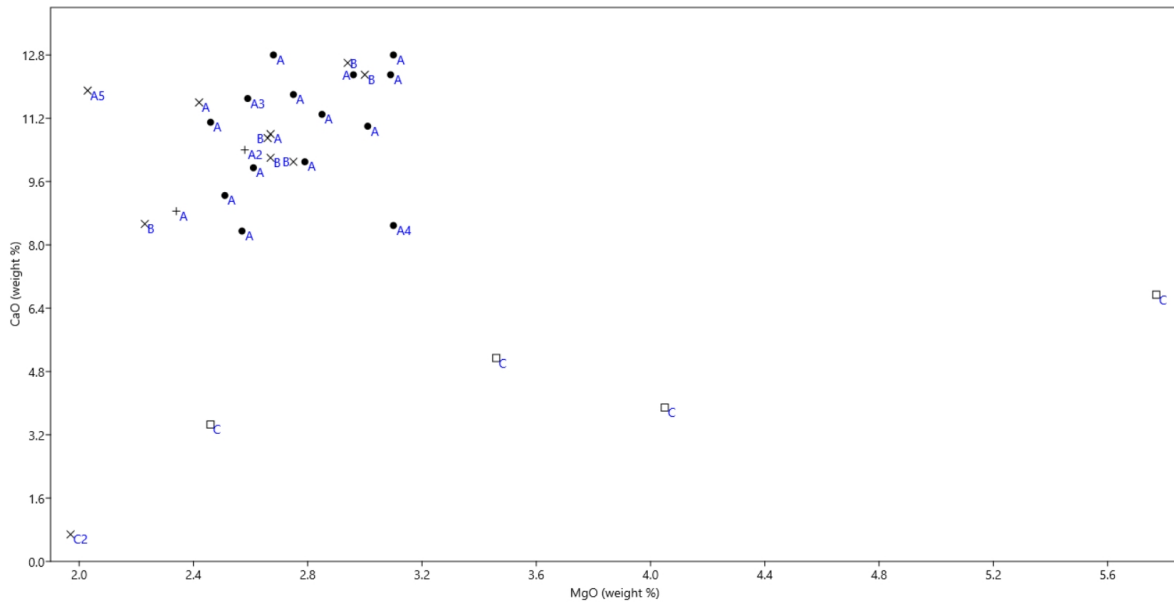


**Fig. 5.1** - Bi-axial graph: MgO and CaO obtained by ED-XRF.

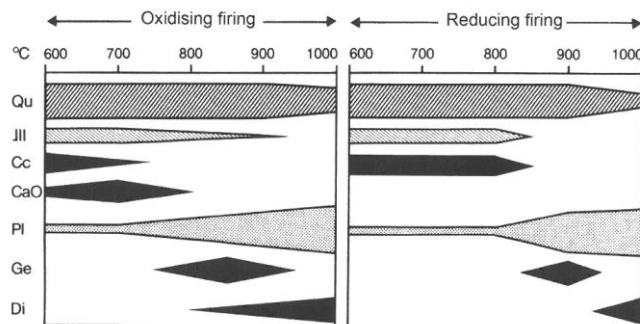


**Fig. 5.2.** – Calcareous rich clays – mineral forming during the firing (after [Noll, Heimann 2016](#)).

The atmosphere and temperature in the ceramic kiln varied as the preservation of calcareous inclusions as limestone, shell or fossils reflect. Depending on the temperature and partially on the oxidizing or redox firing, the calcite intrusions decompose. The difference in the firing regime reflects technological choices. However, this could happen in the same ceramic

workshop. The variance in mineralogical phases can partially reflect the firing conditions (**Fig. 5.2**). In the fabric A the clay with similar raw properties was used (Noll, Heimann 2016), but the variance in size, roundness and composition (i.e. shell temper) of the used temper can be noticed (6 – A4, 9 – A3, 16 – A2, 22 – A5). For instance, the lower firing temperature and oxidizing atmosphere is noticed in sample 22 -A5, Pellicer D, with lots of shells in the temper and frequent abundance of mica/illite (**Table 2-4**).

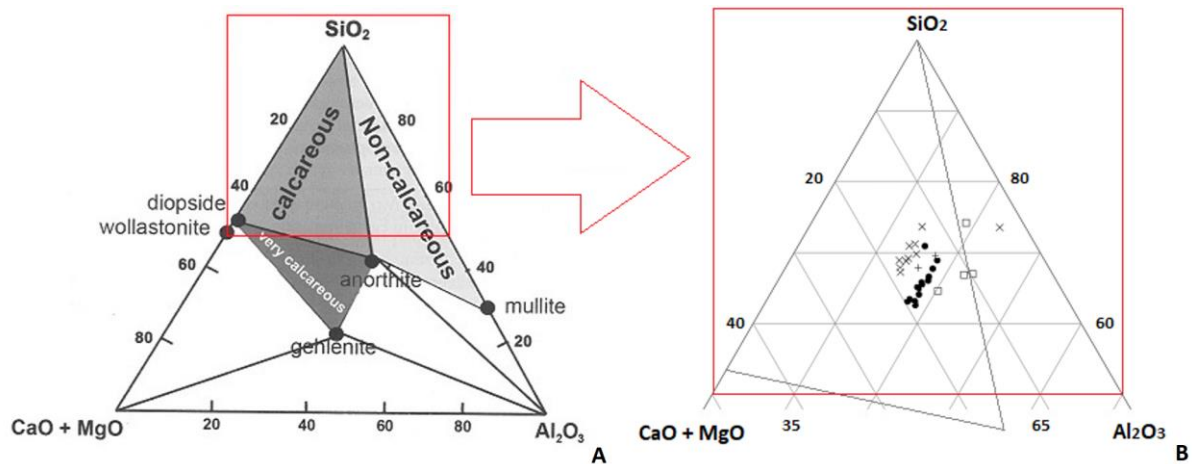


**Fig. 5.3 – A:** Simplified ternary phase diagram  $\text{SiO}_2\text{-Al}_2\text{O}_3\text{-(CaO+MgO)}$  for calcaeous-dolomitic clays (after Noll, Heimann 2016), **B:** Top part of the simplified ternary diagram. Symbols reflect the main archaeological typology (dot – Pellicer B/C, cross – amphorae without protrusion, square – concave bottoms, X – Pellicer D).

The ternary diagram is introduced for the manifestation of differentiation in the presence of CaO with MgO,  $\text{Al}_2\text{O}_3$  and  $\text{SiO}_2$  in calcaeous dolomitic clay (**Fig. 5.3**). In general, the Pellicer B/C have a similar amount of CaO with MgO and a slightly greater presence of  $\text{Al}_2\text{O}_3$ . The local containers have a lower presence of CaO with MgO and a higher amount of  $\text{Al}_2\text{O}_3$ . Sample 30 (C2) is out with the lowest amount of CaO with MgO and the highest abundance of  $\text{Al}_2\text{O}_3$ . Sample 30 was made out from non-calcaeous clay. The percentage of  $\text{SiO}_2$  slightly varies in all groups, but in general, the amount of  $\text{SiO}_2$  among the samples does not show significant deviation. The amount of  $\text{Al}_2\text{O}_3$  partially reflects the ratio of temper/clay but also properties of the clay used (**Fig. 5.3; Table 5**).

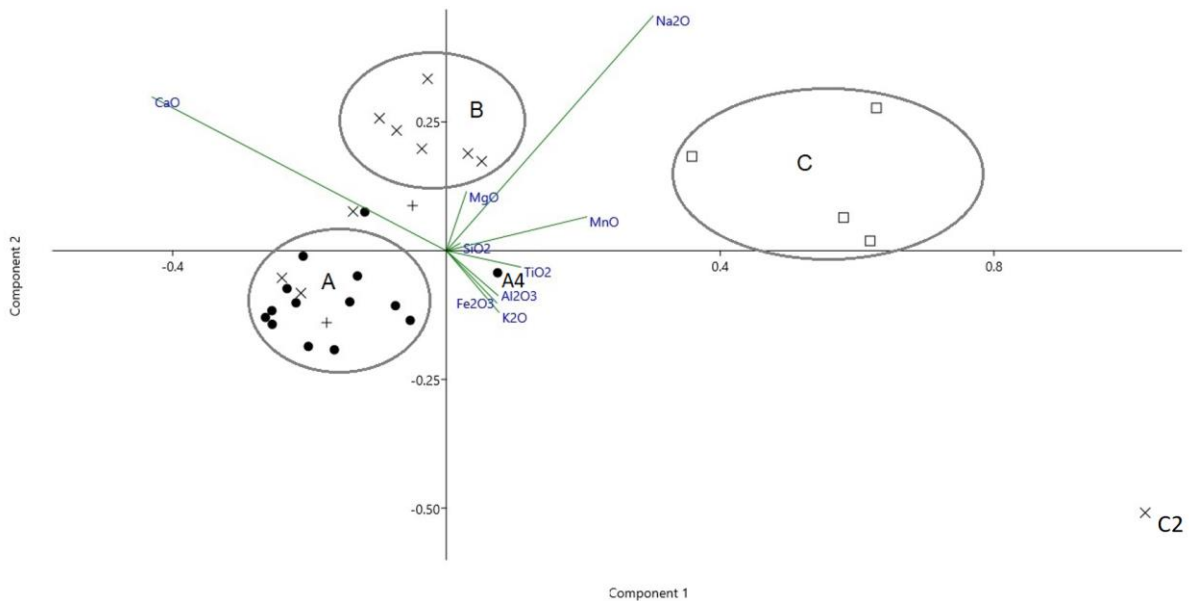


**Fig. 5.4** – Principal component analysis (PCA) of main oxides. The values of oxides were transformed into the logarithmic scale (loading data: **Annex III**), the group of petrographic fabrics marked in circles (**Table 2-5**).

The multivariate statistical analysis (PCA) with major elements provides information regarding the differences in elemental compositions of the samples. The graph presents the variance of the 2 first components. The vectors of oxides (descriptors) are plotted as well. In the orthogonal graph the distribution of objects (samples) reflects the petrography groups (A, B, C). Two outliers are marked as well. The clear chemical outlier is sample 30 (C2; **Fig. 5.4**), due to the sample having the lowest amount of CaO, highest presence of Fe<sub>2</sub>O<sub>3</sub> and K<sub>2</sub>O, and the highest abundance of Al<sub>2</sub>O<sub>3</sub> and Ti<sub>2</sub>O (**Table 5**). Sample 6 (A4) is separated from any group as well, because of variance in the big rounded temper (**Annex I**).

The defined fabric groups point out to various manufacturing traditions in certain types of vessels. Production of amphorae without significant protrusion (II) and of Pellicer B/C (I) is only related with the fabric group A. These amphorae are dated to the same time interval, from 5<sup>th</sup> to 4<sup>th</sup> century BC. In the group is a variability in the temper and the colour of the matrix, but this fabric corresponds to comparable manufacturing traditions and geological settings in terms of raw material. Group B contains only amphorae of the Pellicer D (IV) and variety reports the use of different kinds of marl and temper. The well-sorted temper containing mainly quartz. The firing temperature was higher than in fabric groups A and C.

Fabric group C is represented by all local containers (III) dated to comparable times of existence as ceramic types I and II (from 5<sup>th</sup> to 4<sup>th</sup> century BC). The main characteristics of fabric C are big rounded temper and clay that is less rich in calcite than those in fabrics A and B (**Fig. 5.1**). This can report also diopside and gehlenite content (**Table 4**). Pellicer D amphorae (30 – C2) made out from non-calcareous clay and bimodal temper is associated with this group by similar features in the temper (i.e. volcanic and metamorphic rocks). However, its provenance is probably Cadis (**Table 1-3**).

The younger variant of the amphorae of Phoenician-Punic tradition, the amphorae Pellicer D is partially associated with all fabric groups. Analysed samples of Pellicer D are dated to the 1<sup>st</sup> century BC. The different manufacturing traditions presented in this ceramic type could be associated with more places of its production. The younger Pellicer D, so called coastal type, was made in the Lower Guadalquivir, but probably also in other sites around Cadiz bay area as the different fabric groups can report ([Megías 2017](#)). After the similar geology in all study area and the identified temper inclusions obtained from sediments of lower streams or seaside, it is not possible to distinguish clear provenance. The particles of analysed feldspars by EDS do not reflect any meaningful difference between the fabric groups or ceramic types.

Some analogies for samples from groups A and B are found among the Pellicer B/C and D amphorae already evaluated from the Lower Guadalquivir region ([Megías 2017](#)). That points out to this region importance, especially the area around Seville, in their production, supporting the hypothesis that amphorae of Pellicer B/C found in the Castro Marim site have their origin in the Lower Guadalquivir region. Although, after the geological setting of the Castro Marim, the amphorae of the fabric groups A and B (I, II, IV) could be made also there. The geology of Castro Marim can be associated with the provenance of these amphorae, but the local containers are distinctive in the fabric C. This stress the difference between local and imported ceramic, however of local common ware are only one ceramic type analysed and predefined as the local. For better understanding of the ceramic production in the Castro Marim, in further research other local vessels should be analysed. The variance in preferable and used raw material as technological choices can be also associated only with this specific ceramic type tradition of the local common wares with the concave bottoms.

## 5.2. Content of vessels

Before starting the discussion of the GC-MS data there are information regarding samples selected for analysis that should be emphasized. The 8 shards selected for analysis of contents were the following: five Pellicer amphorae B/C (3, 6, 8, 9, 10), two local common wares (17, 20) and one amphora without protrusion (15). These samples were : 1) excavated and collected from field works which took place almost 20 years ago, 2) come from an archaeological site that was extensively settled in more recent times (e.g. Islamic period, Middle age castle and Modern time), 3) secondary precipitation of carbonates, possibly iron oxides and chemical processes occurring in the ground were detected in the ceramic by petrography of thin sections and SEM-EDS, 4) shards were washed and treated in the archaeological laboratory (i.e. labelling) and later stored in a depositary without controlled atmosphere. All of these processes, both during burial and post-excavation, can affect the organic residue analysis, with added contaminants or leaching out of organic molecules.

Internal standard and the products of the derivatization were clearly identified in all samples, suggesting an effective extraction and derivatization procedures. From the eight analysed samples, only in five of them (3, 6, 9, 10, 20) the compounds identified could be related with the past content of the vessels. In other three samples (8, 15, 17), except some compounds associated with a recent contamination (e.g. a handling by naked hands, plasticizers from packing material, etc.), no other relevant compounds could be associated with possible past contents. A list of the compounds identified in samples 3, 6, 9, 10, 20 is presented in **Table 6**. Figure 35 A and B shows the chromatograms for samples 6 and 20, where the identification of the individual peaks is presented. A weird feature, difficult to explain, is the absolute absence of free fatty acids, neither saturated nor unsaturated, in all the analysed samples with the exception of sample 6. MAG's 16:0 and 18:0 are detected in the samples, but no traces of fatty acids were identified. Esters and terpenoids in general (including plant and animal sterols), are missing from the chromatograms as well (**Fig. 5.5, Table 6**).

In the sample 6, several saturated fatty acids (from C8 to C18), MAG's (C18 and C16), alcohols (even carbon numbered, C18, C26, C30 and C32) and alkanes (uneven carbon numbered, from C19 and C31) were detected. As stated before, sample 6 is unique among the analysed set, because several free fatty acids are detected. The presence of the shorter chain fatty acids

(C6:0, C8:0, C9:0, C:10, C:12 and C:14) could hypothetically be associated with a storage of dairy products. However, other compounds which can be related with a milk product, namely cholesterol and derivatives, branched fatty acids and uneven fatty acids (C15 and C17), are all missing. To prove the hypothesis related with the presence of dairy products in the vessel further analysis is necessary, e.g. by GC-IRMS to get the ratio between carbon isotopes for the C16:0 and C18:0 fatty acids (Dune et al. 2017; Roffer-Salque et al. 2017).

Apart from the fact that fatty acids are missing, sample 20 contains a similar pattern of longer chain alcohols and alkanes as in sample 6. The abundance of odd carbon numbered n-alkanes as well as the prominent presence of longer chain alcohols with an even number of carbon atoms, is an important pattern, and it is significantly different to what is observed in samples 3 and 9. The long chain compounds in samples 6 and 20 are likely related with beeswax used as a sealant for the walls in the ceramic to protect it from leaking a liquid. Although, wax esters (i.e. C46 and C48) are missing, the chromatograms for samples 6 and 20 are comparable to samples that had already been obtained from other archaeological contexts, and in which beeswax was identified (Roffet-Salque et al. 2015). The wax esters in these two samples could have decayed throughout time, yielding long chain alcohols and palmitic or 15-hydroxypalmitic acids, both acids surprisingly absent from the chromatogram of sample 6. The identification of beeswax residues is further proven by the relative ratio between n-alkane C25 and C27, where the C27 peak area is clearly higher than that of C25, whereas the opposite is typical for wax obtained from plant leaf material (Fig. 5.5; Dune et al. 2017; Roffet-Salque et al. 2017; 2015). The presence of beeswax residues indicates a possible usage of the vessels 6 and 20 for storage of liquid products.

Samples 9 and 10 contain MAG's alcohols and alkanes as well, but the longer chain alcohols or alkanes, as observed in samples 6 and 20, are absent. Except for MAG's (14:0, 16:0 and 18:0), we could only identify relatively shorter chain alcohol compounds (C14:OH, C16:OH and C18:OH) and n-alkanes, with the number of carbons going up to C27 in sample 9. Sample 9 yielded slightly more compounds than sample 3, but their pattern is very similar. The presence of only relatively shorter even numbered alcohols and shorter n-alkanes likely points to a plant material origin; however, and again, the fatty acids are strangely missing. Sample 3 contain only n-alkanes up to C25. In sample n-alkanes C25 and C27 are present, but in this



The samples without detectable free fatty acids, observation that we cannot explain, but the fact that the samples had been washed previously can partially account for this issue. To get more information from the analysed samples other extraction method or a re-run of the samples with the mass spectrometer on SIM (single ion monitoring) mode should be done. The acidic extraction method ([Correa-Ascencio, Evershed 2014](#)) is more aggressive and it will lead to the hydrolysis of the MAG compounds, but it is possible that the more effective extraction will yield other free fatty acids. The SIM mode is a more sensitive analytical method, and if  $m/z$  74 ion is chosen then, even if only minute amounts of the fatty acids are present in the extract, peaks will be observed in the chromatograms. Fatty acid Identification will be made based on their retention time, as no mass spectra will be available for the individual compounds when the mass spectrometer is run in SIM mode.

There is a previous publication on the organic contents of amphora Peliccer B/C and D typologies ([Garcia-Fernandez et al. 2017](#)). The authors extracted a total of 31 samples unearthed from the Guadalquivir valley using methanol with sodium hydroxide at 70°C. This is an extraction methodology rarely used, but useful to recover compounds hard to remove from the ceramic body like diacids, which arise from oxidation of unsaturated fatty acids. When applied, this methodology can complement the information gathered with the organic solvent extraction used in this work. Despite the methodology used, authors reported only the presence of fatty acids, saturated and unsaturated, in the samples. Relations between the peak areas of the fatty acids and fatty acids and squalene (a contaminant from ceramic handling) are reported in order to attempt to conclude about the previous contents of the amphorae. The authors conclude that some amphorae were used for olive oil, while others had been used for cured meat and milk by-products, but the chemical basis for these conclusions are not sound.

## Conclusion

The multianalytical protocol implemented in this material study shows the differences between four ceramic types (i.e. Pellicer amphorae B/C, Pellicer amphorae D, amphorae without protrusion and local common wares) and reveal the presence of three fabric groups: A, B and C. The XRD and ED-XRF complemented the information obtained by the petrographic study. The variability in mineralogical phases detected by XRD and chemical composition of the bulk ceramic samples points out the results of petrography and the general character of matrix and temper. The SEM-EDS complements the information and reveals various chemical compositions of the matrix and temper. The fabric groups reflect the different raw materials (clay, temper and their ratio) and some technological specifics.

In general, the geological setting of the Castro Marim and the expected production region of the Pellicer amphorae B/C and D (i.e. Lower Guadalquivir valley and Cadiz area) is similar. The region of Castro Marim as well as the Lower Guadalquivir have presented comparable calcareous dolomitic clays so called marl and clastic sediments from the erosion of hercynian massif. Therefore, in the term of provenance is not possible to objectively distinguish at the base of geological setting of Castro Marim, which fabric groups are local, and which one is related with the imported amphorae. However, the fabric group C represented basically by local common wares suggest the main manufacturing tradition represented in the Castro Marim. The main fabric group A is associated with Pellicer amphorae B/C and amphorae without the protrusion and it is dated to same interval as local common wares (from 5th to 4th century BC). The fabric group B is restricted to 6 samples of younger type Pellicer D dated to 1st century BC. Although, the type Pellicer D present also fabric of group A (3 samples) and C (1 sample). This is related with wide spread of this ceramic type and its production in several centres or regions.

We conclude that firing temperature in the fabric group A was lower than 900°C in oxidizing atmosphere besides some observed variation in temperature regime. It is known ([Megías 2017](#)) that amphorae of Pellicer B/C were produced in more than one workshop. Although the comparable raw materials can be find in the Castro Marim as well, the technical choices of fabric group A reflect the same tradition and probably the same source.

The fabric group B reports higher firing temperature than 900°C as reflect the glassy vitrification. To obtain a vitrification of the ceramic in the ancient double chamber kiln, marl or other clay rich in calcite or dolomite must be used. The calcite works as a flux and allows to form new mineralogical phases (e. g. diopside and gehlenite) in lower temperature. The well-sorted smaller temper (i.e. quartz) and the higher estimated firing temperature suggest that the fabric group B is a ceramic with better final quality than fabric groups A and C. This fabric group is younger and probably, reflects improvements in technology.

For the fabric group C can be concluded slightly lower firing temperature, but the used clay is less enriched in calcite than in the fabric A and B. The clay naturally present smaller subangular quartz inclusions. Bigger rounded grains of temper were added.

The sample 30 (– C2) Pellicer D was identified as clear outlier. This amphora was produced with non-calcareous clay, what reveal a different chemical and mineralogical composition not identified in any other vessel.

Concerning the GC-MS study, five analysed samples reflect the possible residue of past content: four Pellicer B/C (3 – A, 6 – A4, 9 – A3, 10 – A) and one local common ware (20 – C). The residues identified in the Pellicer B/C can report imported edible commodities, however, there is a problem with possible reuse of amphorae. The compound identified by GC-MS show the presence of MAG's, alcohols and alkanes in all samples, but the fatty acids except the one sample of Pellicer B/C (6 – A4) are not detected. This strange fact we cannot sufficiently explain. In future other more aggressive acidic based extraction methods should be used to obtain more information from the samples. The short chain saturated fatty acids suggest in the sample 6 a storage of dairy products, but not all compounds typical of milk products are detected. The presence of a dairy product can in future prove additional IR-GC-MS analysis.

Except for sample 3 where only MAG's are present, other four samples reveal a distinctive pattern between the even and non-even numbers of alkanes and alcohols. The presence of beeswax residues indicates a possible usage of the vessels 6 (A4) and 20 (C) for the manipulation of liquid products. The beeswax was used in ancient times as the sealant. The data obtained from other 2 samples can be associated only with the plant leaves wax material.

It is likely that in these amphorae some solid plant material was stored, like cereals, which would not have yielded large amounts of fat molecules into the ceramic body.

In future research the same multianalytical approach must be applied to more similar vessels in order to get a detailed picture of their production (i.e. raw materials and technology) characteristics. It is expected that the data can contribute to revealing the relations between the different settlements in Punic times. The analysis of other ceramic materials from Castro Marim will lead to distinguishing more relations between local fabric tradition and the character of imported vessels. Further systematic study based on similar methodical approach should discover more about the imported food products and commercial interaction in the Castro Marim site during the Second Iron Age.

## Literature

Arruda, A. M. (1996) – O Castelo de Castro Marim. In *De Ulisses a Viriato. O primeiro milénio a.C.*. Lisboa: Ministério da Cultura, Instituto Português de Museus, Museu Nacional de Arqueologia, 95-100.

Arruda, A. M. (2000) – As cerâmicas de importação do Castelo de Castro Marim no âmbito do comércio Ocidental dos séculos V a III a.C. *Actas del IV Congreso Internacional de Estudios Fenícios y Púnicos*. Servicio de publicaciones de la Universidad de Cádiz. Cádiz, 727-735.

Arruda, A. M. (2009) – Phoenician Colonization on the Atlantic Coast of the Iberian Peninsula. In Dietler, M., López-Ruiz, C. (eds.) *Colonial Encounters in Ancient Iberia: Phoenician, Greek and Indigenous Relations*. Chicago 2009, 113-130.

Arruda, A. M., Freitas, V. T. (2008) – O Castelo de Castro Marim durante os séculos VI e V a.n.e.. In: Jiménez Ávila, J. (ed.) *Sidereum Ana I: El río Guadiana en Época Post-Orientalizante*, Madrid 2008, 429-446.

Arruda, A. M., Oliveira, F., Teixeira de Freitas, V., Soares, A., Manuel Martins, J., Portela, P. (2014) – A cronologia relativa e absoluta da ocupação sidérica do Castelo de Castro Marim. *SAGVNTVM. Papeles del Laboratorio de Arqueología de Valencia* 45 (2013), 100-114.

Arruda, A. M., Viegas, C., Bargão, P., Pereira, R. (2006) – A importação de preparados de peixe em Castro Marim: da Idade do Ferro à Época Romana. *Setúbal Arqueológica* 13, 153-176.

Artioli, G., 2010. *Scientific Methods and Cultural Heritage: An Introduction to the Application of Materials Science to Archaeometry and Conservation Science*. Oxford: Oxford University Press, 2010.

Aubert, M. E. (1995) – From trading post to town in the Phoenician-Punic world. In Cunliffe, B., Keay, S. (eds.) *Social Complexity and the Development of Towns in Iberia, From the Copper Age to the Second Century AD*. *Proceeding of British Academy* 86, 47-65.

Bannert, T. (2017) – *Studium růstu ZnO krystalů ze supersaturovaného alkalického elektrolytu*. Diploma thesis, Brno University of Technology. Brno, 2017.

Bargão, P., Arruda, A. M. (2014) – The Castro Marim 1 Amphora Type: A West Mediterranean Production Inspired by Carthaginian Models. *Carthage studies* 8, 143-160.

Barker, A., J. (2014) - *A Key for Identification of Rock-forming Minerals in Thin-Section citation*. London, 2014.

Barnard, H., Eerkens, J. (2017) – Assessing Vessel Function by Organic Residue Analysis. In Hunt, A. (ed.) *Oxford Handbook of Archaeological Ceramic Analysis*. Oxford University Press, 2017.

Beckhoff, B., Kanngießner, B., Langhoff, N., Wedell, R., Wolff, H. (2006) – Handbook of Practical X-Ray Fluorescence Analysis. Springer, 2006.

Buxeda i Garrigós, J., Madrid Fernández, M. (2016) – Designing Rigorous Research: Integrating Science and Archaeology. In Hunt, A. (ed.) Oxford Handbook of Archaeological Ceramic Analysis. Oxford University Press, 2017.

Carlson, D. (2017) – Quantitative Methods in Archaeology Using R. Cambridge: Cambridge University Press, 2017.

Chic García, G., García Vargas, E. (2004) – Alfares y producciones cerámicas en la provincia de Sevilla. Balance y perspectivas. In Lagóstena, L., Bernal, D. (eds.) Actas del Congreso Internacional Figlinae Baeticae. Talleres Alfareros y Producciones Cerámicas en la Bética Romana (ss. II a.C. – VII d.C.). Cádiz, 12-14 de noviembre de 2003. BAR International Series 1266, 279-348.

Correa-Ascencio, M., Evershed, R. (2014) – High throughput screening of organic residues in archaeological potsherds using direct acidified methanol extraction. Analytical Methods 6-5.

Cuomo di Caprio, N. (2007) – Ceramica in Archeologia 2. Antiche tecniche di lavorazione e moderni metodi di indagine. Studia Archaeologica 144. Roma, 2007.

Dietler, M. (2009) – Colonial Encounters in Iberia and the Western Mediterranean: An Exploratory Framework. In Dietler, M., López-Ruiz, C. (eds.) Colonial Encounters in Ancient Iberia: Phoenician, Greek and Indigenous Relations. Chicago 2009, 3-48.

Dunne, J., Evershed, R., Heron, C., Brettell, R., Barclay, A., Smyth, J., Cramp, L. (2017) – Organic Residue Analysis and Archaeology Guidance for Good Practice. Historic England, 2017.

Emwas, AH., M., Al-Talla, Z., A., Yang, Y., Kharbatia, N., M. (2015) – Gas Chromatography–Mass Spectrometry of Biofluids and Extracts. In Bjerrum, J. (ed.) Metabonomics. Methods in Molecular Biology 1277. Humana Press, New York, 2015, 91-112.

Evershed, R. P. (2008) – Organic residue analysis in archaeology: The archaeological biomarker revolution. Archaeometry 50(6), 895-924.

Fernandez, M., Berastegui, X., Puig, C., Garcia-Castellanos, D., Jurado, M. J., Torne, M., Banks, C. (1998) – Geophysical and geological constraints on the evolution of the Guadalquivir foreland basin, Spain. Geological Society, London, Special Publications 134, 29-48.

Fletcher, W. J. (2005) – Holocene Landscape History of Southern Portugal. Doctoral thesis: University of Cambridge, 2005.

Freestone, I., C. (2001) – Post-depositional Changes in Archaeological Ceramics and Glasses. In Brothwell, D., R., Pollard, A., M. (eds.), Handbook of archaeological science, New York: Wiley, 615-625.

Galán Huertos, E., González Díez, I., Mayoral Alfaro, E., Miras Ruiz, A. (1985) – Las moronitas de las hojas geológicas de Carmona (Sevilla), Jerez de la Frontera y Sanlúcar de Barrameda (Cádiz). Estudio de caracterización. Informe INGEMISA. Sevilla 1985.

García Fernández, F. J., García Vargas, E. (2012) – “Los hornos alfareros de tradición fenicia en el valle del Guadalquivir y su perduración en época romana: aspectos tecnológicos y sociales”. SPAL Revista de Prehistoria y Arqueología de la Universidad de Sevilla 21, 9-38.

García-Fernández, F. J. (2019) – Rumbo a poniente: el comercio de ánforas turdetanas en la costa atlántica de la península ibérica (siglos V-I a. C.) / Westbound: trade in Turdetanian amphorae on the Atlantic coast of the Iberian Peninsula (V-I centuries BC). *Archivo Español de Arqueología* 92 (2019), 119-153.

García-Fernández, F. J. (2009) – As ânforas do tipo B/C de Pellicer no Castelo de Castro Marim. Master thesis: University of Lisbon, 2009.

García-Fernández, F. J. (2015) – Living in the far West: Tradition and Innovation in Turdetania between Late Iron Age and Romanisation. In Danielisová, A., Fernández-Götz, M. (eds) *Persistent Economic Ways of Living. Production, Distribution, and Consumption in Late Prehistory and Early History*. Budapest, 2015, 223-241.

García-Fernández, F. J., Albelda, E. F., Mateos, A., Durán-Barrantes, M. M. (2017). Análisis de residuos orgánicos y posibles contenidos en ánforas púnicas y turdetanas procedentes del valle del Guadalquivir. *SAGVNTVM. Papeles del Laboratorio de Arqueología de Valencia* 48 (2016), 59-87.

Grotzinger, J., Thomas H. Jordan, T. H., Press, F., Siever, R. (2006) - *Understanding Earth*. Fifth edition. New York, 2006.

Heimann, R. B., Maggetti, M. (2014) – *Ancient and Historical Ceramics*. Stuttgart: Schweizerbart Science Publishers, 2014.

Heiri, O., Lotter, A., Lemcke, G. (2001) – Loss on ignition as a method for estimating organic and carbonate content. *Journal of Paleolimnology* 25, 101-110.

Hložek, M. (2012) – *Multidisciplinární technologická analýza neolitické keramiky*. Doctoral thesis: Masaryk University in Brno. Brno, 2012.

Hoffmann, E., Stroobant, V. (2007) – *Mass Spectrometry: Principles and Applications*. Wiley, 2007.

Megías, V. M. (2017) – *Del campo a la ciudad: Producción y comercialización de recipientes anfóricos en el bajo Guadalquivir durante la II Edad del Hierro*. Dissertation thesis: University of Sevilla, 2017.

- Moldoveanu, S. C., David, V. (2018) – Derivatization Methods in GC and GC/MS. In Gas Chromatography - Derivatization, Sample Preparation, Application (working title), 2018. <https://www.intechopen.com/online-first/derivatization-methods-in-gc-and-gc-ms> (1.9.2019)
- Montealegre Contreras, L., Barrios Neira, J. (1996) – Mineralogy of clays in sediments from Neogene deposits in the Guadalquivir Depression (Spain). In Ortega, M., López e I. Palomo, A. (eds.) *Advances in Clay Minerals*, Granada, 1996, 150-152.
- Morales, J. A. (1997) – Evolution and facies architecture of the mesotidal Guadiana River delta (S.W. Spain-Portugal), *Marine Geology* 138, 127-148.
- Moura, D., Gomes, A., Mendes, I., Anibal, J. (2017) – Guadiana River Estuary - Investigating the past, present and future. CIMA, University of Algarve, 2017.
- Mukherjee, A., J., Gibson, A., M., Evershed, R., P. (2008) – Trends in pig product processing at British Neolithic Grooved Ware sites traced through organic residues in potsherds. *Journal of Archaeological Science* 35, 2059-2073.
- Nodari, L., Marcuz, E., Maritan, L., Mazzoli, C., Russo, U. (2007) – Hematite nucleation and growth in the firing of carbonate-rich clay for pottery production. *Journal of the European Ceramic Society* 27, 4665-4673.
- Noll, W., Heimann, B. R. (2016) – *Ancient Old World Pottery: Materials, Technology, and Decoration*. Schweizerbart Science Publishers, 2016.
- Oliveira, J. T. et al. (1982) – Carta Geológica de Portugal, escala 1:200000. Notícia Explicativa da Folha 8. Serviço Geológico de Portugal, Lisboa, 1982.
- Pellicer Catalán, M. (1978) – Tipología y cronología de las ánforas prerromanas del Guadalquivir, según el Cerro Macareno (Sevilla). *Habis* 9, 365-400.
- Petřík, J. (2017) – Petroarchaeological research of ceramic production in the area of Western Carpathians at the end of the Early Bronze Age. Doctoral thesis: Masaryk University in Brno., Brno, 2017.
- Pollard, M., Batt, C., Stern, B. e Young, S. M. M. (2007) – *Analytical Chemistry in Archaeology*. United States of America: Cambridge University Press, 2007.
- Quinn, P. S. (2013) – *Ceramic petrography: The interpretation of archaeological pottery & related artefacts in thin section*. Oxford: Archaeopress, 2013.
- Rahman, M., Abd El-Aty, A., M., Choi, J., Shin, H., Chul Shin, S., Shim, J. H. (2015) – Basic Overview on Gas Chromatography Columns. In Anderson, J., Berthod, A., Pino, V., Stalcup, A. (eds). *Analytical Separation Science*. Weinheim: Wiley, 2015, 823-834.

Ramón Torres, J. (1995) – Las ánforas fenicio-púnicas del Mediterráneo Central y Occidental. Colección Instrumenta 2. Barcelona, 1995.

Renfrew, S., Bahn, P. (2012) – *Archaeology: Theories, Methods and Practice*, New York: Thames and Hudson, 2012.

Riccardi, M. P., Messiga, B., Duminuco, P. (1999) – An approach to the dynamics of clay firing. *Applied Clay Science* 15 (3-4), 393-409.

Roffet-Salque, M., Dunne, J., Altoft, D. T., Casanova, E., Cramp, L. J. E., Smyth, J., Whelton, H. L., Evershed, R. (2017) – From the inside out: Upscaling organic residue analyses of archaeological ceramics. *Journal of Archaeological Science: Reports* 16, 627-640.

Roffet-Salque, M., Regert, M., Evershed, R., Outram, A., Cramp, L., Decavallas, O., Dunne, J., Gerbault, P., Mileto, S., Mirabaud, S., Pääkkönen, M., Smyth, J., Soberl, L., Whelton, H., Alday, A., Asplund, H., Bartkowiak, M., Bayer-Niemeier, E., Belhouchet, L., Zoughlami, J. (2015) – Widespread Exploitation of The Honeybee by Early Neolithic Farmers. *Nature* 534.

Romariz, C., Almeida, C., Oliveira, M. (1979) – Contributions to the geology of Algarve (Portugal) II-Volcanic structures in eastern Algarve (Portugal). *Boletim do Museu e Laboratório Mineralógico e Geológico da Faculdade de Ciências, Universidade de Lisboa* 16, 253-263.

Romero Sáez, A. M. (2018) – Apuntes sobre las dinámicas comerciales de Gadir entre los siglos VI y III a.C. *Gerión* 36 (1), 11-40.

Romero Sáez, A. M., Niveau de Villedary, A. M. (2016) – Pellicer D (Baetica Ulterior coast), Amphorae ex Hispania. Landscapes of production and consumption. <http://amphorae.icac.cat/amphora/pellicer-d-baetica-ulterior-coast> (20. 7. 2016).

Roux, V. (2017) – Ceramic manufacture: the chaîne opératoire approach. In Hunt, A. (ed.) *Oxford Handbook of Archaeological Ceramic Analysis*. Oxford University Press, 2017.

Salvany, J. M., Larrasoña, J. C., Mediavilla, C., Rebollo, A. (2011) – Chronology and tectono-sedimentary evolution of the Upper Pliocene to Quaternary deposits of the lower Guadalquivir foreland basin, SW Spain. *Sedimentary Geology* 241, 22-39.

Schiavon, N., Soria, V., Arruda, A., Beltrame, M., Mirao, J. (2015) – “Losanga” decorated Imitations of Italic Late Republican Black Gloss Tableware from South-Western Iberia: a Multi-analytical/Microchemical Characterization. *Microchemical Journal* 124, 712-718.

Shephard, A. O. (1985) – *Ceramics for the archaeologist*. Washington, 1985.

Sillar, B., Tite, M. S. (2000) – The challenge of ‘Technological Choices’ for Materials Science Approaches in Archaeology. *Archaeometry* 42, 2–20.

South, S. (1968) – Archaeological Evidence of Pottery Repairing. Conference on Historic Site Archaeology Papers 2 (1), 62-71.

Stuart, B., 2007. Analytical techniques in materials conservation. New York: Wiley.

Tite, M. S. (1999) – Pottery production, distribution and consumption: the contribution of the physical sciences. *Journal of Archaeological Method and Theory* 6 (3), 181-233.

Tite, M. S. (2008) – Ceramic production, provenance and use – a review. *Archaeometry* 50 (2), 216-231.

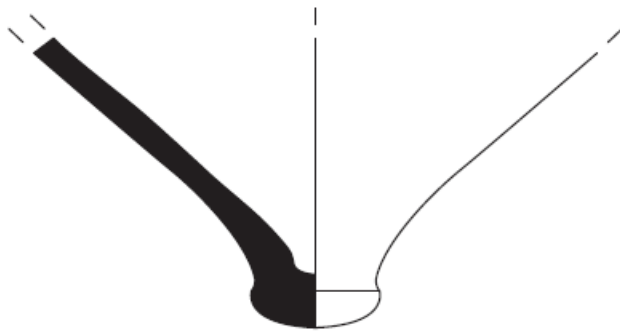
Trindade, M. J., Dias, M. I., Coroado, J., Rocha, F. (2009) – Mineralogical transformations of calcareous rich clays with firing: A comparative study between calcite and dolomite rich clays from Algarve, Portugal. *Applied Clay Science* 42 (3-4), 345-355.

Vargas, E. G. (2016) – Pellicer D (Guadalquivir Valley), Amphorae ex Hispania. Landscapes of production and consumption. <http://amphorae.icac.cat/amphora/pellicer-d-guadalquivir-valley> (20. 7. 2016).

Vieira Ferreira, L. F., Barros, L., Ferreira Machado, I., Gonzalez, A., Pereira, M., Casimiro, T. (2018) – Spectroscopic characterization of amphorae from the 8th to the 7th c. BCE found at the Almaraz settlement in Almada, Portugal. *Journal of Archaeological Science: Reports* 21, 166-174.

Villalobos Megía, M., Pérez Muñoz, A. B. (2006) – Geodiversidad y patrimonio geológico de Andalucía: itinerario geológico por Andalucía: guía didáctica de campo. Consejería de Medio Ambiente. Séville, 2006.

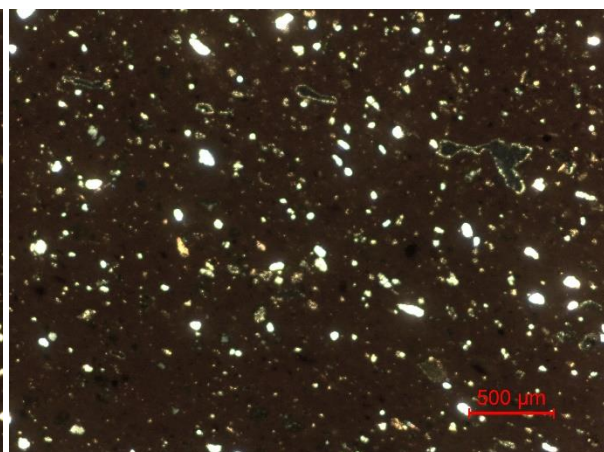
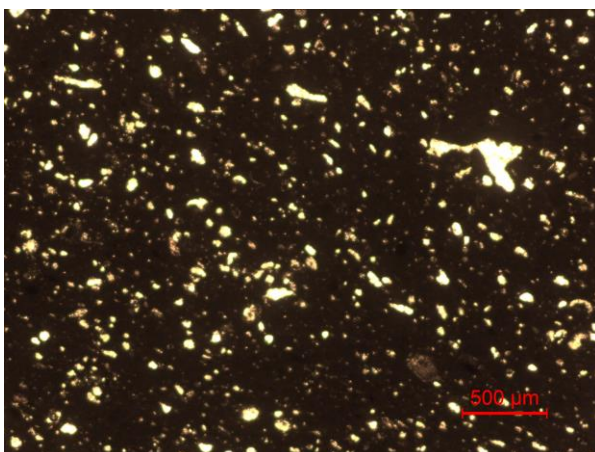
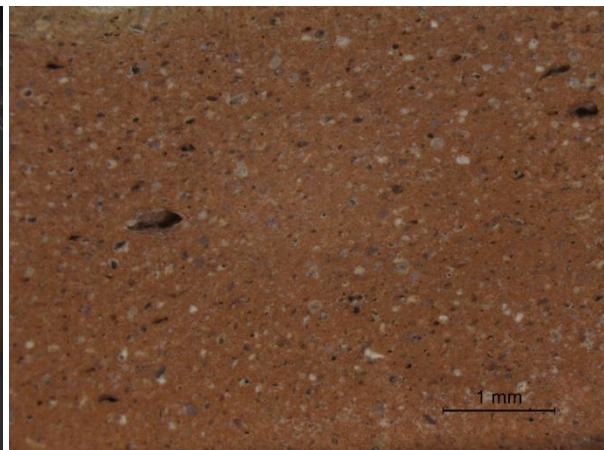
Annex I



1259 [52] - sem contexto  
Produção Guadalquivir  
Pellicer B/C

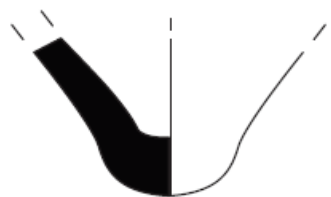


10 cm



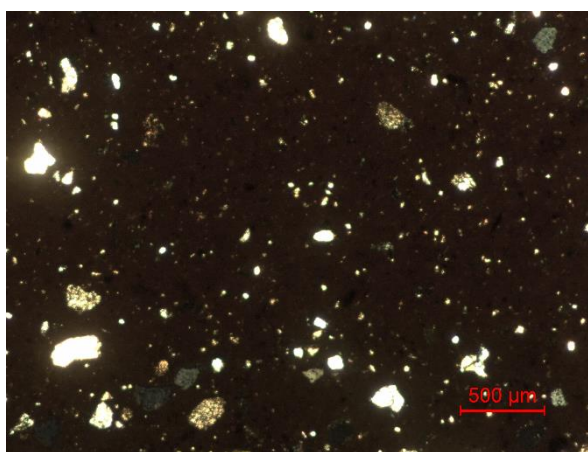
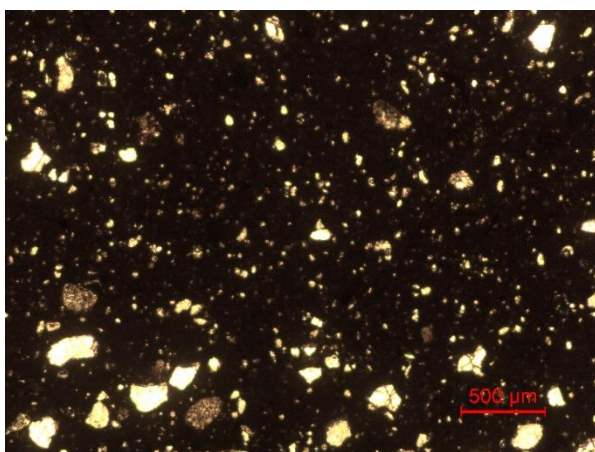
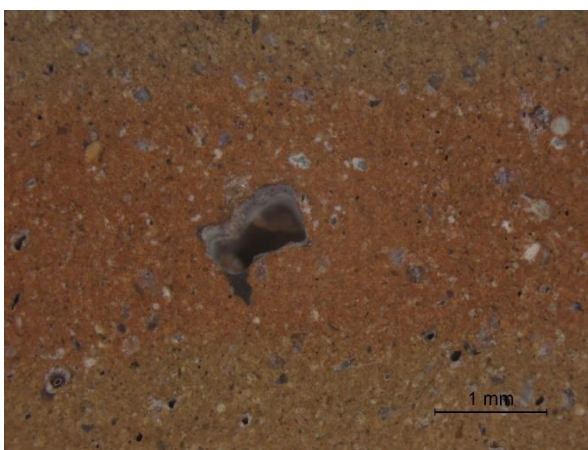
**Sample 1** – drawing and arch. info (1), shard photo (2), cross section (3, 4), thin section (5, 6).

Inventory number: 1259, Year of excavation: 2000, Archaeological context: 1[52]



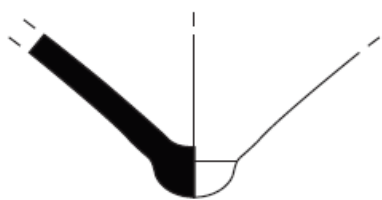
7110 [584] - séc. V/IV  
Produção Guadalquivir  
Pellicer B/C

10 cm



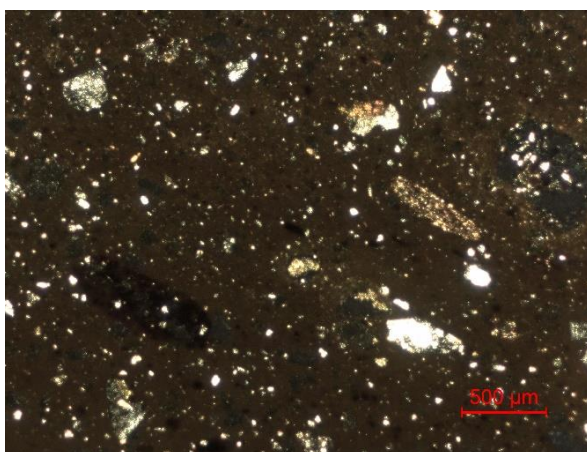
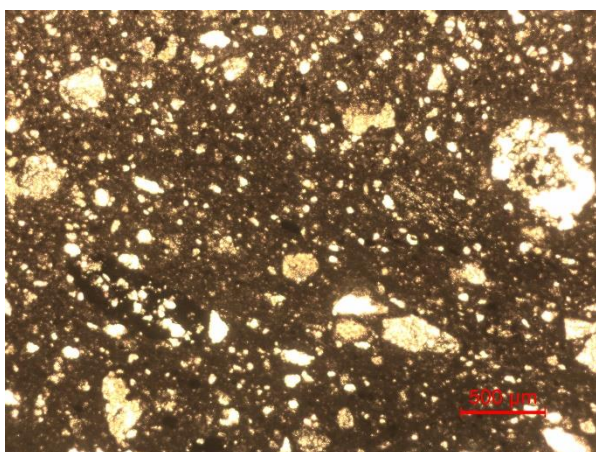
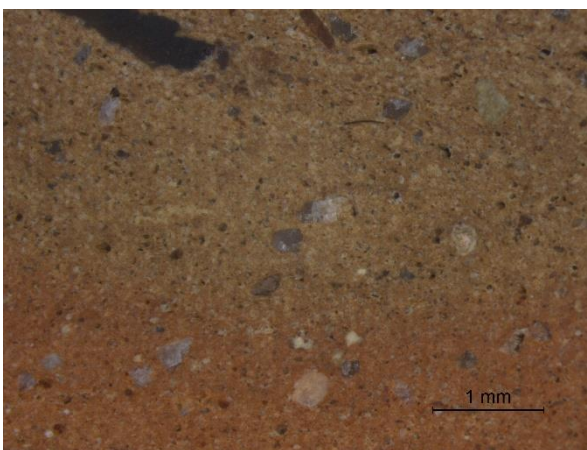
**Sample 2** – drawing and arch. info (1), shard photo (2), cross section (3, 4), thin section (5, 6).

Inventory number: 7110, Year of excavation: 2002, Archaeological context: 1[584]



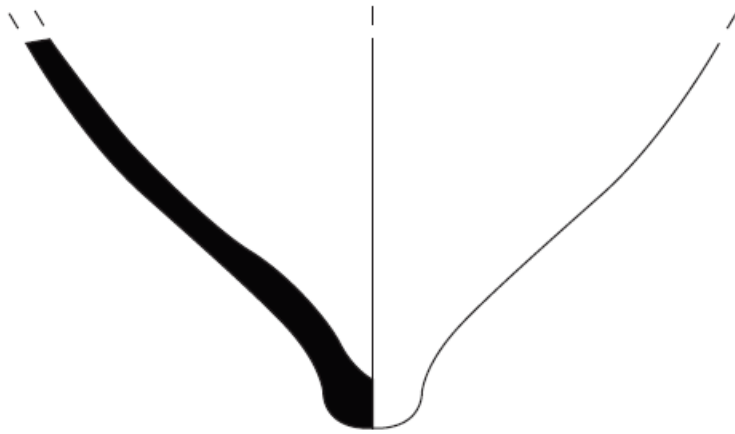
9010 [497] - 2ª metade séc. V a.C.  
Produção Guadalquivir  
Pellicer B/C

10 cm



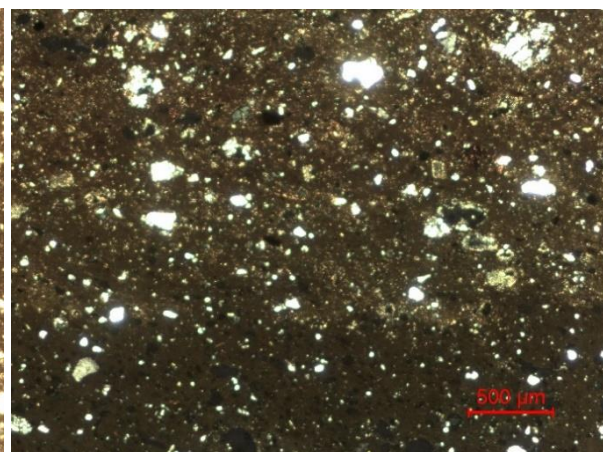
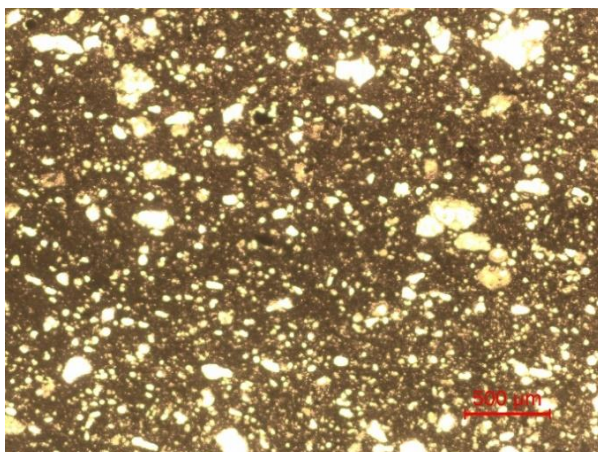
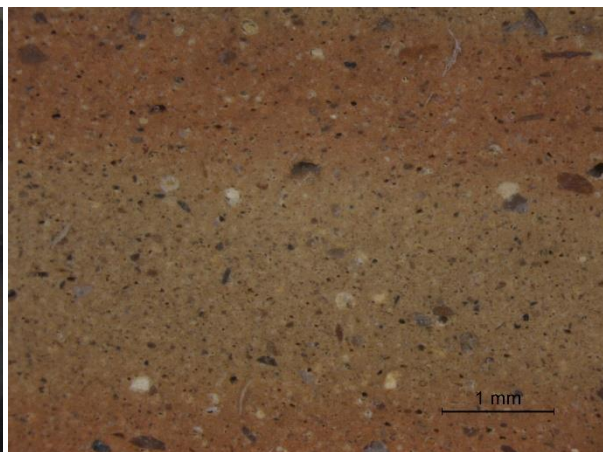
**Sample 3** – drawing and arch. info (1), shard photo (2), cross section (3, 4), thin section (5, 6).

Inventory number: 9010, Year of excavation: 2002, Archaeological context: 1[497]



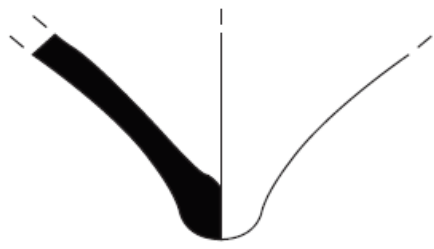
12356 [783] - 2ª séc. V  
Produção Guadalquivir  
Pellicer B/C

10 cm

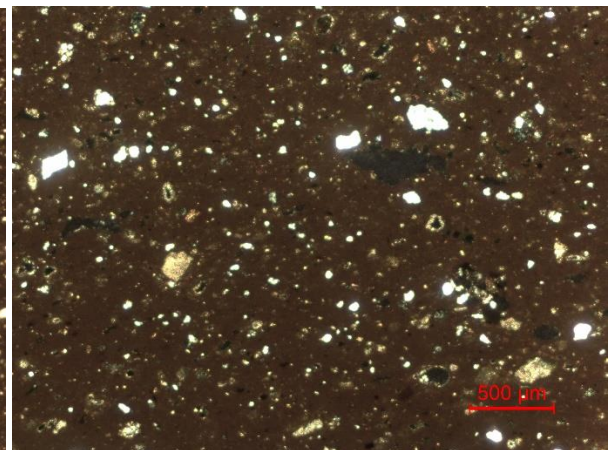
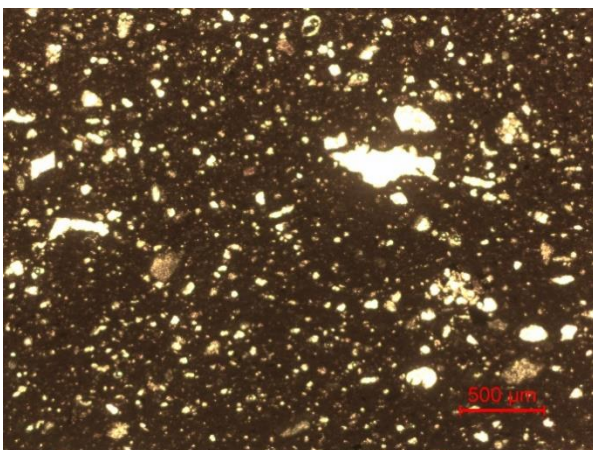
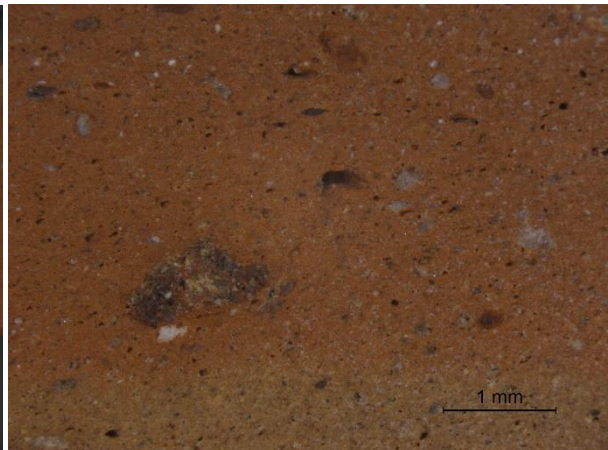


**Sample 4** – drawing and arch. info (1), shard photo (2), cross section (3, 4), thin section (5, 6).

Inventory number: 12356, Year of excavation: 2003, Archaeological context: 1[783]

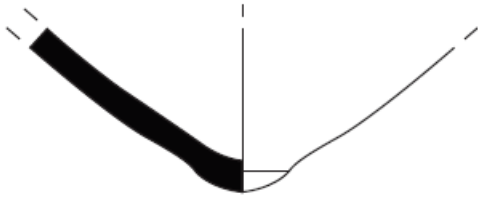


13104 [669] - 2ª metade séc. V a.C.  
Produção Guadalquivir  
Pellicer B/C

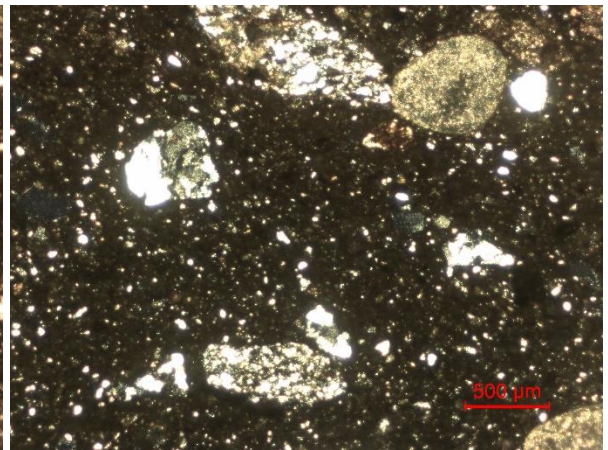
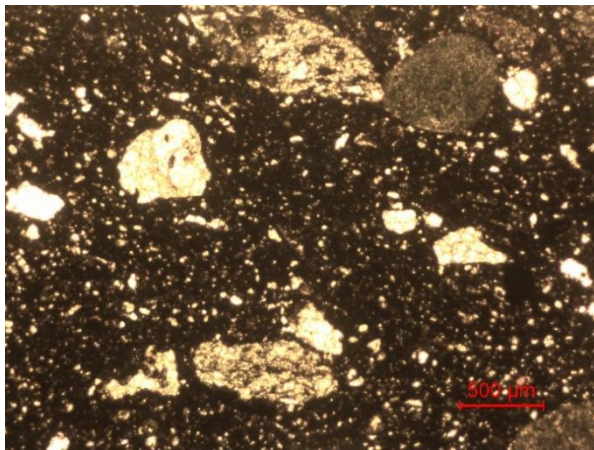
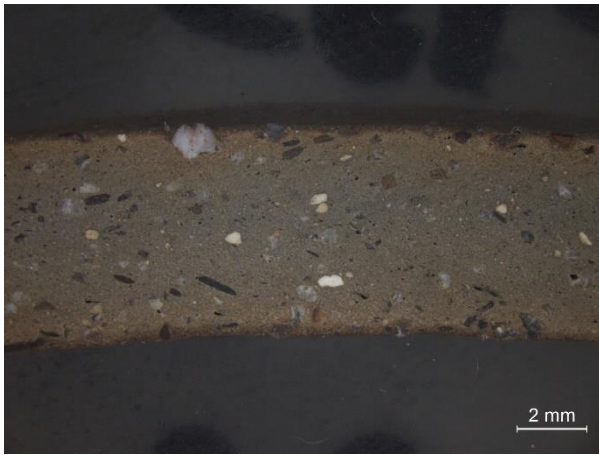


**Sample 5** – drawing and arch. info (1), shard photo (2), cross section (3, 4), thin section (5, 6).

Inventory number: 13104, Year of excavation: 2003, Archaeological context: 1[669]

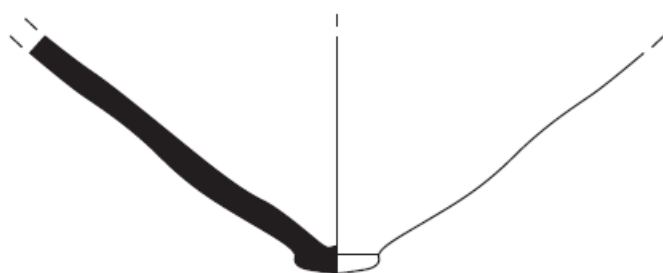


4282 [153] - 2ª metade séc. V  
Produção Guadalquivir  
Pellicer B/C



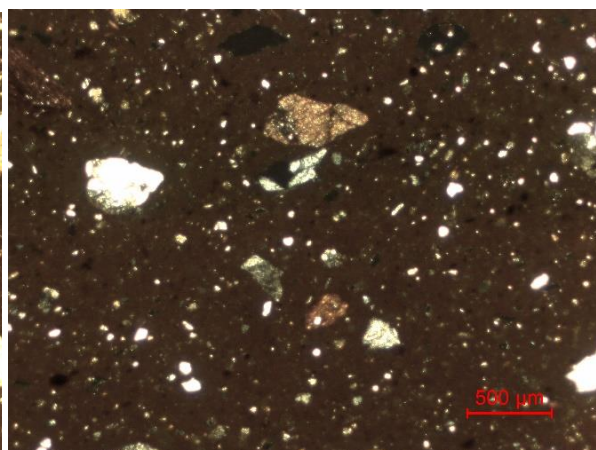
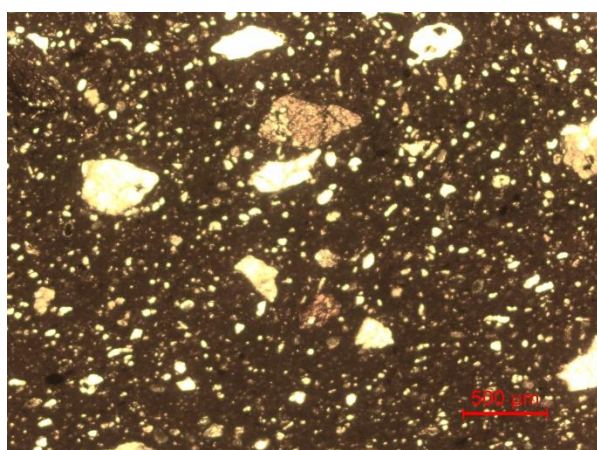
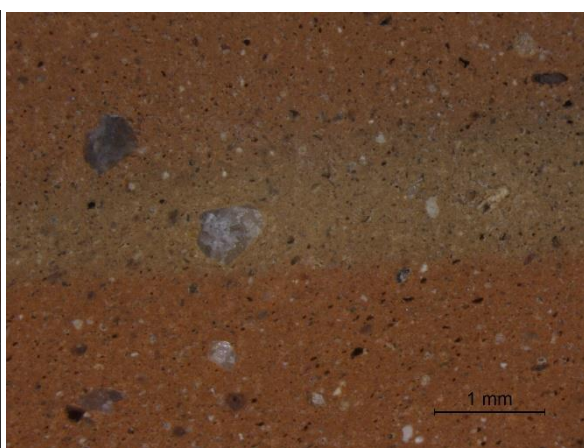
**Sample 6** – drawing and arch. info (1), shard photo (2), cross section (3, 4), thin section (5, 6).

Inventory number: 4282, Year of excavation: 2001, Archaeological context: 1[153]



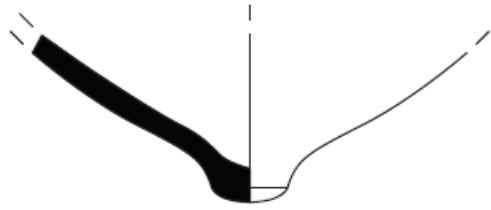
5400 [360] - sem contexto  
Produção Guadalquivir  
Pellicer B/C

10 cm



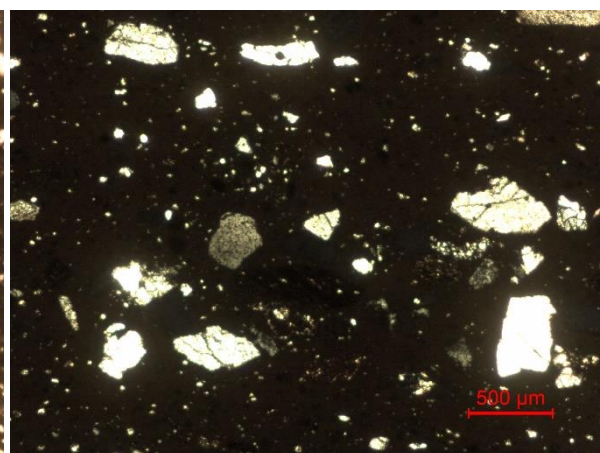
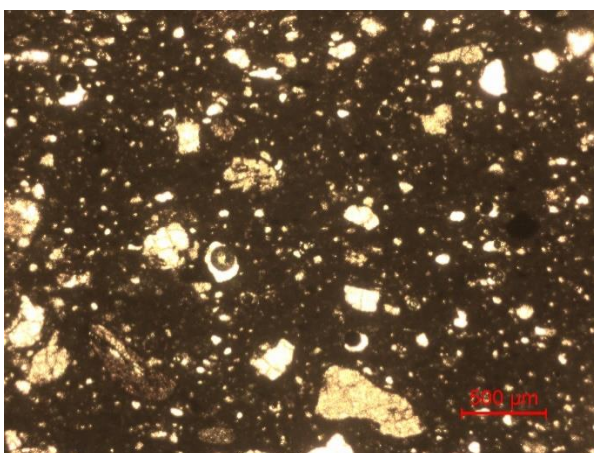
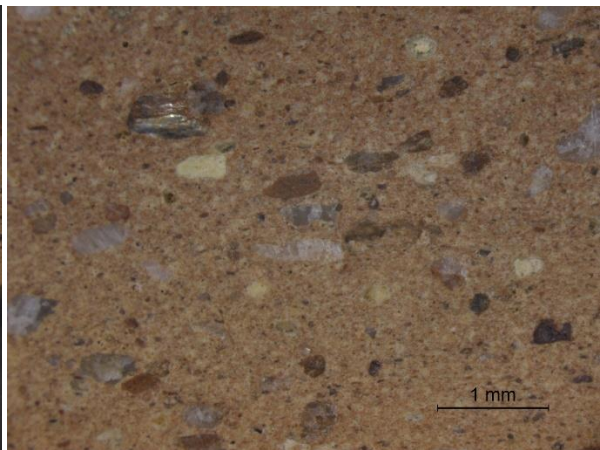
**Sample 7** – drawing and arch. info (1), shard photo (2), cross section (3, 4), thin section (5, 6).

Inventory number: 5400, Year of excavation: 2002, Archaeological context: 1[360]



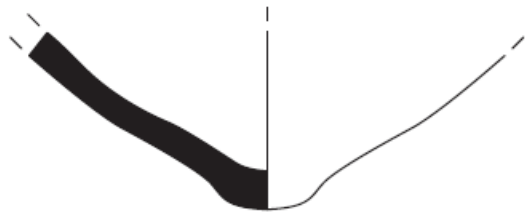
5616 [360] - sem contexto  
Produção Guadalquivir  
Pellicer B/C

10 cm



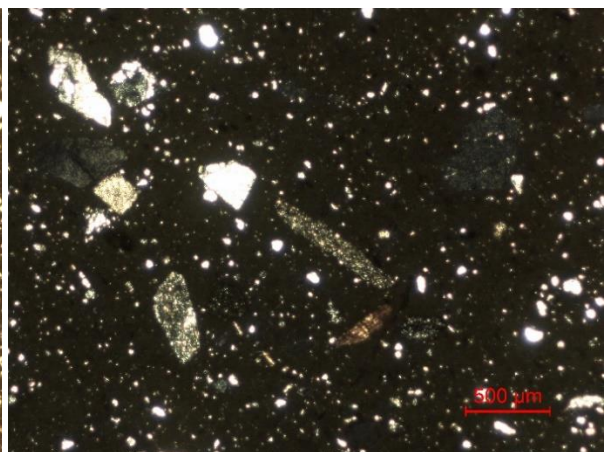
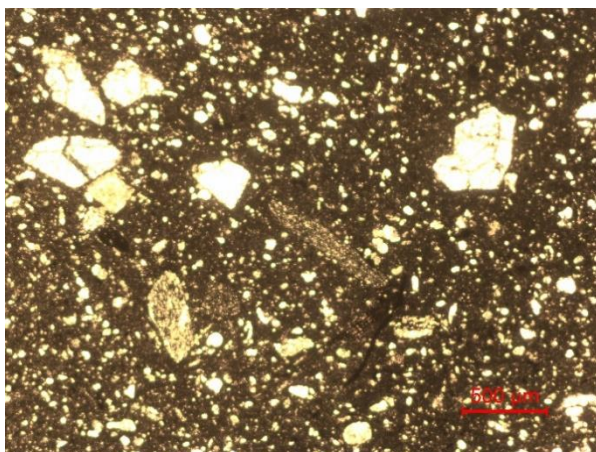
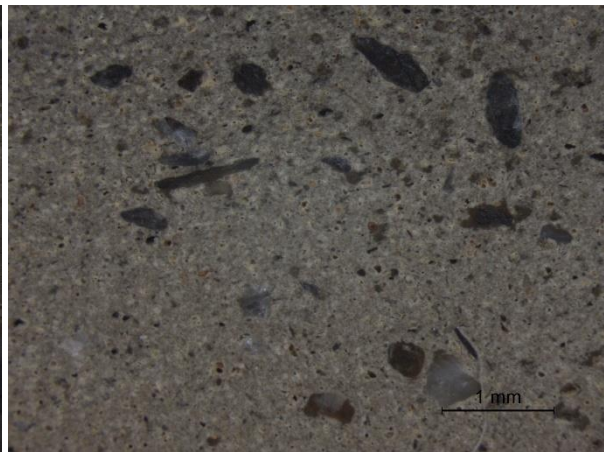
**Sample 8** – drawing and arch. info (1), shard photo (2), cross section (3, 4), thin section (5, 6).

Inventory number: 5616, Year of excavation: 2002, Archaeological context: 1[360]



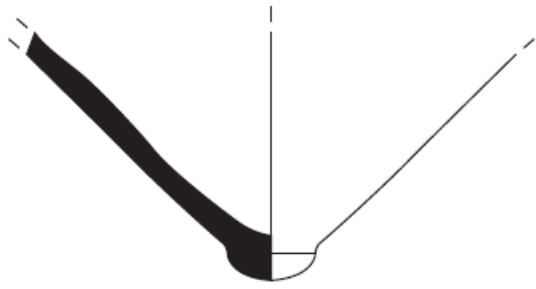
12196 [680] - 2ª metade do século V a.C.  
Produção Guadalquivir (queimada)  
Pellicer B/C

10 cm



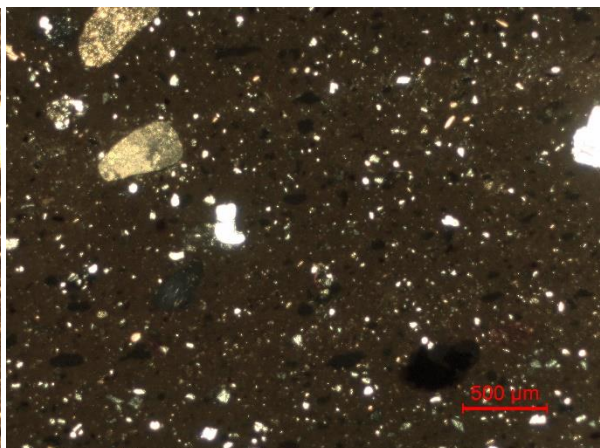
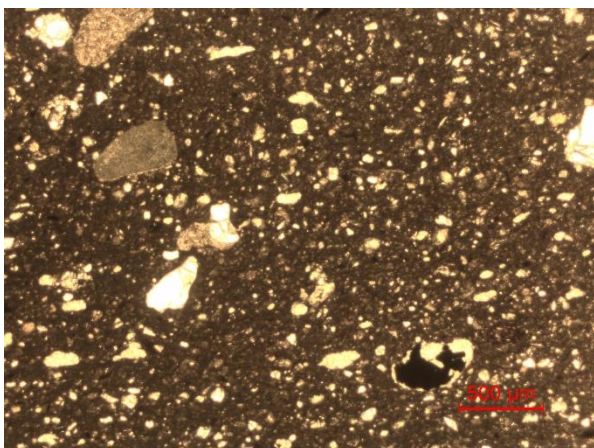
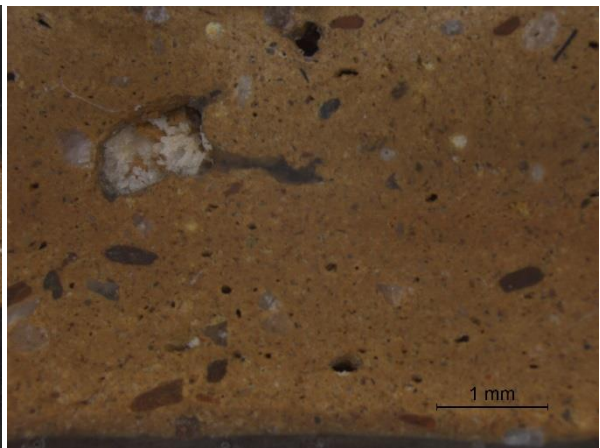
**Sample 9** – drawing and arch. info (1), shard photo (2), cross section (3, 4), thin section (5, 6).

Inventory number: 12196, Year of excavation: 2003, Archaeological context: 1[680]



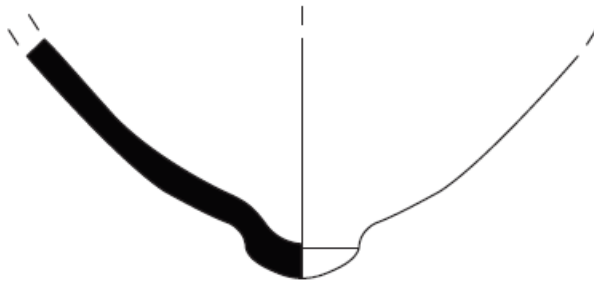
12655 [766] - 2ª metade séc. V  
Produção Guadalquivir  
Pellicer B/C

10 cm



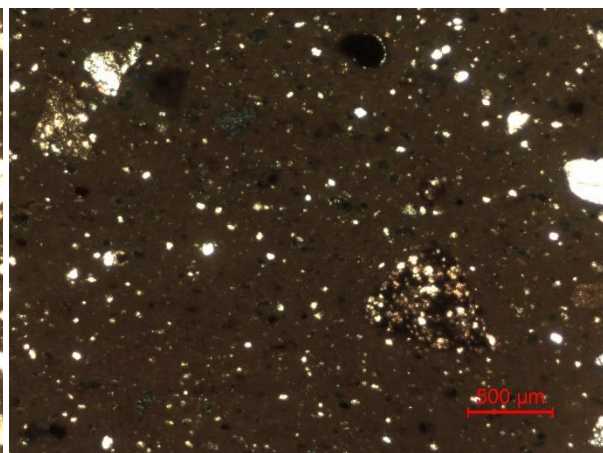
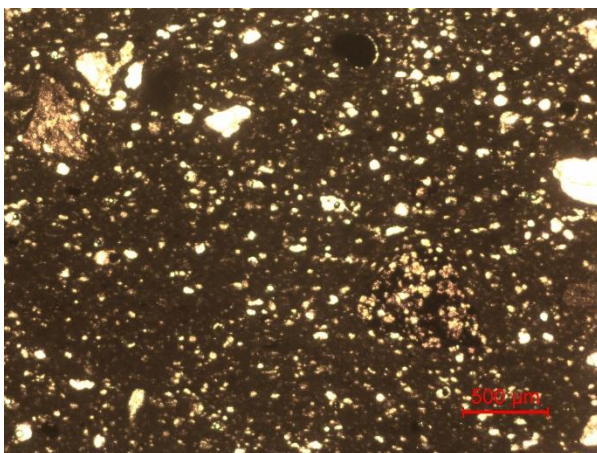
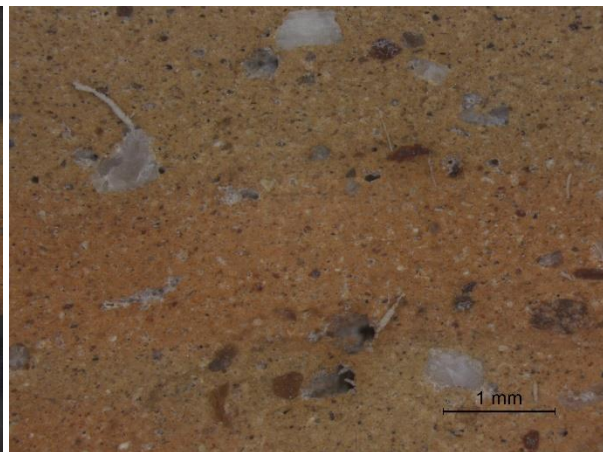
**Sample 10** – drawing and arch. info (1), shard photo (2), cross section (3, 4), thin section (5, 6).

Inventory number: 12655, Year of excavation: 2003, Archaeological context: 1[766]



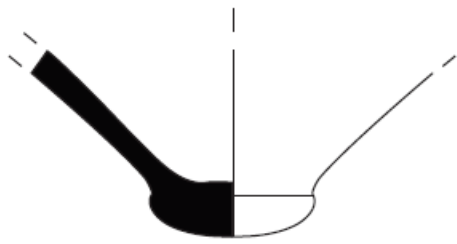
13167 [641] - 1ª metade do séc. IV  
Produção Guadalquivir (gatada)  
Pellicer B/C

10 cm



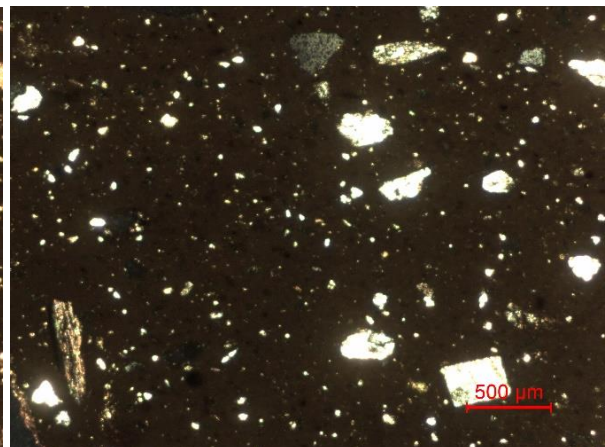
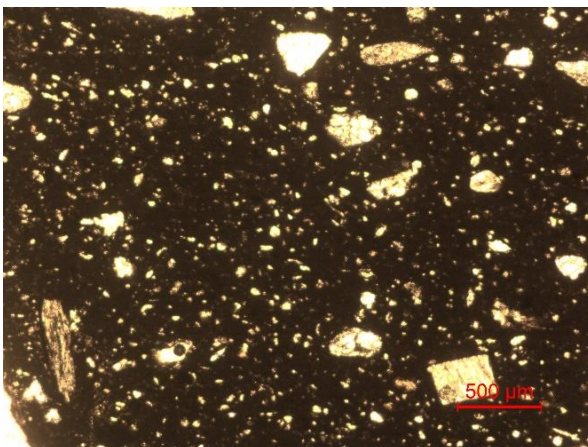
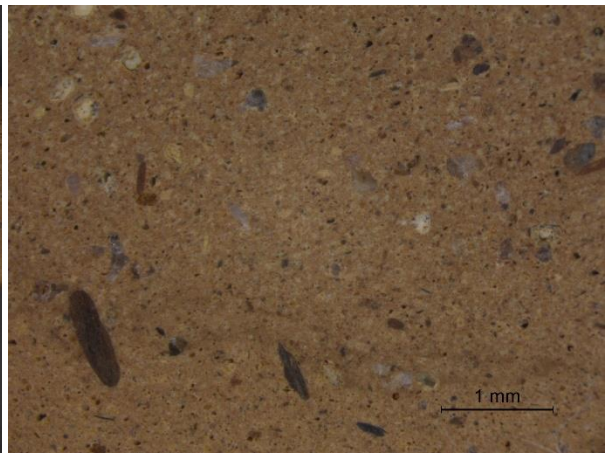
**Sample 11** – drawing and arch. info (1), shard photo (2), cross section (3, 4), thin section (5, 6).

Inventory number: 13167, Year of excavation: 2002, Archaeological context: 1[641]



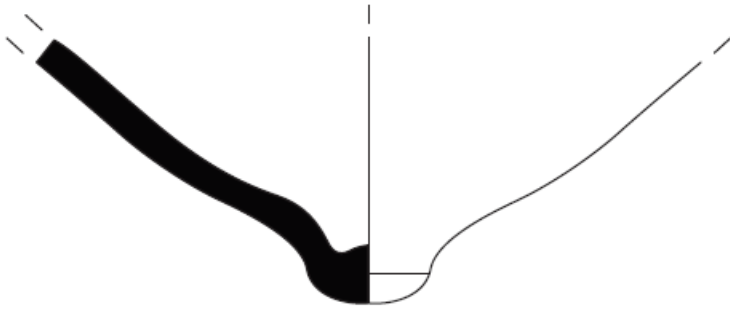
3698 [110] - 2ª metade séc. V  
Produção Guadalquivir  
Pellicer B/C

10 cm



**Sample 12** – drawing and arch. info (1), shard photo (2), cross section (3, 4), thin section (5, 6).

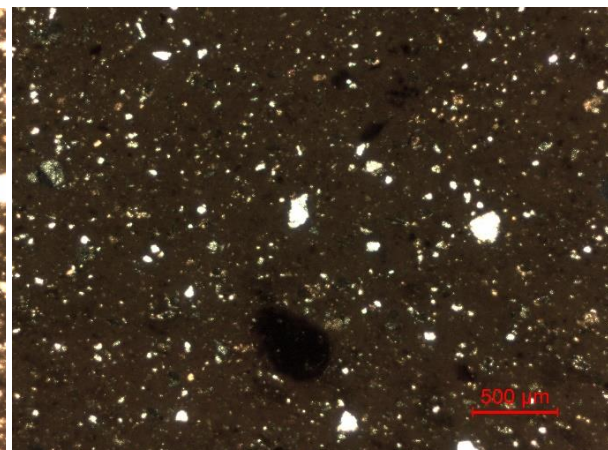
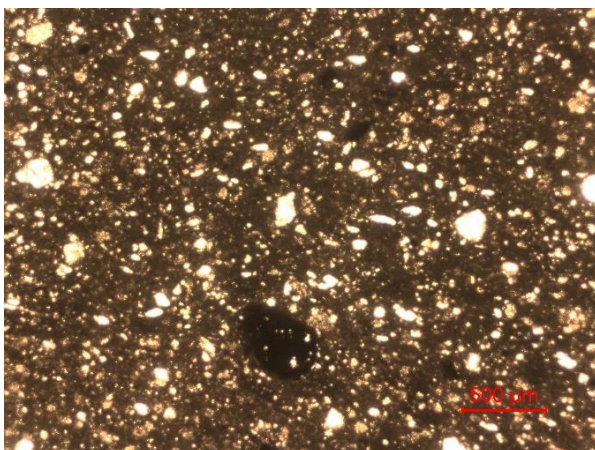
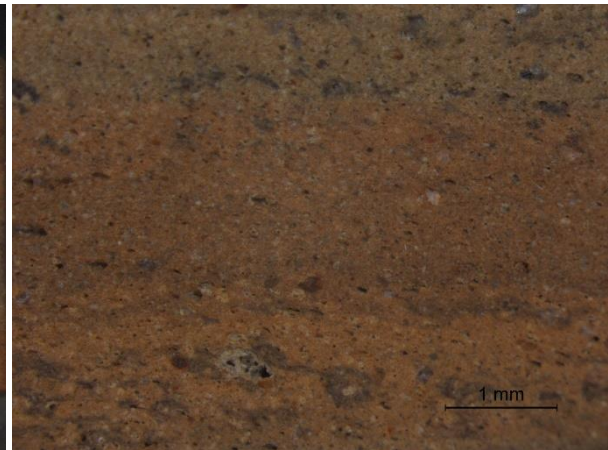
Inventory number: 3698, Year of excavation: 2001, Archaeological context: 1[110]



9082 [442] - séc. IV  
Produção Guadalquivir  
Pellicer B/C

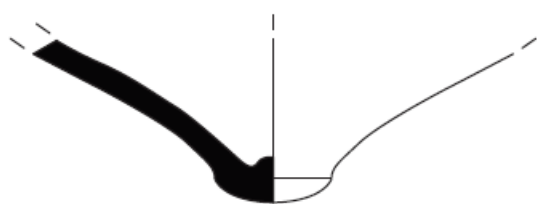


10 cm



**Sample 13** – drawing and arch. info (1), shard photo (2), cross section (3, 4), thin section (5, 6).

Inventory number: 9082, Year of excavation: 2002, Archaeological context: 1[442]

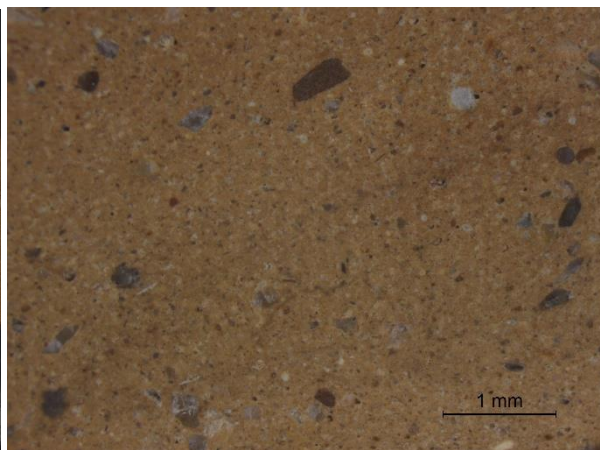


12125 [605] - séc. V/IV a.C.  
Produção Guadalquivir  
Pellicer B/C

10 cm



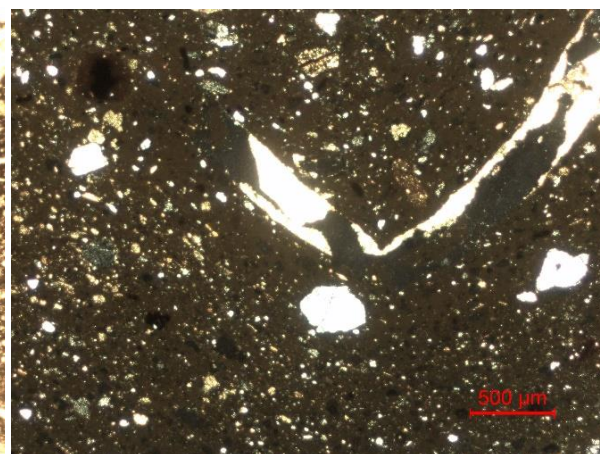
2 mm



1 mm



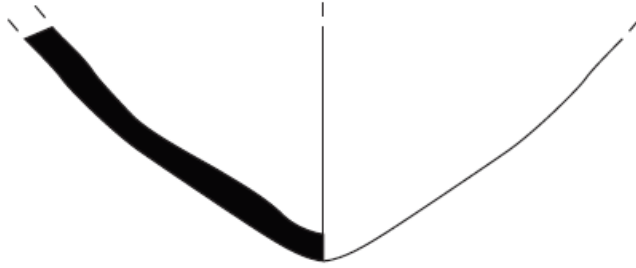
500  $\mu$ m



500  $\mu$ m

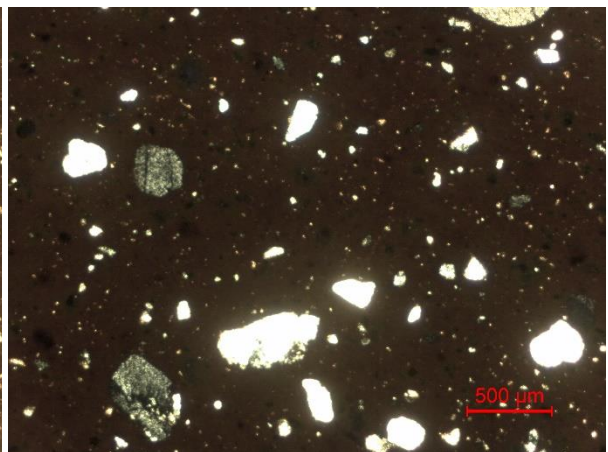
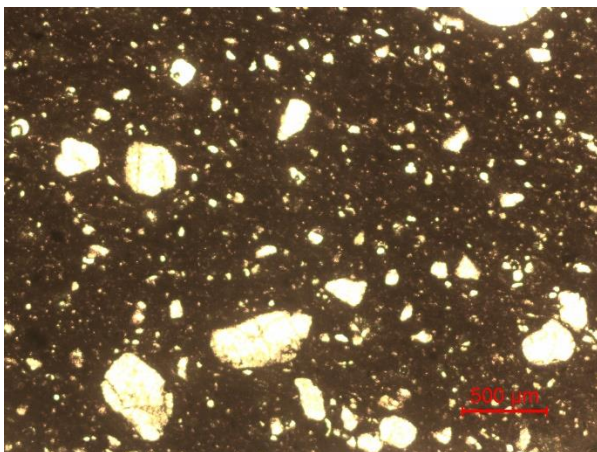
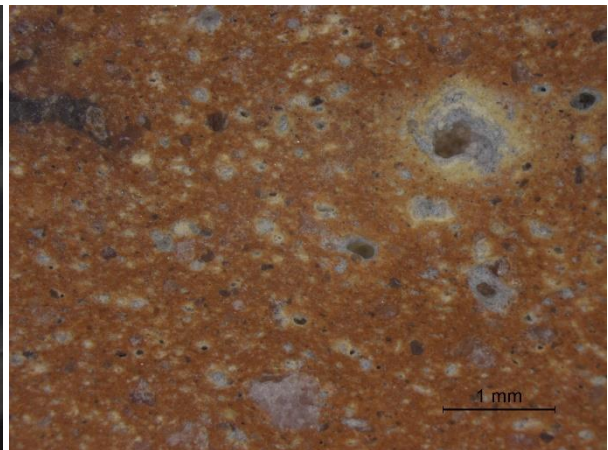
**Sample 14** – drawing and arch. info (1), shard photo (2), cross section (3, 4), thin section (5, 6).

Inventory number: 12125, Year of excavation: 2003, Archaeological context: 1[605]



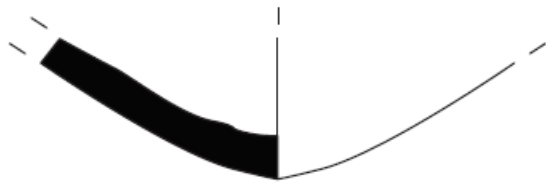
12658 [766] - 2ª metade séc. V  
Produção Guadalquivir  
Pellicer B/C (?)

10 cm



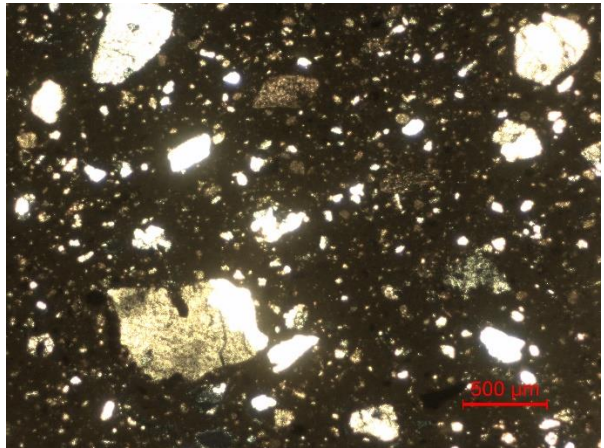
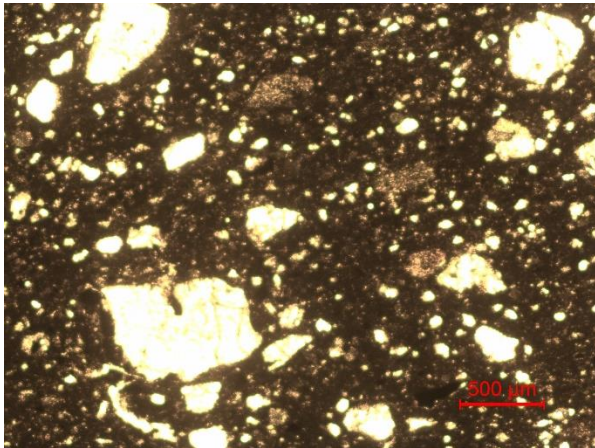
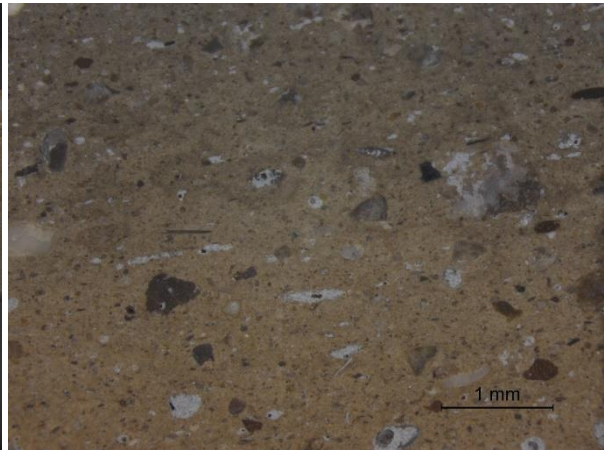
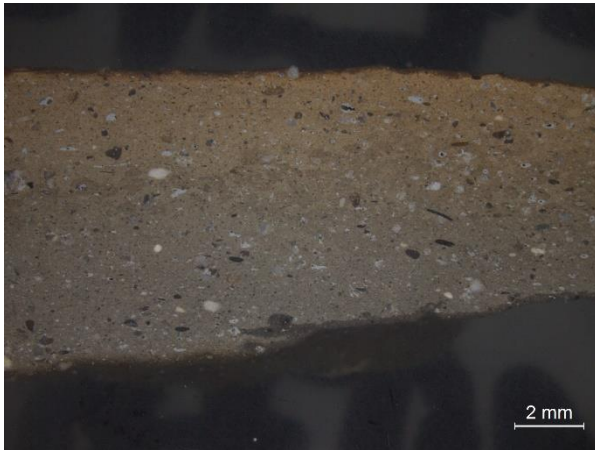
**Sample 15** – drawing and arch. info (1), shard photo (2), cross section (3, 4), thin section (5, 6).

Inventory number: 12658, Year of excavation: 2003, Archaeological context: 1[766]



11078 [983] - séc. V/IV  
Produção Baía de Cádiz  
Possível MPA4

10 cm



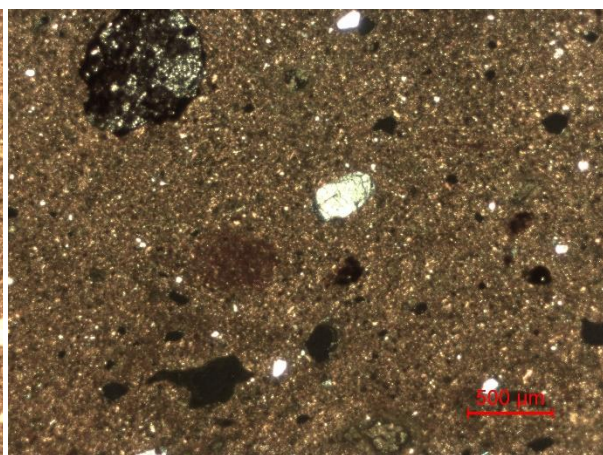
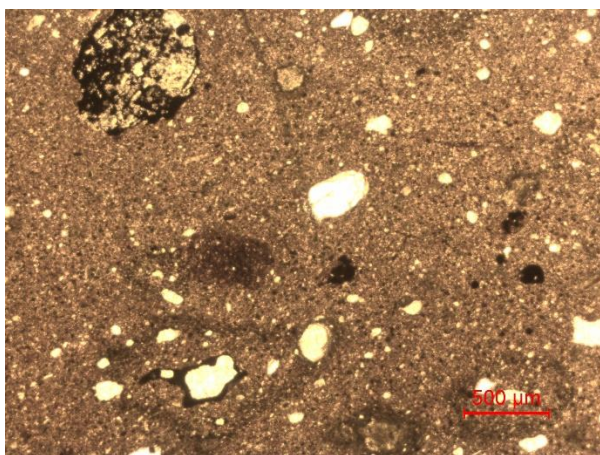
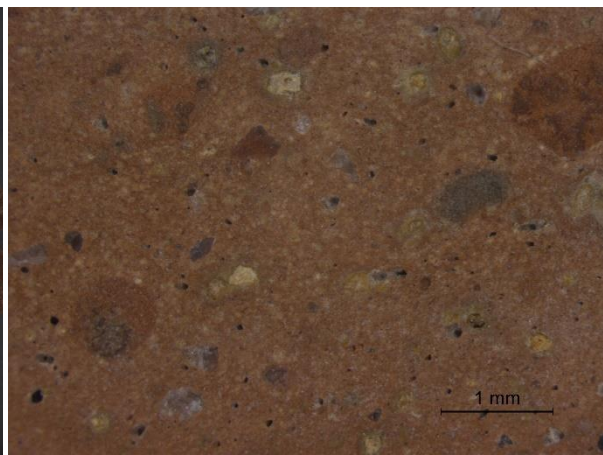
**Sample 16** – drawing and arch. info (1), shard photo (2), cross section (3, 4), thin section (5, 6).

Inventory number: 11078, Year of excavation: 2003, Archaeological context: 1[983]



4175 [149] - séc. V/IV a.C.  
Produção local  
Cerâmica comum

10 cm



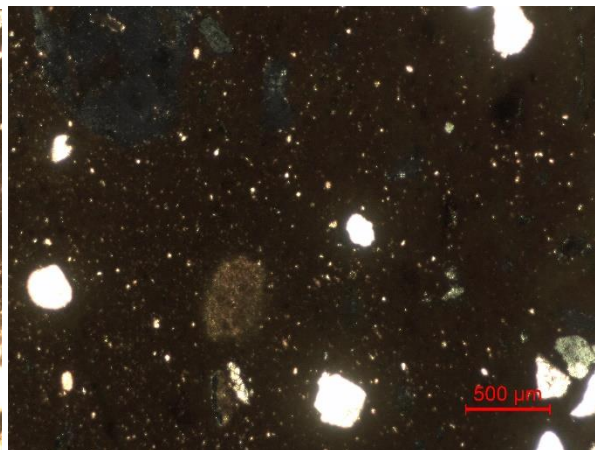
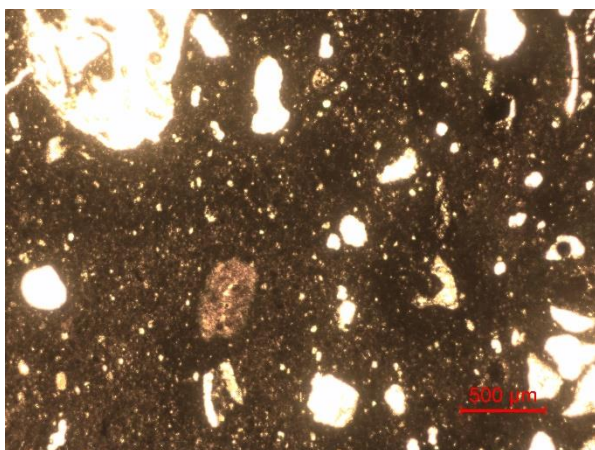
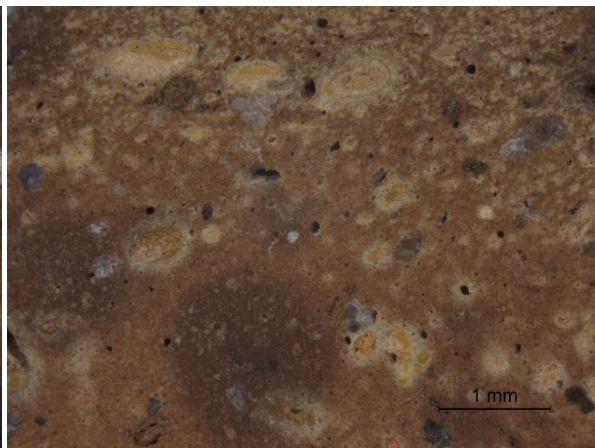
**Sample 17** – drawing and arch. info (1), shard photo (2), cross section (3, 4), thin section (5, 6).

Inventory number: 4179, Year of excavation: 2001, Archaeological context: 1[149]



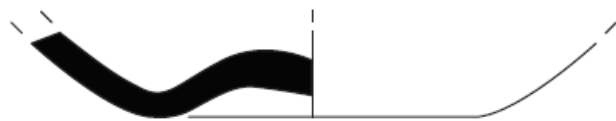
4760 [633] - séc. VI  
Produção local  
Cerâmica comum

10 cm



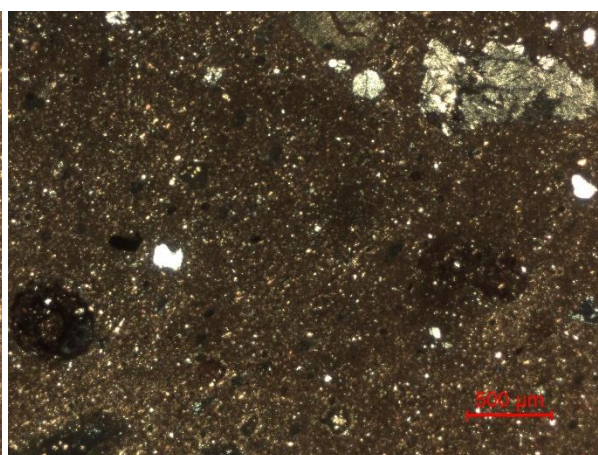
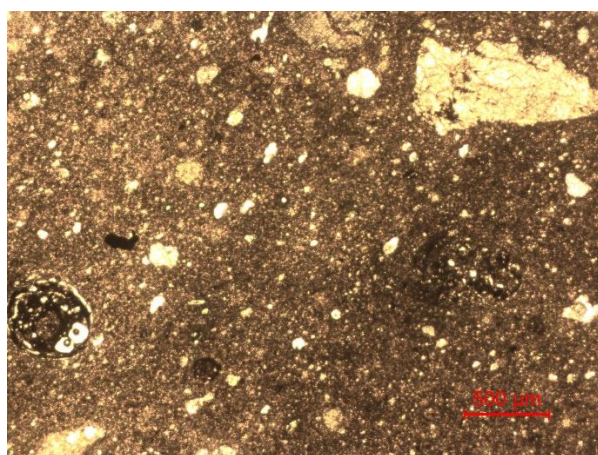
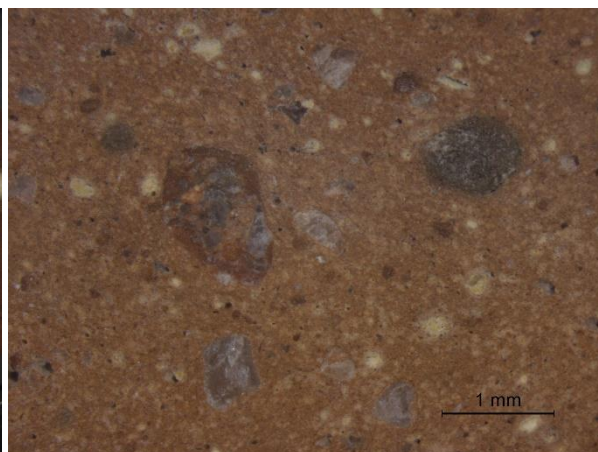
**Sample 18** – drawing and arch. info (1), shard photo (2), cross section (3, 4), thin section (5, 6).

Inventory number: 11760, Year of excavation: 2003, Archaeological context: 1[633]



12047 [775] - séc. V/IV  
Produção local  
Cerâmica comum

10 cm



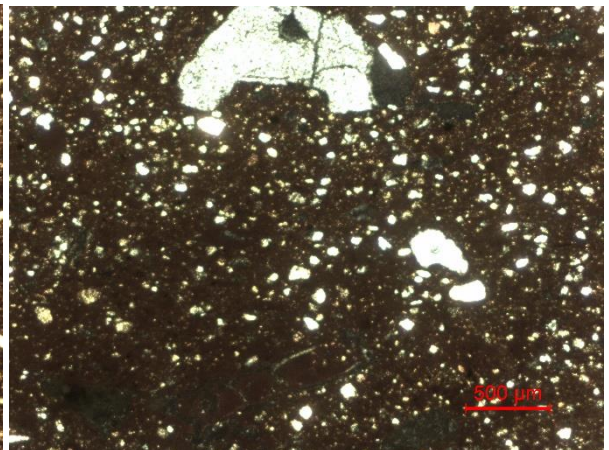
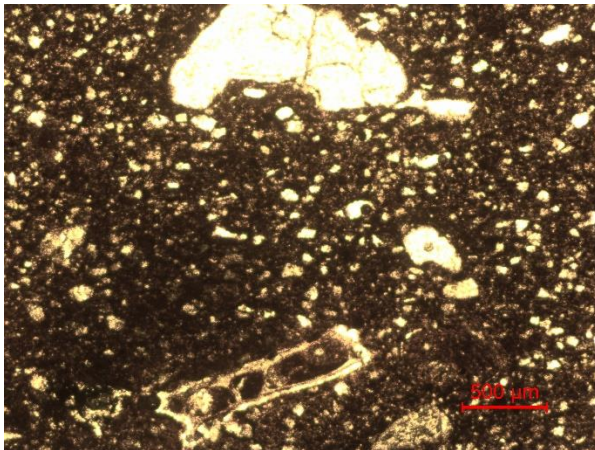
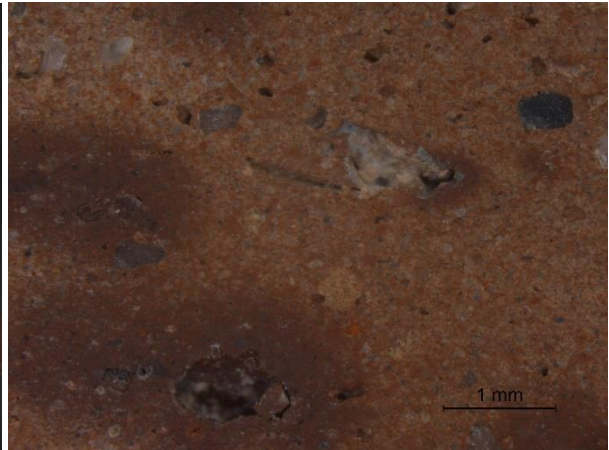
**Sample 19** – drawing and arch. info (1), shard photo (2), cross section (3, 4), thin section (5, 6).

Inventory number: 12047, Year of excavation: 2002, Archaeological context: 1[775]



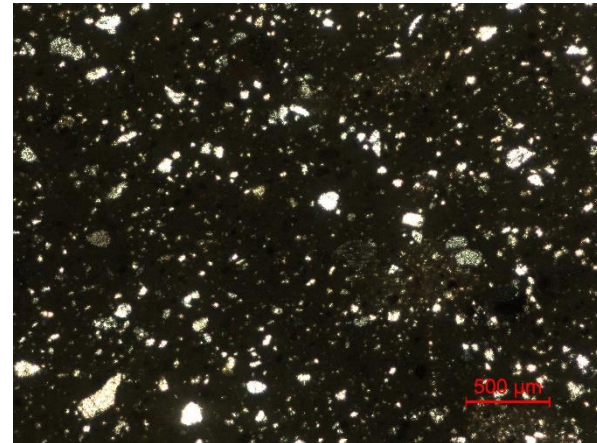
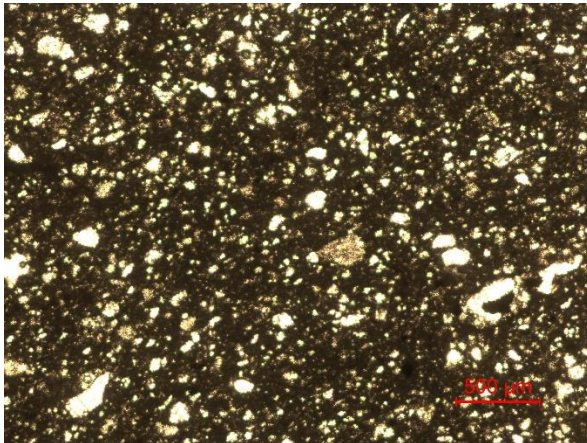
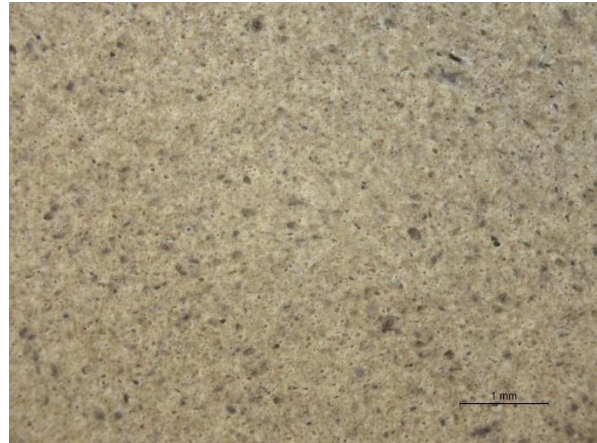
12092 [781] - séc. V/IV  
Produção local  
Cerâmica comum

10 cm



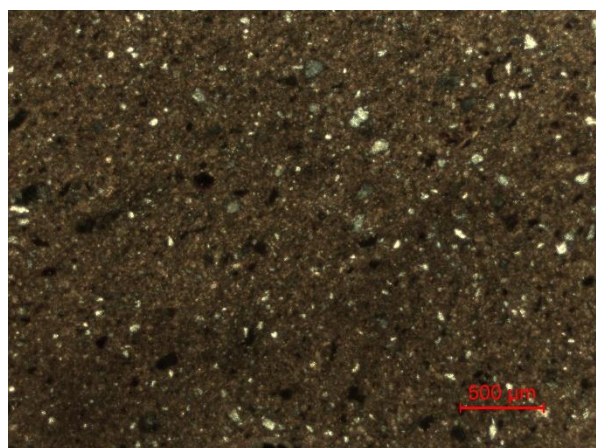
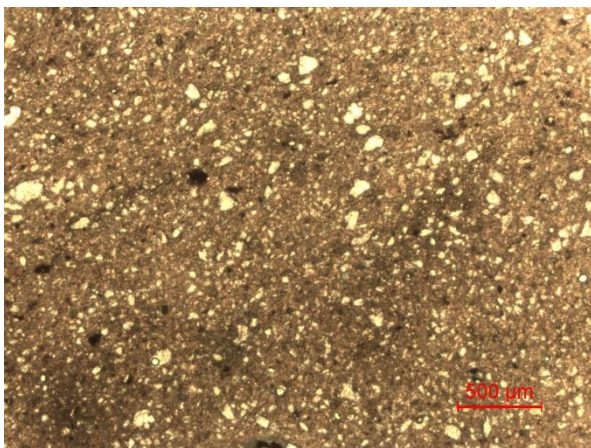
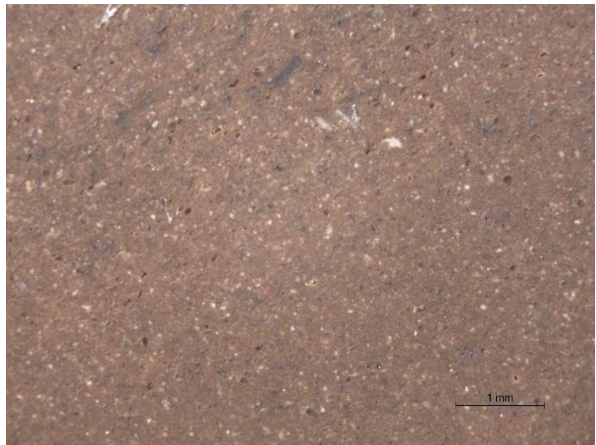
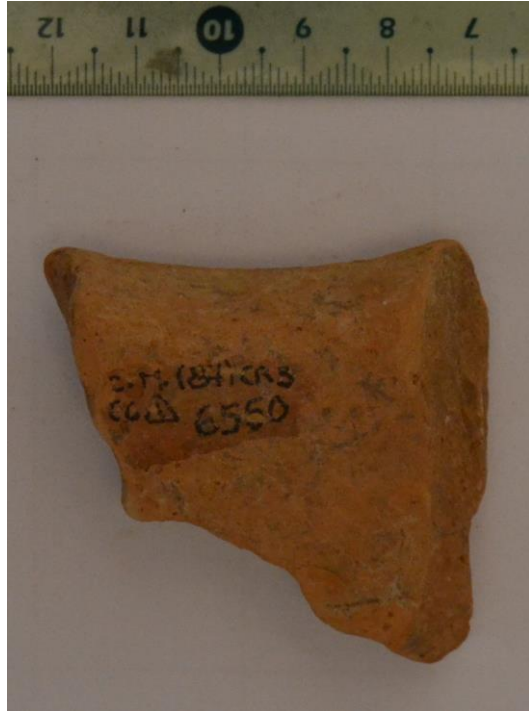
**Sample 20** – drawing and arch. info (1), shard photo (2), cross section (3, 4), thin section (5, 6).

Inventory number: 12092, Year of excavation: 2003, Archaeological context: 1[781]



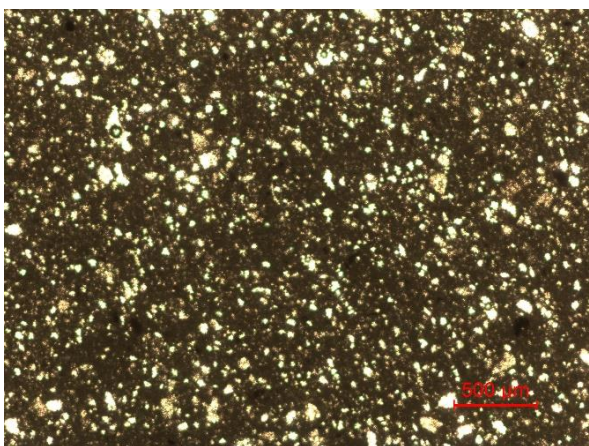
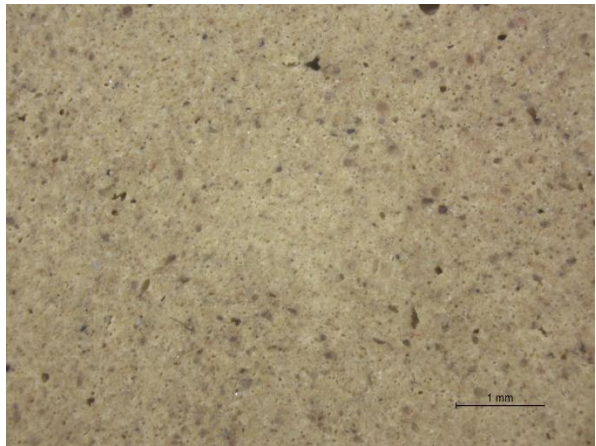
**Sample 21** – shard photo (1, 2), cross section (3, 4), thin section (5, 6).

Inventory number: 3530, Year of excavation: 1987, Archaeological context: CR3 C5



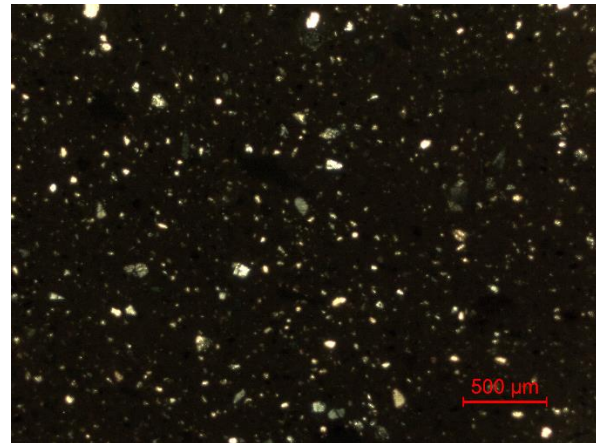
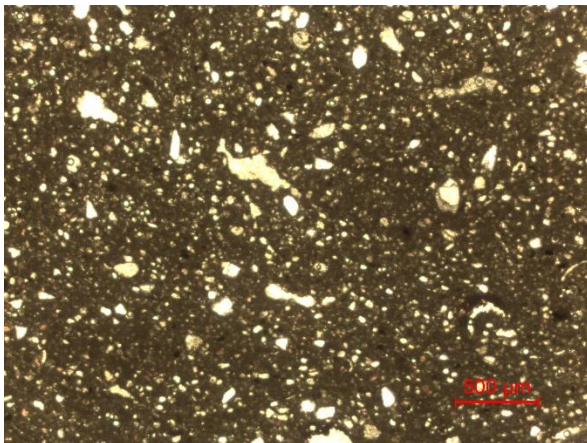
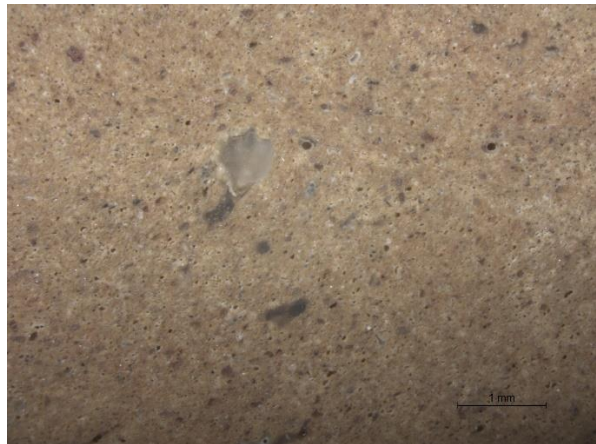
**Sample 22** – shard photo (1, 2), cross section (3, 4), thin section (5, 6).

Inventory number: 6550, Year of excavation: 1987, Archaeological context: CR3 C6



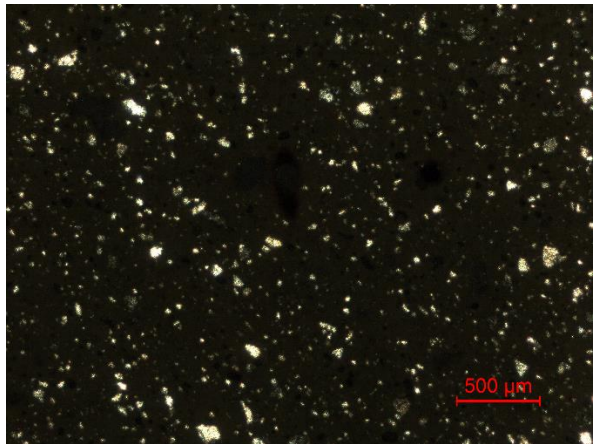
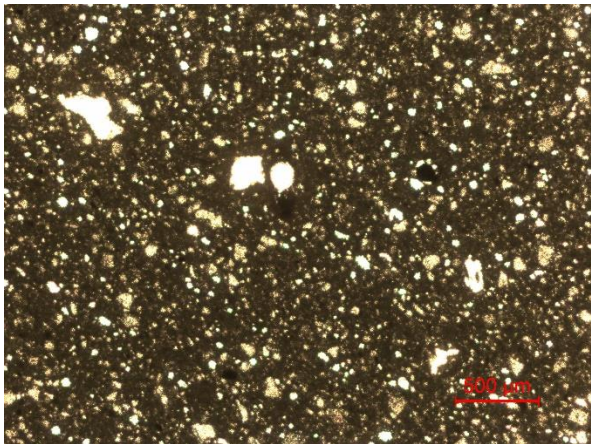
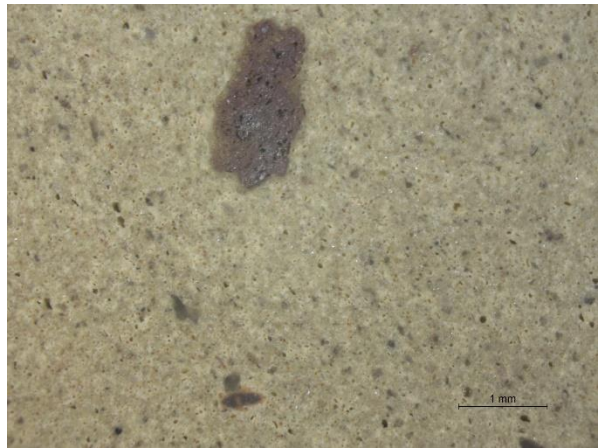
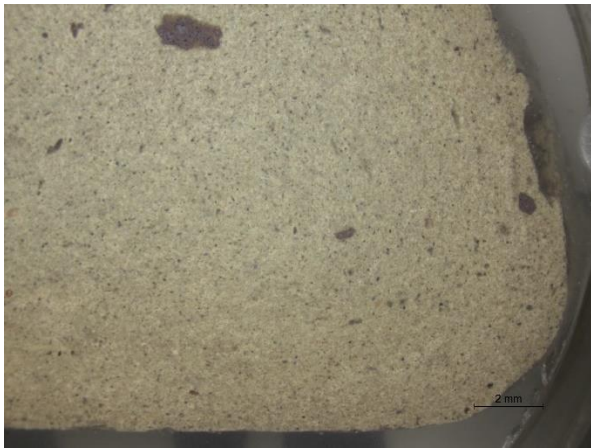
**Sample 23** – shard photo (1, 2), cross section (3, 4), thin section (5, 6).

Inventory number: 7115, Year of excavation: 1987, Archaeological context: CR3 C5



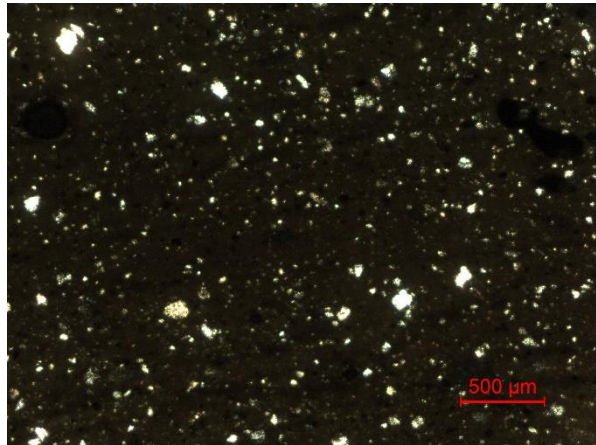
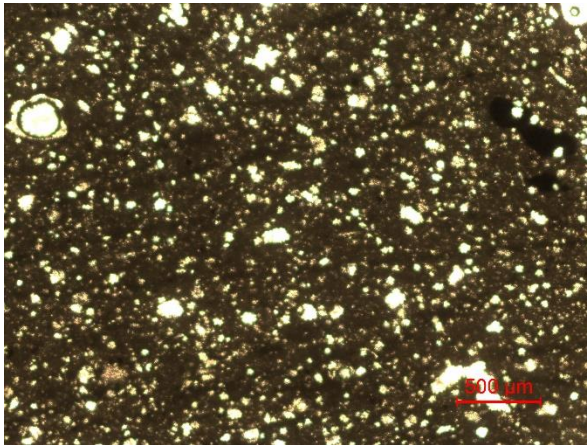
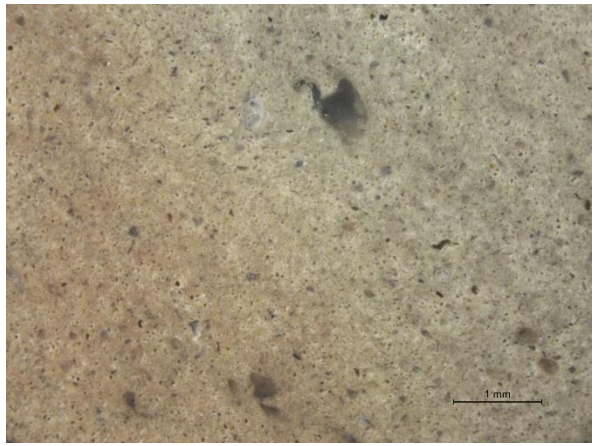
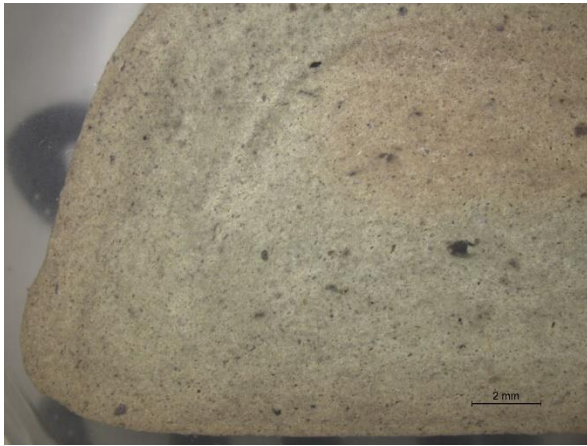
**Sample 24** – shard photo (1, 2), cross section (3, 4), thin section (5, 6).

Inventory number: 7617, Year of excavation: 1987, Archaeological context: CR3 C6



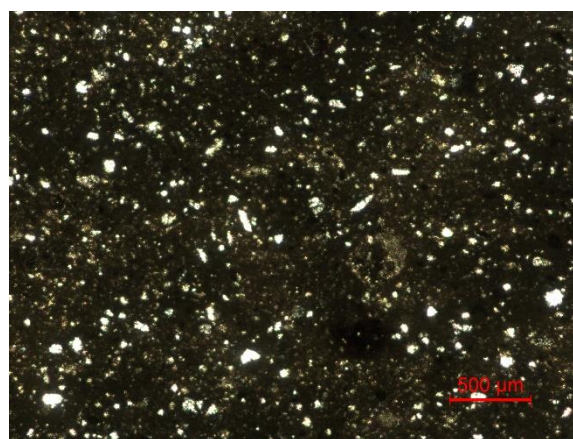
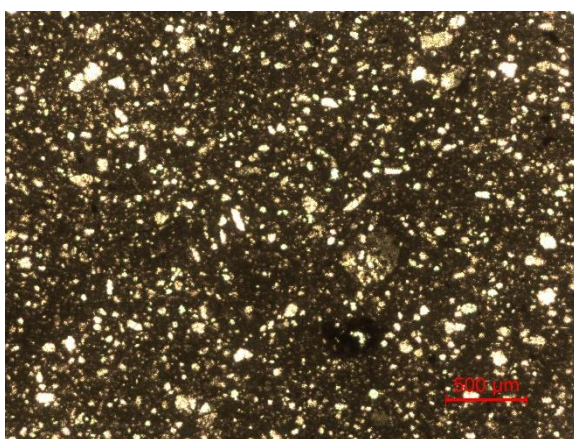
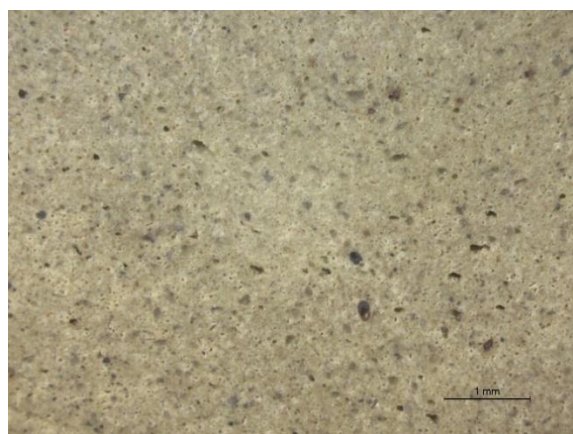
**Sample 25** – shard photo (1, 2), cross section (3, 4), thin section (5, 6).

Inventory number: 7939, Year of excavation: 1987, Archaeological context: CR3 C5



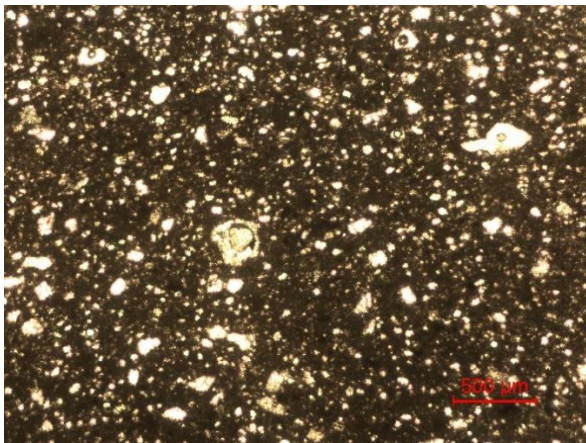
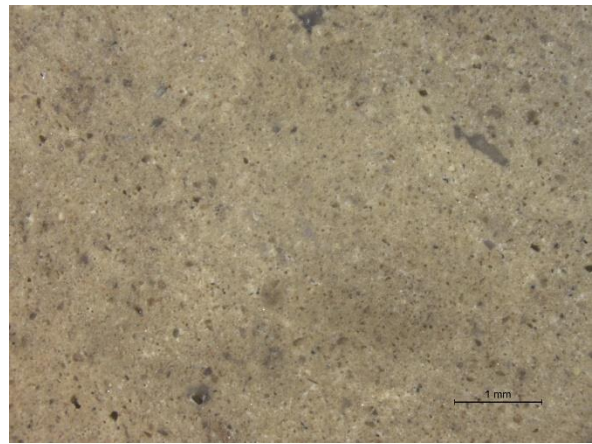
**Sample 26** – shard photo (1, 2), cross section (3, 4), thin section (5, 6).

Inventory number: 8275, Year of excavation: 1987, Archaeological context: CR3 C5



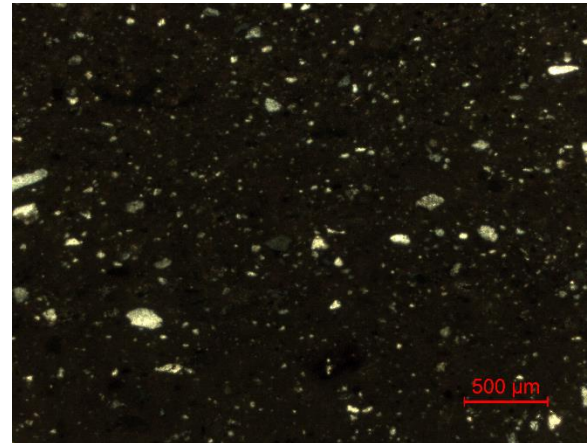
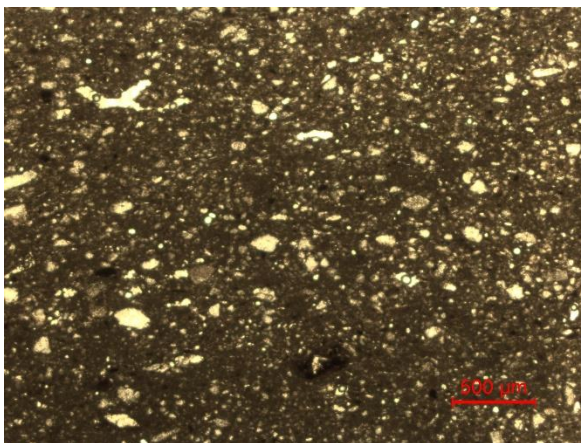
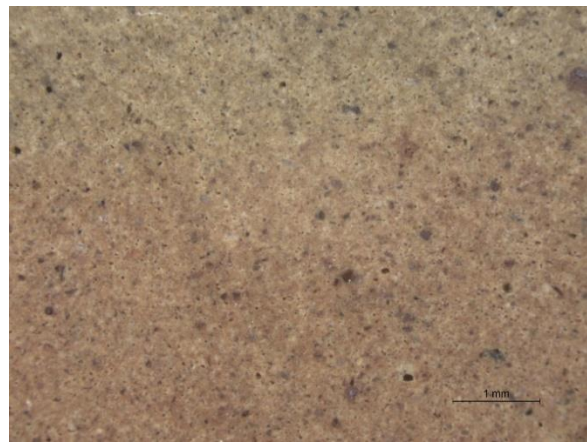
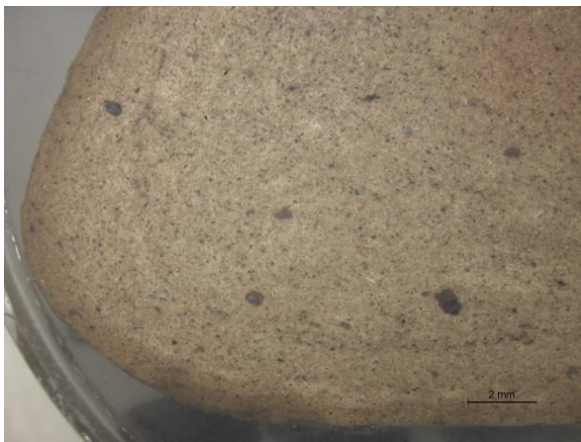
**Sheet 27** – Sample 27: shard photo (1, 2), cross section (3, 4), thin section (5, 6).

Inventory number: 8360, Year of excavation: 1987, Archaeological context: CR3 C5



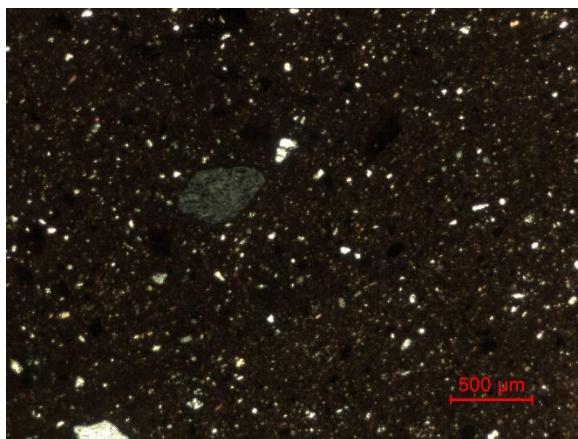
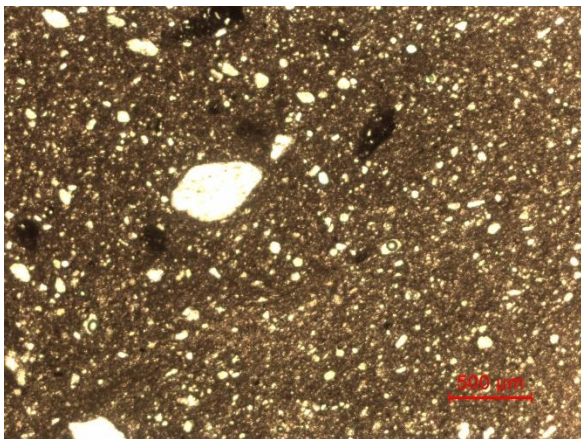
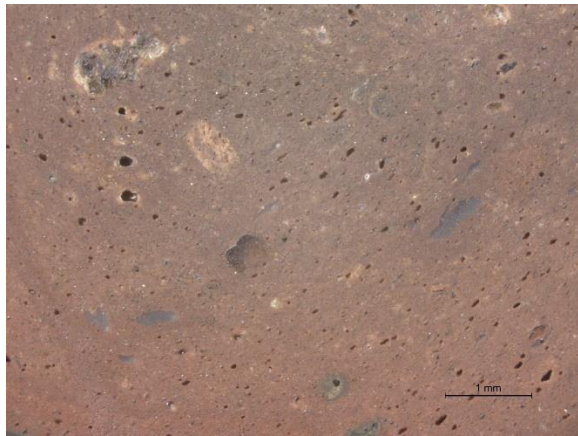
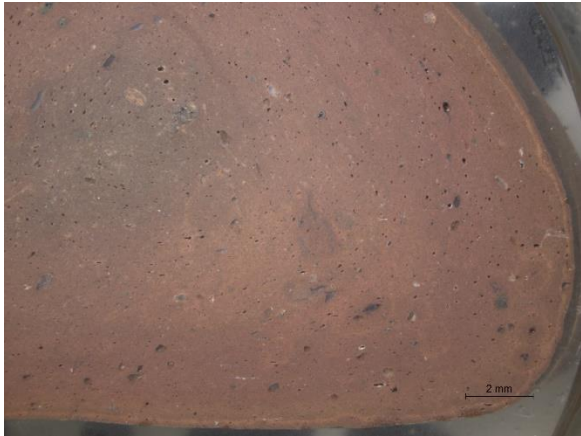
**Sample 28** – shard photo (1, 2), cross section (3, 4), thin section (5, 6).

Inventory number: 9284, Year of excavation: 1987, Archaeological context: CR3 D6



**Sample 29** – shard photo (1, 2), cross section (3, 4), thin section (5, 6).

Inventory number: 9506, Year of excavation: 2002, Archaeological context: 1[385]



**Sample 30** – shard photo (1, 2), cross section (3, 4), thin section (5, 6).

Inventory number: 10529, Year of excavation: 1988, Archaeological context: CR3 C5

## Annex II

Sample	Fabric	Rb	Sr	Y	Zr	Nb	Ba	Th	Cr	Co	Ni	Cu	Zn	Ga	As	Pb	Sn	V	Cs	La	Ta	Ce	U	Cl
1	A	101	363	21	186	17	1580	9	87	20	25	29	81	20	15	12	-6	123	6	35	1	176	3	10
2	A	115	352	24	167	22	1020	11	87	22	24	28	85	18	17	-3	10	129	6	81	1	286	3	13
3	A2	85	185	29	204	13	1360	9	90	22	28	28	96	19	10	14	0	111	7	84	1	143	3	9
4	A	100	365	25	159	21	1280	10	117	21	30	32	92	19	15	17	4	146	7	14	1	175	3	10
5	A	115	370	17	164	16	1370	12	80	21	31	29	87	19	19	3	-5	144	6	55	1	147	3	11
6	A4	101	353	18	158	17	1650	14	204	23	92	38	93	16	20	3	2	118	5	82	1	189	2	16
7	A	111	390	23	176	16	1370	3	92	23	25	37	87	20	18	14	13	117	6	107	1	302	3	10
8	A	67	364	21	163	17	1620	7	117	22	23	33	66	18	15	9	22	99	8	129	1	202	3	11
9	A3	99	359	21	153	12	1670	3	123	21	28	24	102	18	13	18	-8	134	7	321	1	474	3	12
10	A	103	421	19	159	17	1250	11	91	22	27	29	92	21	14	10	24	115	7	68	1	216	3	13
11	A	107	393	20	164	21	1480	3	115	23	32	30	81	19	14	-3	10	137	7	137	1	211	3	10
12	A	111	369	23	174	14	1790	8	109	20	44	34	86	19	22	6	-3	135	7	45	2	147	3	19
13	A	99	330	19	178	19	1660	3	89	21	31	23	85	17	16	15	4	87	5	62	1	245	2	8
14	A	105	392	23	159	16	1540	8	82	20	24	26	81	17	23	4	7	136	6	67	1	123	3	15
15	C2	109	361	18	164	16	1150	6	152	22	48	32	93	20	12	1	2	141	6	84	1	221	3	8
16	A2	169	103	29	217	15	1280	11	69	18	26	31	82	15	13	7	-9	93	7	63	1	225	3	9
17	C	101	324	22	166	18	936	9	91	26	42	43	100	20	13	13	1	102	10	22	2	142	4	15
18	C	114	143	26	149	18	1350	12	60	31	34	46	94	20	19	6	14	85	7	62	2	231	3	14
19	C	166	117	24	172	20	981	9	445	27	210	49	111	21	18	1	15	102	10	54	2	101	4	15
20	C	122	119	28	232	21	977	7	47	20	22	34	77	20	19	0	9	78	7	101	2	190	3	16
21	B	102	278	30	266	13	1600	4	63	16	26	23	67	16	16	14	8	71	6	55	1	203	3	15
22	A/C	151	150	27	160	17	923	3	130	13	56	23	86	17	11	12	20	109	5	103	1	89	2	8
23	B	82	299	23	226	20	1690	5	92	18	26	21	75	16	15	0	-14	66	5	156	1	142	2	11
24	A	80	327	25	242	13	1830	3	55	16	17	18	76	14	13	10	-4	63	6	87	1	243	2	10
25	B	91	346	28	228	16	1360	10	74	17	20	21	63	17	16	11	22	104	5	134	1	156	2	11
26	B	74	322	31	247	19	1650	17	92	17	26	14	70	16	16	8	-14	91	4	35	1	199	2	9
27	B	76	333	30	234	11	1760	2	91	17	28	25	65	16	15	24	3	74	4	27	1	237	2	14
28	B	64	322	33	253	15	1610	2	74	19	27	23	69	17	18	-1	-15	91	6	95	1	179	2	10
29	A	92	329	28	242	10	1600	6	49	17	24	26	66	16	15	0	4	47	6	130	1	206	3	12
30	C3	98	300	24	233	20	1110	14	111	27	61	47	110	22	19	7	13	25	10	68	2	225	4	19

Minor and trace elements from ED-XRF analysis (not presented in Table 5). The values are in ppm after the standard calibration of the equipment.

## Annex III

Sample	Na <sub>2</sub> O	MgO	Al <sub>2</sub> O <sub>3</sub>	SiO <sub>2</sub>	K <sub>2</sub> O	CaO	TiO <sub>2</sub>	Fe <sub>2</sub> O <sub>3</sub>	MnO
1	-0.201	0.479	1.173	1.745	0.415	1.041	-0.143	0.759	-0.959
2	-0.328	0.455	1.152	1.724	0.417	1.053	-0.201	0.714	-1.046
3	-0.215	0.446	1.179	1.736	0.435	1.004	-0.155	0.760	-1.046
4	-0.066	0.471	1.170	1.712	0.431	1.090	-0.180	0.742	-1.000
5	-0.260	0.428	1.179	1.709	0.415	1.107	-0.174	0.746	-1.000
6	-0.222	0.491	1.121	1.782	0.320	0.929	-0.143	0.755	-0.523
7	-0.284	0.439	1.173	1.721	0.422	1.072	-0.180	0.732	-1.097
8	-0.180	0.410	1.176	1.760	0.513	0.922	-0.137	0.747	-1.046
9	-0.260	0.413	1.167	1.732	0.439	1.068	-0.167	0.728	-1.046
10	-0.201	0.400	1.173	1.748	0.444	0.966	-0.131	0.747	-0.959
11	-0.357	0.391	1.161	1.727	0.449	1.045	-0.143	0.758	-0.921
12	-0.319	0.417	1.173	1.739	0.473	0.998	-0.114	0.757	-1.000
13	-0.208	0.491	1.146	1.709	0.401	1.107	-0.161	0.724	-1.000
14	-0.357	0.490	1.143	1.706	0.420	1.090	-0.194	0.712	-0.959
15	-0.215	0.369	1.179	1.779	0.307	0.947	-0.143	0.777	-1.222
16	-0.004	0.412	1.121	1.743	0.462	1.017	-0.194	0.679	-1.000
17	0.462	0.539	1.248	1.725	0.587	0.711	-0.022	0.840	-0.638
18	0.152	0.761	1.223	1.727	0.423	0.829	-0.071	0.820	-0.638
19	0.193	0.607	1.279	1.738	0.574	0.590	0.009	0.877	-0.569
20	0.279	0.391	1.207	1.802	0.431	0.539	-0.018	0.738	-0.745
21	0.161	0.348	1.072	1.800	0.418	0.931	-0.155	0.624	-1.097
22	-0.268	0.307	1.021	1.734	0.367	1.076	-0.208	0.616	-0.921
23	0.093	0.477	1.072	1.757	0.297	1.090	-0.187	0.626	-1.046
24	-0.092	0.384	1.072	1.756	0.365	1.064	-0.180	0.640	-0.959
25	0.104	0.439	1.093	1.796	0.312	1.004	-0.161	0.651	-1.097
26	0.161	0.468	1.083	1.754	0.236	1.100	-0.161	0.642	-0.921
27	0.104	0.425	1.068	1.787	0.212	1.029	-0.161	0.639	-1.097
28	0.107	0.427	1.104	1.772	0.408	1.009	-0.131	0.672	-0.959
29	-0.237	0.427	1.068	1.752	0.420	1.033	-0.143	0.704	-1.097
30	0.117	0.294	1.290	1.790	0.549	-0.167	0.041	0.857	-0.854

Loading matrix for PCA analysis (the values for oxides transformed into the logarithmic scale).

PC	Eigenvalue	% variance
1	0.1013	59.8970
2	0.0325	19.1860
3	0.0231	13.6650
4	0.0069	4.1025
5	0.0036	2.1003
6	0.0011	0.6224
7	0.0004	0.2440
8	0.0002	0.1055
9	0.0001	0.0773

Element	PC 1	PC 2	PC 3	PC 4	PC 5	PC 6	PC 7
Na <sub>2</sub> O	0.5121	0.7734	-0.2829	0.1674	0.1131	0.0888	-0.0769
MgO	0.0495	0.1941	0.3896	0.3785	-0.5964	-0.5340	0.1277
Al <sub>2</sub> O <sub>3</sub>	0.1277	-0.1473	0.1221	0.3865	-0.1316	0.4636	-0.4129
SiO <sub>2</sub>	0.0335	0.0243	-0.1056	-0.1522	-0.0504	0.1225	0.5620
K <sub>2</sub> O	0.1302	-0.2027	0.1456	0.5326	0.7075	-0.3218	0.1327
CaO	-0.7286	0.5059	0.2824	0.1631	0.1945	0.2448	0.0884
TiO <sub>2</sub>	0.1838	-0.0537	0.0344	0.0995	-0.0370	0.2696	0.6746
Fe <sub>2</sub> O <sub>3</sub>	0.1251	-0.1720	0.1980	0.3481	-0.1801	0.4841	0.0858
MnO	0.3474	0.1114	0.7751	-0.4636	0.1988	0.0801	-0.0596

The variance for calculated principal components (PC).

# Annex IV



## Phoenician-Punic amphorae from Castro Marim, Portugal: provenance and contents of Pellicer amphora types B/C and D

Adam Gašpar <sup>(a,c)</sup>, Ana Margarida Arruda <sup>(b)</sup>, Cristina Dias <sup>(a)</sup>, José Mirão <sup>(a)</sup>, Elisa de Sousa <sup>(b)</sup>, Ana Manhita <sup>(a)</sup>

a. HERCULES Laboratory, University of Evora, Portugal, Largo Marquês do Marialva 8, 7000-554 Evora, Portugal  
 b. UNIARQ - Centro de Arqueologia da Universidade de Lisboa, Faculdade de Letras, Alameda da Universidade, 1600-214 Lisboa, Portugal  
 c. Department of Archaeology and Museology, Faculty of Arts, Masaryk University, Arna Nováka 1, 602 00 Brno, Czech Republic



### INTRODUCTION

#### CONTEXT AND RESEARCH QUESTIONS

- Typical hilltop site in the river delta the Castle of Castro Marim
- There was vigorous trade in Bay of Cadiz during the Second Iron Age
- The large sized amphorae used for the transport of food products

**Is it possible to distinguish differences in the composition of the ceramics in terms of the provenance?**

**What were the possible past food contents of the 8 selected bottoms?**

Castro Marim in the Iberian Peninsula

The Guadiana river, swampy area and the hilltop in middle

Geological setting of Cadiz bay and Lower Guadalquivir (Salvany et al. 2021)

The Pellicer B, C and D (after Pellicer Catalán 1972)

Examples of double-chamber ceramic tiles that were introduced by the Phoenicians, and commonly used during the Second Iron Age (Cosimo di Caprio 2007)

Section of the analysed samples of bottoms

- A: Pellicer B/C (variant I)
- B: Pellicer B/C (variant II)
- C: Pellicer B/C (variant III)
- D: similar to Pellicer B/C
- E: bottom of *Musa amphorae*?
- F: local containers with concave bottom

In terms of availability of raw materials for ceramic production, the Castro Marim site has similar geological settings than those in the Lower Guadalquivir area (common presence of calcite-dolomitic clay – marl and naturally sorted material by river or sea from the erosion of Sierra Morena).

### SAMPLES AND METHODS

#### DATA SET OF 30 SAMPLES

**4 ceramic types from various archaeological contexts**

- 14 bottoms of Pellicer B/C (5<sup>th</sup>-4<sup>th</sup> cent. BC)
- 2 bottoms of like Pellicer B/C (5<sup>th</sup>-4<sup>th</sup> cent. BC)
- 4 local containers (5<sup>th</sup>-4<sup>th</sup> cent. BC)
- 10 rims of Pellicer D (1<sup>st</sup> cent. BC)

#### MULTIANALYTICAL PROTHOCOL

- Petrography of thin sections
- Powder XRD
- ED-XRF of fused beads
- SEM-EDS of selected thin sections
- GC-MS – lipid extraction: CHCl<sub>3</sub>/MeOH, 2:1

### RESULTS

#### CERAMIC STUDY

The ceramic study discovered 3 different fabric groups

	Pellicer B/C	Amphorae like B/C	Local container	Pellicer D
Fabric A - 19 samples	x	x		x
Fabric B - 6 samples				x
Fabric C - 5 samples			x	x

#### RESULTS OF PETROGRAPY

The fabric - stereo-microscopic images of representative samples

Examples of temper inclusions in Fabric A

#### XRD

Legend: ● - Pellicer B/D, + - Amphorae like Pellicer B/C, x - Pellicer D, □ - local container

#### XRF

Principal component analysis (PCA) of the main oxides. Variance of the first two components (PC1 and PC2)

#### SEM

Pellicer D - Fabric B: Elemental mapping with glassy vitrification

#### CONTENT STUDY – GC-MS

Four samples from the content study reveal a presence of beeswax, plant leave wax and possibly a dairy product

	Milk	Bees wax	Plant wax
Pellicer B/C	x	x	x
Pellicer B/C			x
Pellicer B/C			x
Local container		x	

### DISCUSSION AND CONCLUSIONS

#### CERAMIC STUDY

The fabric group C represented basically by local containers suggests the main manufacturing tradition represented in the Castro Marim. The fabric group A is associated with Pellicer amphorae B/C and Amphorae like Pellicer B/C and it is dated to the same time interval as the local containers (from 5th to 4th century BC). The fabric group B is restricted to 6 samples of younger type Pellicer D dated to 1st century BC. However, in the ceramic type Pellicer D fabric of group A (3 samples) and C2 (1 sample) are also present. This is related to the wide spread of this ceramic type, and its production in several centres or regions.

In future research the same multi-analytical approach must be applied to more vessels in order to get a detailed picture of their production (i.e. raw materials and technology) characteristics. It is expected that the data can contribute to revealing the relations between the different settlements in Punic times. The analysis of other ceramic materials will lead to distinguishing more relations between the local fabric tradition and the character of imported vessels.

#### CONTENT STUDY

Concerning the GC-MS study, the residues identified in the Pellicer B/C indicate a possibly imported edible commodity. The three Pellicer B/C and one local container present residues which can be related with their past content. The identified compounds show the presence of MAG's, alcohols and alkanes in all samples, but fatty acids are absent, except for one sample of Pellicer B/C. This strange fact we cannot explain. In future other more aggressive acidic based extraction methods should be used to obtain more information. The short-chain saturated fatty acids suggest a storage of dairy products, but not all typical compounds are detected. It can be proven by an additional IR-GC-MS analysis in future. The beeswax residue suggests that the vessels were possibly used for the manipulation of liquid products. The beeswax was used in ancient times as the sealant. The data obtained from other 2 samples can be associated only with the plant leaves wax material. It is likely that in these amphorae some solid plant material was stored, like cereals, which would not have yielded large amounts of fat molecules into the ceramic body. Further systematic study will discover more about the imported food products and commercial interaction in the Castro Marim site.

**Bibliography** Cuomo di Caprio, N. (2007) – Ceramica in Archeologia 2. *Antiche tecniche di lavorazione e moderni metodi di indagine*. Studia Archaeologica 144. Roma, 2007.  
 Pellicer Catalán, M. (1978) – Tipología y cronología de las ánforas prerromanas del Guadalquivir, según el Cerro Micasero (Sevilla). *Habis* 9, 335-400.  
 Salvany, J. M., Larrosaña, J. C., Mediavilla, C., Rebollo, A. (2011) – Chronology and tectono-sedimentary evolution of the Upper Pliocene to Quaternary deposits of the lower Guadalquivir foreland basin, SW Spain. *Sedimentary Geology* 241, 22-39.

THE EMAIL OF FIRST AUTHOR  
 adam.gaspar@gmail.com

Acknowledgements: this work was carried out with the financial support of the EACEA agency of the EU under the ERASMUS+ MUNDUS ARCHMAT Master Project (FPA2013-0238).